Effect of electrostatic deflectors and associated fringe fields on spin coherence time for the measure of electric dipole in a storage ring

Julien Michaud

Communauté
UNIVERSITÉ Grenoble Alpes

THÈSE

Pour obtenir le grade de

DOCTEUR DE LA COMMUNAUTÉ UNIVERSITÉ GRENOBLE ALPES

Spécialité : Physique Subatomique et Astroparticules
Arrêté ministériel : 25 mai 2016

Présentée par

Julien MICHAUD

Thèse dirigée par **Jean-Marie De Conto**,
Université Grenoble Alpes

préparée au sein du **Laboratoire de Physique Subatomique et de Cosmologie**
dans **l'École Doctorale de Physique**

Effet des déflecteurs électrostatiques et des champs de fuite associés sur la cohérence de spin pour la mesure du moment électrique dipolaire du proton sur anneau de stockage

Effect of electrostatic deflectors and associated fringe fields on spin coherence time for the measure of the proton electric dipole moment in a storage ring

Thèse soutenue publiquement le **25 septembre 2019**,
devant le jury composé de :

Monsieur Christophe Furget
Professeur, Université Grenoble Alpes, Président
Monsieur Jörg Pretz
Professeur, Université RWTH Aachen - Allemagne, Rapporteur
Monsieur Fabian Zomer
Professeur, Université Paris-Sud, Rapporteur
Monsieur Bertram Blank
Directeur de recherche, CENBG, Examinateur
Monsieur Dominique Rebreyend
Directeur de recherche, LPSC, Examinateur

Remerciements

La recherche fondamentale - et en particulier la physique - a toujours fait partie de mes projets et mes passions. Déjà, dès mon plus jeune âge, j'embêtais mon entourage avec des tonnes de questions et des idées d'expériences farfelues. L'obtention du diplôme de doctorat représente pour moi un grand accomplissement vers ce rêve qui est de contribuer à l'élargissement de nos connaissances sur le monde qui nous entoure et l'amélioration de nos technologies.

Ce haut-fait, je le dois à un travail assidû et laborieux lors de ces trois dernières années, mais aussi et surtout à ces personnes qui m'ont entouré, soutenu et conseillé. A défaut de ne pouvoir doubler le nombre de pages de ce manuscrit en remerciements (oh oui qu'il en faudrait des pages !), je vais tâcher de n'oublier personne, tout en restant synthétique.

Tout d'abord, je tiens à remercier les membres de mon jury de thèse, à commencer par Fabian et Jörg, qui ont accepté de subir la laborieuse lecture de mon manuscrit. Mes prochains remerciements vont à Christophe, pour avoir accepté de présider mon jury de thèse et enfin à Dominique et Bertram pour avoir joué le rôle d'examinateurs. Je vous remercie tous pour vos remarques constructives, pour vos questions et vos corrections.

Cette thèse n'aurait jamais vu le jour, ni son aboutissement, sans l'aide et les avis précieux de Jean-Marie. Je te remercie chaleureusement pour ton soutien, ta patience et ton implication ces trois dernières années. J'ai passé les trois années les plus enrichissantes de ma vie, scientifiquement comme humainement, et beaucoup de ce mérite te revient.

Je tiens à remercier particulièrement les collègues qui m'ont entouré pendant cette thèse. Un grand merci à Maud, pour ta sympathie et ta disponibilité. Un grand merci également à Yolanda qui m'a beaucoup aidé avec ces montagnes de calculs, mais aussi à Thomas, Thomas et Thomas, Julien, Patrick et tous les autres.

Mention spéciale à David et Jacob pour avoir suivi de près l'avancement de ma thèse, et pour l'implication que vous y avez mis.

Peu le savent, mais le LPSC est doté d'une force gigantesque : un organisme (presque) international qu'on appelle le Bidul. Merci les gars pour ces moments magiques ! Big up à Kiki, Laulau, Ju l'autre, Seb, Flo, Mathieu (merci pour les débug!), Toto, Rola, Alex, Dilia... et les autres ! J'espère que je ne vais pas trop vous manquer (sisi je vais vous manquer !).

Il y a le boulot, mais aussi un paquet de gens autour. Je tiens à remercier les meilleurs des collocs Killian, Elie, Elisa, Caro (puis Eustache, Richter, la reine des neiges et tous leurs amis) ! C'était inoubliable !! Je remercie aussi toute la bande de copains, de Grenoble, Bordeaux, EMF/TML.

Quand on parle de ces gens autour, je ne peux pas ne pas penser à remercier mes parents, qui, bien que loin, m'ont soutenu ces trois dernières années, mais aussi toutes les années précédentes.

Last but not least, un mega merci à ma Sheeshee pour m'avoir soutenu ces dernières semaines (j'ai du être insupportable). Merci aussi pour tes conseils stylistiques, parce que c'est pas sorcier c'est mieux avec des belles couleurs !

Merci !

Contents

Introduction

Particle accelerators are one of the most efficient ways to study matter and elementary particles, as proven by the recent discovery of the Higgs Boson on the Large Hadron Collider. The JEDI collaboration proposes to measure the value of the proton electric dipole moment (EDM) with a precision of 10^{-29} e.cm using a storage ring.

A measurement of such a value of EDM, above the extremely small prediction of the Standard Model would lead to new physics, by adding an additional source of CP violation. The CP violation is one of the three conditions necessary to explain the non understood asymmetry between matter and antimatter in the universe.

In order to achieve this 10^{-29} e.cm precision, one needs to store the measured particles for many seconds in an electric field : a storage ring appears as an ideal solution for charged particles. One of the main issues consists in keeping the beam spin-coherent during the whole duration of the measurement. An excellent control of systematics and understanding of the spin dynamics to perform this measurement are mandatory.

The electrostatic deflectors used in the experiment to provide both bending and EDM-induced spin precession could lead to systematic errors and spin decoherence. The internal part of the deflectors and especially their fringe fields need to be understood, in terms of trajectories and spin dynamics.

This thesis provides models for fields, trajectories, spin dynamics and also results about the spin decoherence induced by the deflectors.

The first part is dedicated to the context around EDM measurements, and will then focus on the storage ring method. Also a first approach to the spin precession equation and spin coherence time will be done, and the problematics about the electrostatic deflectors exposed.

The second part describes in details the analytic or semi-analytic models we developed. The first model describes the electric fringe field of the deflector, using conformal mapping.

This model takes into account boundary conditions like the vacuum chamber or a diaphragm and proposes universal formulas as a function of the ratio between gap and radius. The second model concerns trajectories in the deflector and the fringe fields.

It is using an Hamiltonian integration, variation of parameters and quadrature formulas to integrate the previously found field. This is done at the second order.

The last model is about spin dynamics and allows the user to compute the total spin precession in the deflector or the fringe fields by using a list of integrals of the field. The final spin transfer solution is a function of the initial conditions (x,px,y,py,dz,ΔP/P) at the second order.

The last part shows the implementation on BMAD and the different effects of deflectors/fringe fields on the spin coherence time.

Introduction - Français

Les accélérateurs de particules sont aujourd'hui un des moyens les plus efficaces pour sonder la matière et les éléments qui la composent.

La collaboration JEDI propose de mesurer la valeur du moment électrique dipolaire (EDM) du proton (voire deuton) avec une précision plusieurs ordre de grandeur supérieure aux limites actuelles, par le moyen d'un anneau de stockage.

La mesure d'un moment éléctrique dipolaire permanent permettrait l'ajout de sources de violation de CP supplémentaires. La violation de la symétrie CP est une des trois conditions nécessaires à l'explication de l'asymétrie matière/antimatière de l'Univers.

En vue de parvenir à une telle précision, les particules doivent être stockées pendant une longue durée dans des champs électriques et/ou magnétiques : dans le cas de particules chargées, un anneau de stockage se présente comme une excellente solution.

Un des principaux défis consiste à conserver la polarisation en spin du faisceau pendant toute la durée de l'expérience. Un excellent contrôle des systématiques et de la dynamique de spin sont alors obligatoires.

Les déflecteurs électrostatiques utilisés dans l'expérience à la fois pour guider les particules et pour entraîner la précession du spin liée à la présence d'EDM sont source d'erreurs systématiques et de décohérence de spin. La partie interne des déflecteurs et aussi leurs champs de fuite doivent être compris et maîtrisés, en termes de trajectoires et de dynamique de spin.

Ma thèse fournit un modèle pour le calcul de champ, trajectoires et dynamique de spin dans un déflecteur électrostatique.

La première partie est dédiée au contexte autour de la mesure d'EDM, et se précisera sur le cas particulier de la mesure proposée par JEDI. L'équation de précession du spin sera présentée ainsi que les objectifs de la thèse.

La seconde partie décrit en détails tous les outils analytiques ou semi-analytiques qui ont été développés pour répondre à nos besoins spécifiques. Ces outils seront ensuite utilisés dans la partie suivante.

La troisième partie concerne les résultats et l'élaboration du modèle de champs, de trajectoire et de spin. Le modèle de champ, établi par transformation conformes, est un modèle universel dépendant uniquement du ratio gap/rayon du déflecteur. Il prend en compte les conditions aux limites telles qu'une chambre à vide ou un diaphragme.

La résolution des équations du mouvement se fait à partir des équations d'Hamilton, au second order, par une méthode perturbative et en utilisant la méthode de la variation des constantes.

La dynamique de spin, quant à elle, est obtenue par la résolution de l'équation Thomas-BMT par une méthode perturbative. Les fonctions de transfert obtenues

dépendent des coordonnées de l'espace des phases à l'entrée du déflecteur. Elles sont totalement analytiques dans le cas de la partie centrale du déflecteur, et semi-analytiques pour les champs de fuites, où elles font intervenir une liste d'intégrales particulières, calculées avant la simulation.

La dernière partie concerne l'analyse et le test du modèle à l'aide d'un code de calcul appelé BMAD.

Chapter 1

Theory and motivations

Contents

1.1 Measuring the electric dipole moment of a charged hadron

1.1.1 The electric dipole moment (EDM) and its context

The matter-antimatter asymmetry problem

The matter-antimatter asymmetry problem, also known as the baryon asymmetry problem, comes from the observed difference between the quantity of matter and anti-matter in the observable universe.

This asymmetry has been determined using data from the Planck satellite on the cosmic microwave background. The ratio of baryons over photons in the universe is given by [2]:

$$\eta = \frac{n_B - n_{\bar{B}}}{n_\gamma} = (6.047 \pm 0.074).10^{-10}$$

where n_B and $n_{\bar{B}}$ are respectively the density of baryons and anti-baryons, and n_γ the density of photons.

Andreï Sakharov (1967) described the necessary conditions for such an asymmetry, called baryogenesis, with three criteria:

- At least one B-number violating process.
- C and CP violation.
- Interactions outside of thermal equilibrium.

These three conditions are not yet satisfied. As we will see in the next section, the actually known sources of CP violation are totally insufficient to explain such an asymmetry.

CP violation

From 1957 and the discovery of the parity symmetry violation, the three discrete symmetries of nature C (charge symmetry), P (parity symmetry) and T (time reversal symmetry) play an important role in the Standard Model. In the same year, Lev Landau proposed the CP symmetry as the fundamental symmetry of nature. However, in 1964 Christenson and al. [4] observed a CP violation in the decay of neutral kaons into two pions.

Historically, the first introduction of CP violation in the Standard Model was done in 1973 with the CKM matrix which contains information on the strength of the flavour-changing weak interaction, and experimentally proven with the discovery of the bottom quark and finally the top quark in 1994.

CP violation could also be allowed by the PMNS matrix which describes the mixing between the neutrino masses and flavors.

Nowadays, it is assumed that the CPT symmetry is conserved.

Electric dipole moment

In a classical and general definition, the electric dipole moment (EDM) is a measure of the separation of positive and negative electrical charges within a system. More precisely, for a particle, the EDM, written d, quantifies the coupling of the spin **S** of the particle with the external electric field **E** with the Hamiltonian:

$$H^{EDM} = d\mathbf{E}.\mathbf{S}$$

Because the EDM vector is similar to a spatial separation of charges, it is odd under parity and even under time reversal. This is not the case with magnetic dipole moments (MDM), that are even under parity and odd under time reversal.

As the EDM/MDM must be either parallel or antiparallel to the spin of the particle, applying the T or P reversal transformation will change the relative orientation of the EDM/MDM. The particle will then not be the same (see fig (1.1)), and the T symmetry violated.

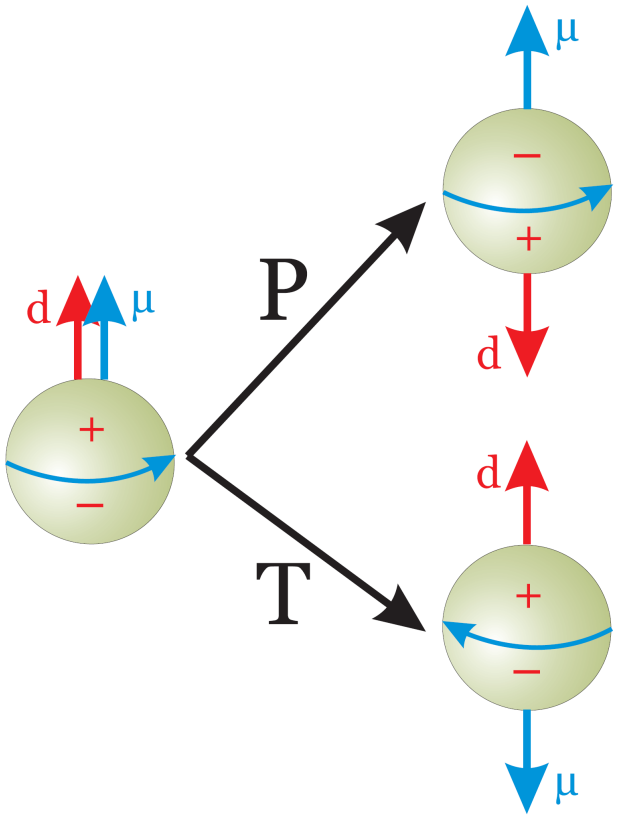

Figure 1.1: Violation of the P and T symmetries due to the presence of an EDM and a MDM [3].

As the CPT symmetry must be conserved, violating T means violating CP.

Many measurements of elementary or composite particles EDM have already been done (see fig 1.2). The current limit for the neutron EDM is set at 10^{-26}e cm. There is not yet a direct measurement of charged hadrons EDM, the current limit for the proton EDM was obtained from an indirect measurement of a mercury atom.

However, a direct measurement for protons and deuterons can be taken using storage rings (more details section 1.1.3).

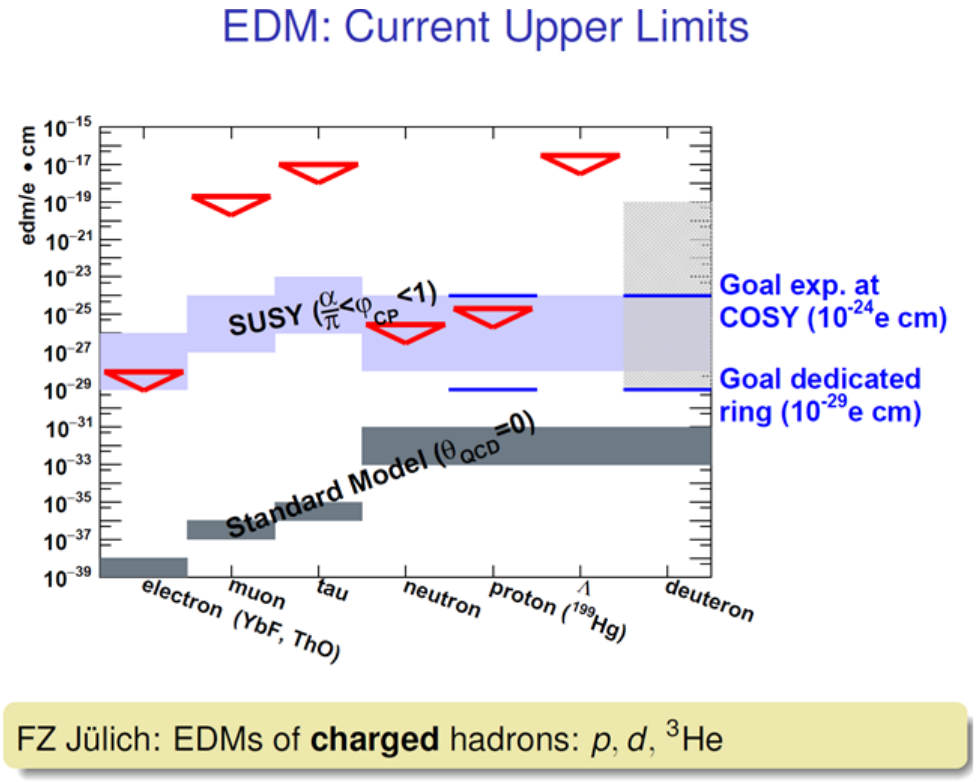

Figure 1.2: Current limits and predictions for different particles EDMs. The red arrows show the current upper limits measured for the EDMs, the two grey areas show the predicted values for the EDMs, from the Standard Model and the Supersymmetry. Blue lines represent the limits aimed by the JEDI collaboration.

Measuring the EDM of charged hadrons up to a certain limit will add more constrains on models such as the supersymmetry. The predictions from the standard model, in the order of $10^{-32} - 10^{-31}$ are too small to be measured by the proposed storage ring method in section 1.1.3.

The JEDI collaboration

The JEDI (Jülich Electric Dipole moment Investigations) collaboration was created in 2011 and is composed by around 150 persons. The JEDI collaboration proposes to increase the current upper limit on charged hadrons EDM by some orders of magnitude. The experiment will be done using a storage ring filled with protons or deuterons.

A research and development program is currently taking place on the COSY (COoler SYnchrotron) storage ring (fig. 1.3) at Jülich, Germany. The first goal is to propose a proof of principle using COSY to make a first measurement of an EDM up to 10^{-24}e cm.

Figure 1.3: Top-side view of the storage ring COSY at Jülich, Germany.

1.1.2 Spin precession equation

We give here a first general approach on the spin precession equation. This equation, called the Thomas-BMT equation, is fundamental to understand the spin dynamics of a particle in systems like storage rings.

General form of the T-BMT equation

Let us first consider a particle at rest, in electric and magnetic fields. The spin evolution of this particle is expressed as the coupling between the electric dipole moment and the electric field, and the coupling between the magnetic moment and the magnetic field as (eq 1.1):

$$\frac{d\vec{S}}{dt} = \vec{d} \times \vec{E} + \vec{\mu} \times \vec{B} \tag{1.1}$$

where $\vec{E}$ and $\vec{B}$ are respectively the electric and magnetic fields, $\vec{d}$ and $\vec{\mu}$ quantities linked to the electric dipole moment and the magnetic dipole moment and $\vec{S}$ the spin vector.

In most cases, charged particles like protons and deuterons are not at rest and we need to express the spin dynamics in the laboratory frame.

By applying the Lorentz boost, equation (1.1) transforms to the Thomas-BMT equation [10], giving the spin evolution in the laboratory frame relative to direction of flight:

$$\frac{d\vec{S}}{dt} = \vec{\Omega} \times \vec{S} \tag{1.2}$$

with

$$\vec{\Omega} = \vec{\Omega}_0 - \vec{\Omega}_{cyc} = -\frac{e}{m}(G\vec{B} + (\frac{1}{\gamma^2 - 1} - G)(\frac{\vec{\beta} \times \vec{E}}{c}) + \frac{\eta}{2}(\frac{\vec{E}}{c} + \vec{\beta} \times \vec{B})) \tag{1.3}$$

where γ is the usual Lorentz gamma factor.

G is the anomalous magnetic moment: G = $\frac{g-2}{2}$ and d = $\frac{\eta q \hbar}{2mc}$ the value of the electric dipole moment.

This equation is a simplified case, where $\vec{B}$ is fully perpendicular to the momentum. For more information, see [1].

Terms of T-BMT equation

One can notice that eq. (1.3) can be separated in two parts:

- A first part containing the G-factor that represents the spin rotation induced by the magnetic moment:

$$G\vec{B} + \left(\frac{1}{\gamma^2 - 1} - G\right) . \left(\frac{\vec{\beta} \times \vec{E}}{c}\right) \tag{1.4}$$

- A second part containing the η factor proportional to the value of the electric dipole moment d:

$$\frac{\eta}{2}(\frac{\vec{E}}{c} + \vec{\beta} \times \vec{B}) \tag{1.5}$$

In the case of a fully longitudinal momentum of the beam, a transverse horizontal electric field and a longitudinally polarized beam, which correspond to the design situation (presented in 1.1.3), the magnetic part of the equation leads to an horizontal rotation of the spin.

In the same configuration, the electric part of the equation leads to a vertical rotation of the spin as shown in the fig. 1.4.

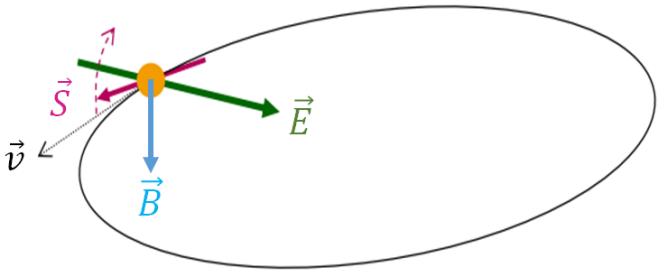

Figure 1.4: Spin rotation induced by the electric dipole moment in the case of the designed scenario.

In the case of a fully electric ring (for protons only), it becomes possible to have two beams present together in the machine in clockwise and counter-clockwise directions.

By doing so, a large fraction of the systematic errors can be eliminated: one beam represents the time-reverse of the other, and the difference will show only time-odd effects such as the EDM [5], and radial B-fields.

1.1.3 EDM measurement experiment and scenarios

General measurement method

In most EDM measurement experiments, electric fields are proposed to interact with the EDM. A difference with other experiments like neutron EDM experiments is the positive charge of the proton (or deuteron, helion ...), which implies that the particle is moving due to the electric field. A solution to this is the use of a storage ring, which allows the particle to feel the electric field and still be confined.

According to the T-BMT equation (1.3), the magnetic and electric moments contributions to the spin can be isolated, as they induce a spin precession around different axis.

In order to get a measurable EDM signal (vertical polarization), one needs to cancel the magnetic moment part contribution to the spin, either exactly (frozen-spin scenario) or in average (quasi-frozen spin scenario).

This condition implies that (1.4) = 0:

$$G\vec{B} + \left(\frac{1}{\gamma^2 - 1} - G\right) . \left(\frac{\vec{\beta} \times \vec{E}}{c}\right) = 0$$

Fully electric frozen-spin scenario

A first method to cancel this term consists in avoiding all magnetic fields and using a particular energy such that $G\vec{B} = 0$ and $\left(\frac{1}{\gamma^2-1} - G\right) = 0$.

This particular energy is called the "magic energy" or "magic condition" and corresponds to:

$$\gamma_0 = \sqrt{1 + \frac{1}{G}} \tag{1.6}$$

For protons, this energy corresponds to $\gamma_0 \simeq 1.2481$ or $E_k \simeq 230$MeV. This method cannot be applied on deuterons, which have a negative G factor (for proton G ≈ 1.7928).

Such a method implies the use of only electric fields for both bending and vertical spin precession. According to the involved energies, strong electric fields are needed, at the order of 10^7V/m for a radius near 30-40 meters, as mentioned in the following chart and figure (1.5):

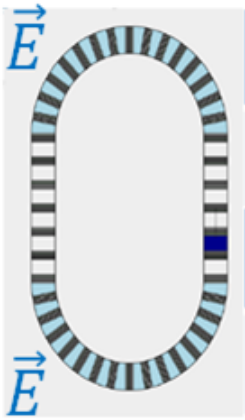

Particle	Energy	Gamma
Protons	230 MeV	1,24
Radius	**Efield**	**Ring length**
32m	13 MV/m	500m

Figure 1.5: Example of frozen spin lattice with typical values.

Combined magnetic and electric fields frozen spin scenario

It is also possible to get a frozen-spin scenario with combined electric and magnetic field such that eq(1.5) = 0. Figure (1.6) shows an example of $\vec{E} \times \vec{B}$ scenario.

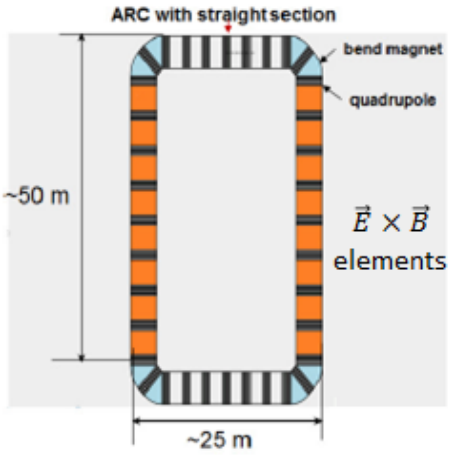

Figure 1.6: Example of frozen spin lattice with crossed electric and magnetic fields.

Quasi frozen-spin (QFS) scenario

Another solution is to force the magnetic term to have an average value equal to zero over a turn. This solution implies the use of both electric and magnetic fields. Magnetic and electric fields should apply an opposite contribution to the spin.

In that case, the spins are oscillating around the initial polarization in a small area such that the vertical precession is not perturbed. Many lattices have been proposed, and a few examples are shown below [15] in fig 1.7.

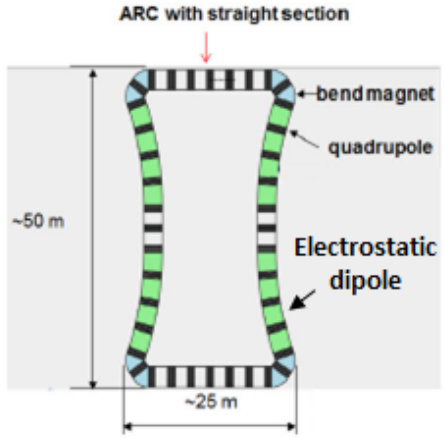

Figure 1.7: Example of quasi-frozen spin lattice with successive E and B fields [6].

Parameters	With « B + E » elements on arcs	QFS with straight deflector		QFS with curve deflector	
Energy	270 MeV	270 MeV		270 MeV	
E field	120 kV/m	120 kV/m		120 kV/m	
Circumference of ring	145.8 m	148.9 m		167.1 m	
B field	0.46 T	Arc : 1.5 T	Straight section : 0.082 T	Arc : 1.5 T	Straight section : 0 T
Radius of magnet curvature	9.2 m	2.3 m	∞	2.3 m	42 m
Lenght of B or/and E deflector	16x1.8 m	4x1.8 m	8x3.6 m	4x2.3 m	8x3.6 m
Number elements per ½ ring	16	4	8	4	8

Figure 1.8: Typical parameters of quasi-frozen spin lattices.

1.1.4 Spin coherence time

Spin coherence time (SCT)

As the different particles of the beam do not have the same phase-space parameters, they will not perform the same trajectory and will have different velocities. The differences of phases due to the different spin tunes of the particles will add up with time and induce a progressive horizontal depolarization of the beam (see fig 1.9).

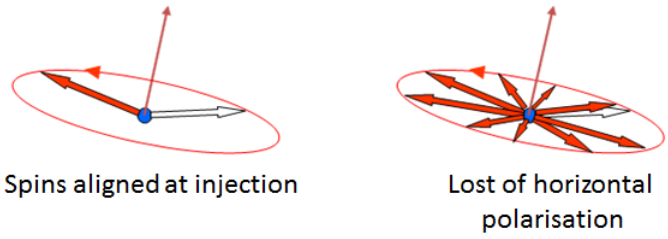

Figure 1.9: Coherent beam (left) versus non coherent beam (right). The white arrow represents the direction of propagation while the red arrows represents the orientations of the spin of the particles.

The spin coherence time is usually defined as the time during which the spins of the particles are not scattered more than one radian (horizontally). As the vertical spin build up depends of the horizontal state of the polarization (eq 1.2), keeping the beam horizontally coherent is necessary to create the vertical polarization one needs to measure an EDM signal.

In order to achieve the wanted precision of 10^{-29} e.cm, a spin coherence time of 1000 seconds has to be reached [5].

1.2 Objectives of the thesis

The main purpose of this study is to evaluate the effect of the electrostatic deflectors on the spin coherence time. Both the internal part of the deflector and the fringe fields will affect the spin, so the entire deflector has to be taken into account.

The present models for fringe fields are incomplete (e.g. no boundary conditions) or too simplified concerning the precision required for an EDM study. Also, the tracking codes generally use Runge-Kutta tracking or simplified models for fringe fields and do not consider fringe fields as an independent element. Runge-Kutta tracking is very time consuming. It does not give explicitly the dependence versus the field components and provides no way to analyse the problem and to optimize the machine.

In order to achieve the best precision in the simulation, we decided to do everything analytically and implement these analytical formulas in a tracking code.

This model appears to be a universal model for every configuration (Gap / Radius) of the deflector. The potential/field, motion transfer functions and spin transfer functions are given as a function of universal integrals, integrated once and for all and stored in a separate file.

Another axis of study is to evaluate the creation of a fake EDM signal (vertical polarization) due to imperfections or fringe fields.

The next figure (1.10), shows in a synthetic and schematic way the work that has been done during this thesis. The complete path of operations is represented, from the computation of the electric field, to the final implementation in the BMAD tracking code:

- Chapter 2.1.2: The electrostatic field of a deflector (straight or cylindrical, with any gap/radius ratio) is computed by conformal mapping. Boundary conditions are included. This thesis results as an analytic description of the field, with its multipolar components.
- Chapter 2.4.2: We compute a list of integrals of the field by using quadrature methods. These integrals are universal and need to be computed once and for all. This list of numbers is stored in a text file.
- Chapter 2.4.1: We solve the motion (chapter 2.2.1) and spin (chapter 1.1.2) equations by using a perturbative method specifically developed.
- Chapter 3.2 and 3.3: We get fully analytical and universal formulas for spin and trajectories in both the inner and the fringe field parts of the deflector. These formulas have been implemented in different routines for tracking purposes.
- Chapter 4: Application of this model on a machine scenario to study the effect of the whole deflector on the spin dynamics.

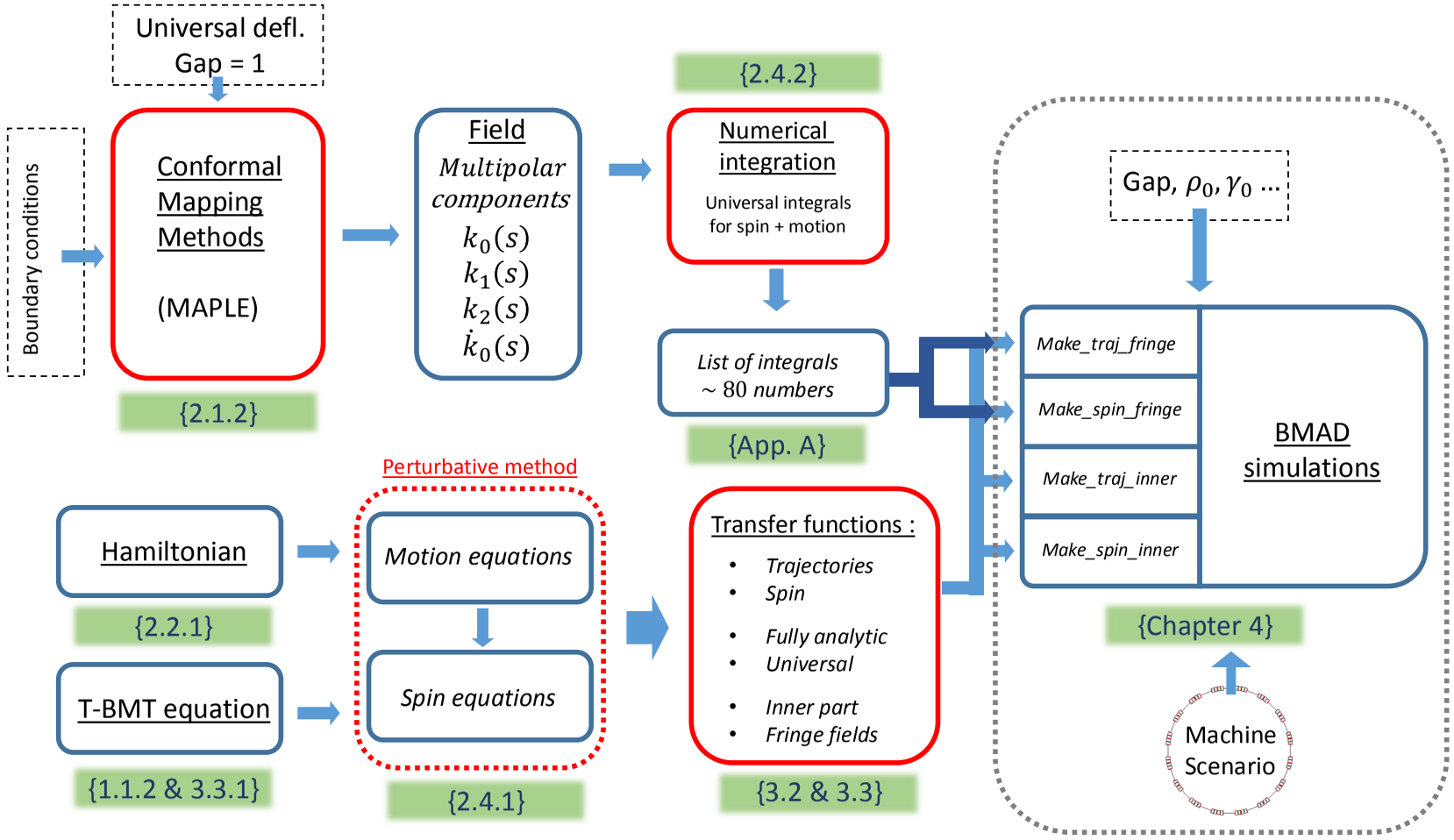

Figure 1.10: Summary of all the operations done to obtain the spin tracking routines. The red boxes show the methods we developed specifically to solve the problem. Black dotted boxes stand for the input initial conditions of the model. Green areas send back to the chapters where these elements are explained.

1.2.1 Computation time and precision

Tracking a beam of particles generally requires lots of computation power and time. The lattice that is studied in chapter 4 is made of hundreds of elements. Tracking a beam of millions/billions of particles on a few million turns (few seconds of flight) can lead to real computation problems such as:

- Computation time: as explained below, computation time can increase dramatically when we rise the number of particles/turns or elements in the lattice. In order to keep the computation time reasonable, we need to develop faster and more efficient methods.
- Lack of computation power: even if the computation power has exponentially increase in recent years, we can still hurt the limit of processing in such a simulation, and having more efficient simulations can decrease the economical and environmental cost of it.
- Accuracy: numerical integrations or tracking methods usually admit uncertainties that can increase with the number of turns or computation time. Having analytic methods, if possible, provide exact and generally faster results.

One way to avoid or decrease the disadvantages mentioned above is to provide analytical results up to the latest possible step of the simulation. These results must be calculated only once and implemented in the tracking code.

The results should be as much universal and integrated as possible so that the study of a new scenario requires a minimum number of operations (as a difference with a model using field maps for example).

We estimate the computation time to be at least a factor 100 faster with the analytical formulas compared to standard methods, like Runge-Kutta.

We provide in this document analytical (or semi-analytical) formulas for the electrostatic field, particles trajectories and spin both in the internal and fringe fields parts of an electrostatic deflector.

There is no need to compute the field with additional codes like finite elements.

Understanding the physical quantities

It is mandatory in this measurement to have a precise value of the spin coherence time of the beam. The spin decoherence is created by plenty different effects, and having a good mastery on these effects can be the solution to maximize the spin coherence time.

The use of analytical models has the advantage to bring out the different sources of decoherence.

The model proposed in this thesis reveals the contribution of the phase space vector components $(x, p_x, y, p_y, d_z, \Delta P/P_0)$ up to the second order (linear, squared and crossed components) on the spin dynamics.

In this way, we plan to understand and master the physical quantities and eventually give an analytic analysis of the effects.

1.2.2 Electrostatic deflectors problematic: internal part

We call an electrostatic deflector the electric dipole used to provide the electrical bending of the particles in the storage ring. An electrostatic deflector is composed by two plates with respectively low and high potentials to provide the bending electric field. These plates can be parallel in the case of a straight deflector or curved for a cylindrical deflector.

The following picture shows a cylindrical electrostatic deflector with the different dimension parameters used in the following.

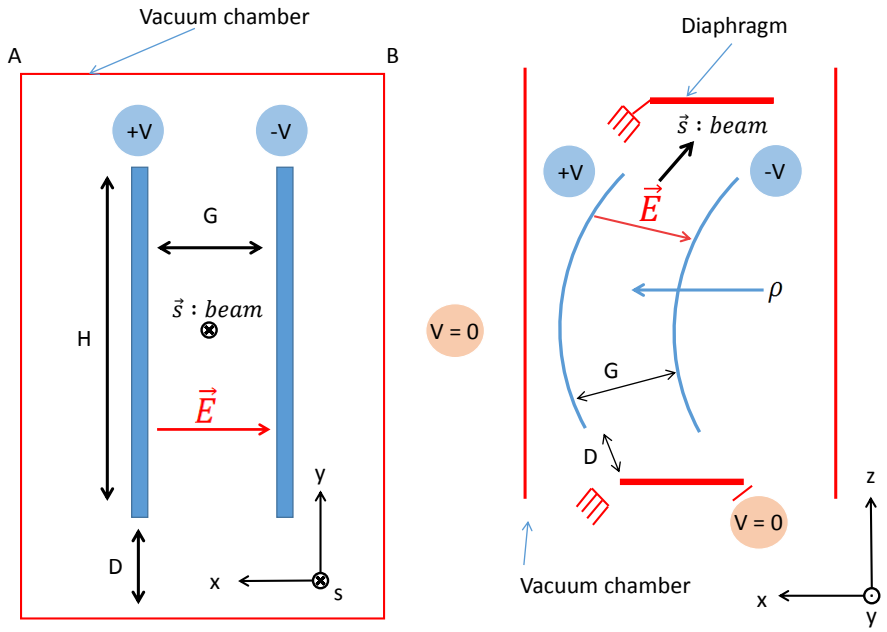

Figure 1.11: Left: View from the beam axis. Right: View from the top of the deflector. +V and -V are the high and low potentials respectively. $\vec{E}$ is the electric field ($\approx$ 13MV/m). H the height of the deflector, G is the gap between the electrodes ($\approx$ 30 mm) and D the distance to the vacuum chamber (we estimated with a finite elements analysis that D $\approx$ 5.G for homogeneity reasons). ρ is the radius of curvature ($\approx 30m$) and s the beam direction.

In order to provide a precise and efficient model, one needs to take into account the electrodes and boundary conditions (in our case we consider the vacuum chamber and a diaphragm at a distance D from the electrodes).

1.2.2.1 Particles trajectory in the inner part of the deflector

In order to know the spin dynamics in the deflector, one first needs to compute the trajectories of the particles inside it.

The trajectory of the reference particle is straightforward and follow the zero equipotential (a circle for cylindrical deflector).

The computation for the others particles has been done up to the second order, under the form of transfer functions of $[x, px, y, py, dz, \frac{\Delta P}{P_0}]$.

We expose in part 2.2 the details of the calculation, using Hamiltonian methods and variation of constants.

1.2.2.2 Spin dynamics in the deflector

In the particular case of the reference particle, whose position and momentum are exactly the design ones, and if the electrostatic deflector is a perfect (alignment, shape...) hard-edge deflector, the spin is supposed to stay aligned with the momentum of the reference particle, due to the magic condition of the T-BMT equation (see eq 1.6).

However, the particles of the beam are not the ideal reference-particle and are distributed among the usual 6-vector $[x, px, y, py, dz, \frac{\Delta P}{P_0}]$. This is going to induce a change in the energy, trajectory length or integrated field of the particles all over the deflector, leading to a faster spin decoherence.

We propose in part 3.3.2 a computation of transfer functions for the spin motion up to the second order of $[x, px, y, py, dz, \frac{\Delta P}{P_0}]$. We used an analytic perturbation method, up to the second order of perturbation, that is described in part 2.4.1.

1.2.3 Fringe fields of the electrostatic deflector

We previously saw that the internal part of the deflector can affect the beam polarization. The fringe fields present the same effects as the internal part, but also additional effects, that we will discuss in a few lines.

The fringe fields are defined in our case as the field that is not part of the internal part of the deflector. This corresponds to the area where the field along the reference trajectory is no more considered as constant and fully perpendicular to the beam direction.

Figure (1.12) is showing the fringe field generated by two parallel plates [17].

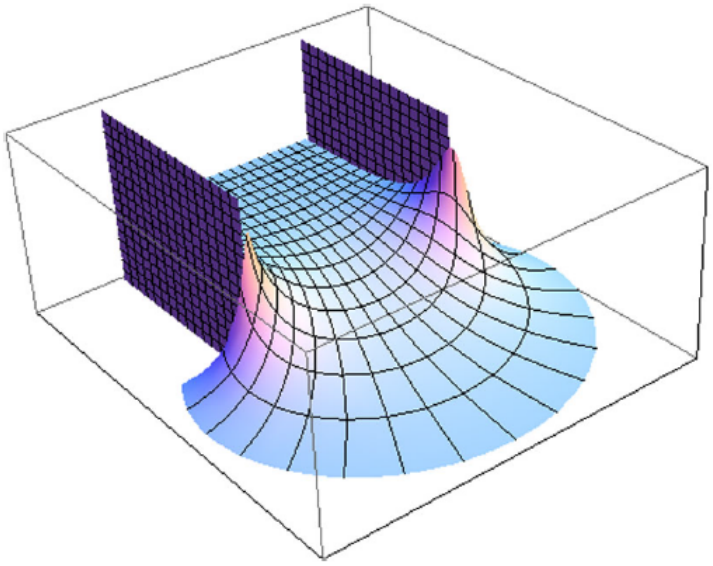

Figure 1.12: Representation of the fringe field generated by two parallel plates [17].

Thus, the fringe field has additional properties:

- Non constant $\vec{E}$ field: nominal at the edge of the deflector and going to zero at the diaphragm or infinity.
- Emergence of additional transverse components of the electric field.
- Longitudinal component is no longer zero and has to be taken into account.

These changes on the field implies that the field is no more the designed electric bending field in this part of the deflector. Not only the trajectories are modified but the spin dynamics itself.

The fringe field is a complicated element to describe, because it is not acting like a drift, nor like a dipole, but something in between. The trajectory of the particle is no more a straight line or a circle, even for the reference particle.

Usually, models are made on purpose and deeply depend on the geometry of the problem (we can think particularly about the Enge functions). These models provide really suitable results concerning beam dynamics. However, they can be insufficient when dealing with high accuracy spin dynamics.

The problematics here consists to find analytically the transfer functions for the trajectory and the spin dynamic in order to study the effect of fringe fields in the global lattice dynamics, especially the effect on the spin coherence time.

1.2.3.1 Electrostatic field computation

A great understanding of the electrostatic fringe fields is important to compute correctly the spin dynamics inside.

We compute in part 3.1 analytic formulas for the fringe field of a straight or curved electrostatic deflector, including boundary conditions like a diaphragm or the vacuum chamber.

Analytical formulas allow us to have exact and almost immediate values for the field at each point of the deflector.

The model we give is a universal model depending only on the ratio between the gap and the radius of the deflector, for a given distance to the diaphragm: this model can be applied to many cylindrical or straight deflector.

It avoids us the use of a field map, and so facilitates the machine design when it comes to change such values on a deflector.

1.2.3.2 Particles trajectory in fringe fields

Part 3.2.3 explains the computations for the trajectories of the particles in the fringe fields, using perturbation methods and quadrature integrations.

The trajectories for both the reference particle and the other particles have to be computed.

1.2.3.3 Spin dynamics in fringe fields

Fringe fields can be a great source of spin decoherence, as they introduce new components of the field and the trajectories are not the ideal ones.

Understanding the global effects of the fringe fields is fundamental if we want a total control on the spin coherence time. In order to get a reasonable computation time, the most computations have to be done once for all, before the code runs. We show in part 3.3.3 how we compute analytically and semi-analytically.

1.2.4 Spin coherence time on a machine scenario

The last chapter of this thesis will be dedicated to the implementation of the model and the associate analysis. I will present the BMAD tracking code that is used to do the simulations and the machine scenario I studied.

The machine is a fully electric ring, including deflectors and fringe fields. The main objective is to evaluate the spin coherence time on such a scenario, and the principal causes of the decoherence.

1.3 Théorie et motivations - Résumé en français

L'asymétrie matière/antimatière, définie par la différence observée entre la quantité de matière et d'antimatière dans l'Univers, a été déterminée récemment en utilisant les données du satellite Planck.

Andreï Sakharov (1967) a décrit les trois conditions nécessaires à l'apparition de cette asymétrie :

- Violation du nombre baryonique.
- Violation des symétries C et CP.
- Intérations hors équilibre thermique.

Les sources de violation de la symétrie CP sont aujourd'hui insuffisantes pour satisfaire les conditions de Sakharov.

La présence d'un moment électrique dipolaire (EDM) apporterait une source de violation de CP supplémentaire.

La collaboration JEDI (Jülich Electric Dipole moment Investigations) propose de mesurer la valeur de l'EDM de hadrons (proton, deuton voire hélion) avec une précision plusieurs ordre de grandeurs supérieurs aux valeurs actuelles. La limite actuelle pour le proton est de 10^{-26}e cm.

Equation de précession du spin La dynamique du spin d'une particule chargée dans des champs électriques et magnétiques est décrite par l'équation de T-BMT :

$$\frac{d\vec{S}}{dt} = \vec{\Omega} \times \vec{S}$$

avec

$$\vec{\Omega} = -\frac{e}{m}(G\vec{B} + (\frac{1}{\gamma^2 - 1} - G)(\frac{\vec{\beta} \times \vec{E}}{c}) + \frac{\eta}{2}(\frac{\vec{E}}{c} + \vec{\beta} \times \vec{B}))$$

où γ est le facteur relativiste de Lorentz, G le moment anormal magnétique : $G = \frac{g-2}{2}$ et η défini via $d = \frac{\eta e\hbar}{4mc}$ la valeur du moment électrique dipolaire.

Cette équation peut être séparée en deux parties distinctes : une partie magnétique (faisant intervenir G) et une partie électrique (proportionnelle à η).

Dans le cas idéal, avec un champ électrique transverse et une vitesse purement longitudinale, la partie magnétique va créer une polarisation horizontale du faisceau tandis que la partie électrique va créer une polarisation verticale.

Dans le but d'obtenir un signal EDM mesurable, nous devons annuler la précession crée par la partie magnétique de l'équation du T-BMT :

- Avec un anneau de stockage purement électrostatique. Ce scénario est appelé le scénario "frozen spin", car en l'absence de champ magnétique et à une énergie de faisceau particulière (appelée énergie magique), la précession horizontale du spin se retrouve gelée et n'évolue plus avec le temps.
- Un scenario type "frozen spin" avec des champs croisés ExB.
- Un scénario type "quasi frozen spin", où l'oscillation du spin dans l'anneau de stockage est en moyenne nulle sur un tour.

Objectifs de la thèse Je propose dans cette thèse des outils pour calculer analytiquement les champs, trajectoires et spins d'un faisceau de particules dans un déflecteur électrostatique, incluant les champs de fuite.

Les modèles actuels de champs de fuite sont insuffisants pour des mesures d'EDM, et parfois lents.

Le modèle présenté dans cette thèse est un modèle universel, dépendant uniquement du ratio gap/rayon du déflecteur. Le modèle de champs de fuite inclut les conditions aux limites comme un diaphragme ou la chambre à vide, et permet une modélisation rapide du déflecteur, sans recalculer des cartes de champs.

De plus, le modèle est un modèle analytique, qui permet une meilleure compréhension de la dynamique de spin, par exemple par l'isolation des différents effets lors des simulations.

Chapter 2

Methods and tools used

Contents

2.1 Electrostatic fields computation

As mentioned is the part 1.2.3, fringe fields can be a source of spin decoherence. To take fringe fields into account, many models are using the so-called empiric Enge profile or the hard-edge approximation such that the integral of the transverse field in the new deflector is the same as the one in the first one including fringe fields:

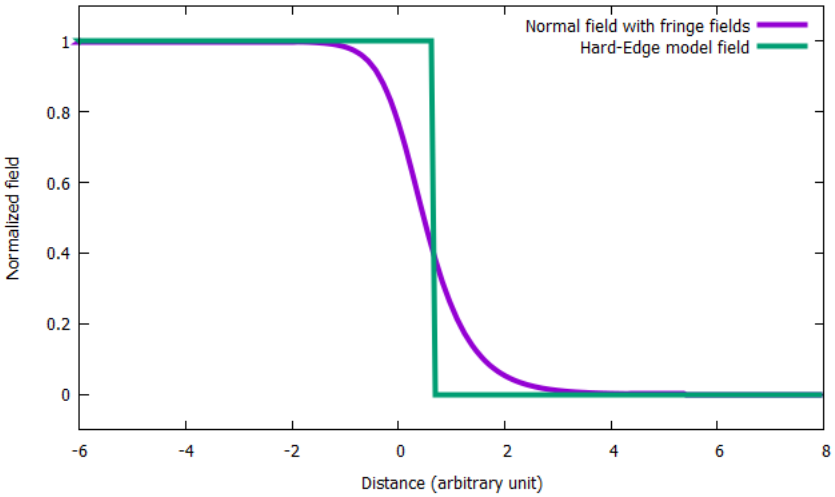

Figure 2.1: Representation of the field (electric or magnetic) along the beam trajectory, with regular and hard-edge model.

These models give us an approximation of the field values, but no information about the field derivatives that are explicitly involved in the spin dynamics (see chapter 3.3.3 for the contributions of the field components and there derivatives).

This approximation can be sufficient in some cases, but is not in ours, as EDM measurements required an extreme precision. Few models exist for the electrostatic fringe fields, as the use of the Enge functions [20].

However, these methods have sometimes the inconvenience to have non-vanishing field, and not to take into account boundary conditions like the vacuum chamber or a diaphragm. We propose here an analytical method based on conformal mapping to compute a more realistic fringe field.

2.1.1 Complex fields

About analytic functions and complex fields

We recall in this paragraph the tools and notations used in the following.

Let us assume a complex function f such that:

$$f(z) = A + i \cdot B \tag{2.1}$$

where z is the complex variable $z = x + i \cdot y$. This function is analytic, i.e. differentiable with respect to z if and only if it fulfills the Cauchy conditions:

$$\frac{\partial A}{\partial x} = \frac{\partial B}{\partial y} \qquad \text{and} \qquad \frac{\partial B}{\partial x} = -\frac{\partial A}{\partial y} \tag{2.2}$$

In virtue of the Schwartz theorem, A and B are harmonic functions and are solutions of the Poisson equation with no charges.

The lines where A (respectively B) is constant are orthogonal to the A (respectively B) gradient. If A are the equipotentials, so the isovalues of B are the field lines and vice versa [7].

The complex electrostatic potential is:

$$\underline{V} = V + i \cdot B \tag{2.3}$$

where V is the usual electrostatic potential and B the flow of the electric field.

The complex electrostatic field is:

$$\underline{E} = -\frac{d\underline{V}}{dz} \tag{2.4}$$

From (2.2) and (2.4) we can write:

$$\underline{E} = -\frac{d\underline{V}}{dz} = \frac{\partial V}{\partial x} - i \cdot \frac{\partial V}{\partial y} \tag{2.5}$$

and finally:

$$\underline{E} = E_x - i.E_y \tag{2.6}$$

where E_x and E_y are the components of $\vec{E}$.

2.1.2 Conformal mapping

A conformal mapping or conformal transformation is a transformation of the complex plane that locally preserves the angles, i.e. the field lines and equipotential lines. An analytic function is conformal at any point where it has a nonzero derivative.

One direct implication of this statement is that the orthogonality of the equipotentials and field lines is conserved.

The electrostatic potential V_1 at a point z is equal to the electrostatic potential V_2 at a point $Z = f(z)$ where f is a conformal transformation. Let us illustrate with an example.

Let z be a complex number in the complex plane:

$$z = x + i.y \tag{2.7}$$

The conformal transformation

$$Z = X + i.Y = f(z) = \frac{1}{\pi}.[1 + z + e^z] \tag{2.8}$$

transforms the infinite planar capacitor in the x, y plan [-∞,+∞] $\times$ [-π,+π] to a semi-infinite planar capacitor in the X, Y plan with a gap equal to 2 and ending at $X = 0$ (see fig 2.2, showing equipotential lines and field lines):

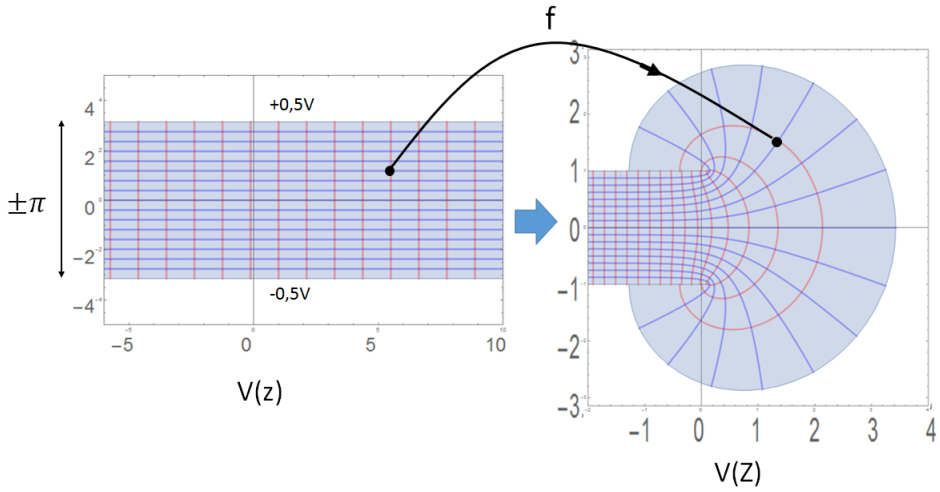

Figure 2.2: Semi-infinite capacitor obtained by conformal mapping, from an infinite capacitor. Horizontal (blue) lines are the equipotentials and vertical (red) lines are the field lines.

The potential at a point $Z = f(z)$ is exactly the same as the potential at the associated point z. In the case of opposite charged electrodes with $+0.5$V and -0.5V, the potential in the first system is well known as:

$$V(Z) = V(z) = \frac{Im(z)}{2\pi} = \frac{y(Z)}{2\pi} \tag{2.9}$$

If one wants to know the potential at any Z point, one needs to know the inverse mapping (function) of f. We will discuss this inverse function in a few paragraphs.

The Lambert function: application to the semi-infinite capacitor fringe field

As mentioned above, we need to inverse the conformal mapping if we want to get the potential in the final system. In z, the function

$$Z = \frac{1}{\pi}.[1 + z + e^z] \tag{2.10}$$

has the solution [21]:

$$z = \pi Z - 1 - W(e^{\pi Z - 1}) \tag{2.11}$$

where $W(z)$ is called the Lambert function.

The Lambert function has some usefull properties [22]:

$$W(x.e^x) = x \tag{2.12}$$

$$e^{W(x)} = \frac{x}{W(x)} \tag{2.13}$$

$$W'(x) = \frac{W(x)}{x \cdot (1 + W(x))} \tag{2.14}$$

From that, we can deduce the complex electrostatic field and potential:

$$\underline{V}(Z) = \pi Z - 1 - W\left[e^{\pi Z - 1}\right] \tag{2.15}$$

$$\underline{E}(Z) = \frac{1}{1 + W\left[e^{\pi Z - 1}\right]} \tag{2.16}$$

The following picture shows the transverse electric field (E_y) along the reference trajectory ($x = 0$) for the electric field given by formula (2.16):

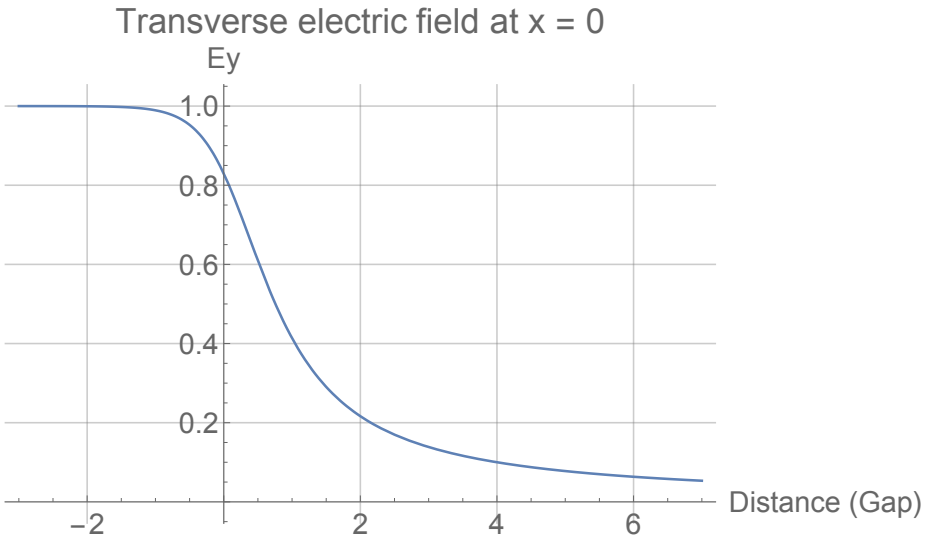

Figure 2.3: Normalized transverse electric field along the reference trajectory obtained by conformal mapping with one single transformation. The horizontal axis is given in Gap units.

We mentioned and explained in this section the different tools that are necessary to compute a more accurate model of fringe fields, including realistic electrodes and boundary conditions. The complete description and computation of this model is given in section 3.1 as well as the results and a comparison with finite elements calculations.

From parallel plates to a cylindrical deflector

The transition from a straight deflector (composed by 2 parallel plates) to a curved, or cylindrical deflector can be done again using conformal mapping.

The exponential function has the property to curve lines when it is question of conformal mapping.

As an example, the transformation:

$$f(z) = \rho_0 \cdot e^{i\left(\frac{G}{\rho_0}\right)\cdot z} \tag{2.17}$$

transforms a straight deflector similar to the one showed in fig (2.2) into a curved deflector of gap G[1] and radius ρ_0.

In the following, we will make all the computations for a straight deflector with a gap $G = 1$. The function (2.17) gives directly the field in a curved deflector. In this way, we can get universal and direct formulas for the field of a curved deflector, depending on the G/ρ_0 ratio.

[1]at first order. The second order relative error is proportional to $G/\rho \approx 10^{-5}$. This has no influence on the beam dynamics, only on the real position of the electrodes, as the field is correct.

2.2 Particles trajectories

This section gives an overview about the tools and methods we are using to describe the trajectories of the particles.

On the one hand, one needs to compute the trajectories inside the internal part of the deflector, of the form of a transfer matrix or 2nd order transfer functions.

On the other hand, we need to compute the trajectories inside the fringe fields of the deflector using the field computed in part 3.1.

2.2.1 Electrostatic Hamiltonian expression

The best correct way to compute the equations of motion in an electrostatic deflector is the use of the Hamilton equations.

We describe in this part the mandatory formulas to deduce the equations of motion. We give the Hamiltonian in curvilinear coordinates, where the independent coordinate is no longer the time but the position along the reference trajectory.

Fig (2.4) shows which coordinates system is used in the following:

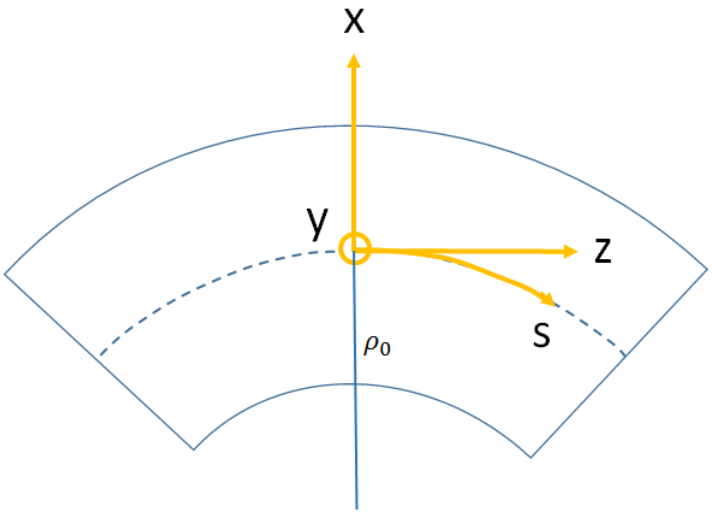

Figure 2.4: Drawing that shows the coordinate system. The longitudinal coordinate along the constant radius of the deflector is noted s , the transverse horizontal coordinate is x and the transverse vertical coordinate is y. We use a direct system (x, y, s).

In the following, the subscript 0 will stand for the reference particle and the design case.

Hamiltonian expression

We first suppose a positive charge q and V the electrostatic potential and give the Lagrangian:

$$\mathcal{L} = -mc^2\sqrt{1 - \frac{v^2}{c^2}} + qV \tag{2.18}$$

In cylindrical coordinates:

$$v^2 = \dot{x}^2 + \dot{y}^2 + \rho^2\dot{\theta}^2 \tag{2.19}$$

where $\rho = x + \rho_0$, and the dots the derivatives with respect to time.

We give the conjugate momenta:

$$p_x = \frac{\partial \mathcal{L}}{\partial \dot{x}} = m\gamma\dot{x} \tag{2.20}$$

$$p_y = \frac{\partial \mathcal{L}}{\partial \dot{y}} = m\gamma\dot{y} \tag{2.21}$$

Let be $v_s = \rho_0 \cdot \dot{\theta}$ the longitudinal velocity along the reference trajectory. We can now rewrite v as:

$$v^2 = \dot{x}^2 + \dot{y}^2 + \frac{\rho^2}{\rho_0^2} \cdot v_s^2 \tag{2.22}$$

and

$$\frac{\partial \mathcal{L}}{\partial v_s} = m\gamma\frac{\rho^2}{\rho_0^2} = p_s \tag{2.23}$$

The temporal Hamiltonian is given by [11]:

$$\mathcal{H} = \sqrt{p^2 \cdot c^2 + m^2 \cdot c^4} - qV \tag{2.24}$$

We know the expression of the total energy:

$$\gamma mc^2 = \mathcal{H} + qV \tag{2.25}$$

From 2.24 and 2.25 we can deduce:

$$p_s = \left(1 + \frac{x}{\rho}\right) \cdot \frac{1}{c} \cdot \sqrt{\gamma^2 \cdot m^2 \cdot c^4 - c^2(p_x^2 + p_y^2) - m^2 \cdot c^4} \tag{2.26}$$

If we divide (2.26) by the reference momentum p_0, we obtain the normalized momentum $\bar{p_s}$ with $\bar{p_x} = \frac{p_x}{p_0}$ and $\bar{p_y} = \frac{p_y}{p_0}$:

$$\bar{p_s} = \frac{p_s}{p_0} \tag{2.27}$$

The Hamiltonian we are concerned with is nothing else than the negative value of $\bar{p_s}$. This quantity is the Hamiltonian in the case where the curvilinear coordinate along the reference trajectory replace time in the classical Hamiltonian (see Alex Dragt [12] for a demonstration).

$$\mathcal{H} = -\bar{p_s} = -\left(1 + \frac{x}{\rho}\right) \cdot \sqrt{\frac{\gamma^2 - 1}{\gamma_0^2 \beta_0^2} - (\bar{p_x^2} + \bar{p_y^2})} \tag{2.28}$$

Expression of the Lorentz γ factor

Let E be the total energy of the (single charged) particle such as:

$$E = \gamma_0 mc^2 - q\mathcal{V} + \Delta E \tag{2.29}$$

where γ_0 is the Lorentz gamma factor of the reference particle, $\mathcal{V}$ the local electrostatic potential and $\Delta E = E - E_0$ the intrinsic difference in energy between the reference particle and the particle before entering the deflector or the fringe field with $E_0 = \gamma_0 mc^2$ (and not the reference kinetic energy). When entering the element, the particle loses an energy $q\mathcal{V}$. $-q\mathcal{V}$ takes a minus sign as E decreases when we get closer to the positive electrode.

We can express the gamma factor with $E = \gamma \cdot m \cdot c^2$ as:

$$\gamma = \gamma_0 \cdot \left(1 - \frac{q\mathcal{V}}{E_0} + \frac{\Delta E}{E_0}\right) \tag{2.30}$$

By using the relation $q \cdot \mathcal{V} = E_0 \cdot \beta_0^2 \cdot V$ we have the final γ expression:

$$\gamma = \gamma_0 \cdot \left(1 - \frac{\gamma_0^2 - 1}{\gamma_0^2} \cdot \left[V - \frac{\Delta P}{P_0}\right]\right) \tag{2.31}$$

V is the electrostatic potential function, given in part 3.1 (logarithm in the case of a cylindrical deflector, with $V = \ln(1 + x/\rho_0)$ or computed by conformal mapping in the case of fringe fields).

For many reasons, the use of $\frac{\Delta P}{P_0}$ instead $\frac{\Delta E}{E_0}$ is more convenient. This change can be done with the following formula:

$$\frac{\Delta P}{P_0} = \frac{\gamma_0^2}{\gamma_0^2 - 1} \cdot \frac{\Delta E}{E_0} \tag{2.32}$$

2.2.2 Variation of constants method

We now have an expression for the Hamiltonian according to the equations (2.27) and (2.31). The equations of motion cannot be found directly due to the complexity of the potential V especially.

We can split the Hamiltonian in an integrable part and a non integrable part. The non integrable part should be small and plays the role of a perturbation.

$$\mathcal{H} = \mathcal{H}_0 + \tilde{\mathcal{H}} \tag{2.33}$$

We can solve the integrable Hamiltonian using the Hamilton equations:

$$\dot{q} = \frac{\partial \mathcal{H}}{\partial p}; \quad \dot{p} = -\frac{\partial \mathcal{H}}{\partial q} \tag{2.34}$$

where q and p are the generalized coordinates.

The solutions for the integrable Hamiltonian $\mathcal{H}_0$ are of the form:

$$\begin{cases} q_0 = q_0[K_1, K_2, s] = K_1 \cdot \cos(\omega s) + K_2 \cdot \frac{\sin(\omega s)}{\omega} \\ p_0 = p_0[K_1, K_2, s] = -K_1 \cdot \omega \cdot \sin(\omega s) + K_2 \cdot \cos(\omega s) \end{cases} \tag{2.35}$$

where K_1 and K_2 are the integration constants.

We look for the solution of the total Hamiltonian $\mathcal{H}_0 + \tilde{\mathcal{H}}$ by writing:

$$\begin{cases} q_0 = q_0[K1(s), K2(s), s] = K_1(s) \cdot \cos(\omega s) + K_2(s) \cdot \frac{\sin(\omega s)}{\omega} \\ p_0 = p_0[K1(s), K2(s), s] = -K_1(s) \cdot \omega \cdot \sin(\omega s) + K_2(s) \cdot \cos(\omega s) \end{cases} \tag{2.36}$$

where

$$\frac{dK_1}{ds} = \frac{\partial \tilde{\mathcal{H}}}{\partial p}$$

$$\frac{dK_2}{ds} = -\frac{\partial \tilde{\mathcal{H}}}{\partial q}$$

This is the so called variation of constants (or also variation of parameters) method for ordinary differential equations.

We have:

$$\frac{dq}{ds} = \frac{\partial q}{\partial s} + \frac{\partial q}{\partial K_1} \cdot \frac{\partial K_1}{\partial s} + \frac{\partial q}{\partial K_2} \cdot \frac{\partial K_2}{\partial s} = \frac{\partial \mathcal{H}_0}{\partial p} + \frac{\partial \tilde{\mathcal{H}}}{\partial p}$$

$$\frac{dp}{ds} = \frac{\partial p}{\partial s} + \frac{\partial p}{\partial K_1} \cdot \frac{\partial K_1}{\partial s} + \frac{\partial p}{\partial K_2} \cdot \frac{\partial K_2}{\partial s} = \frac{\partial \mathcal{H}_0}{\partial q} + \frac{\partial \tilde{\mathcal{H}}}{\partial q}$$

If the perturbation $\mathcal{H}$ is equal to zero we have:

$$\frac{\partial q}{ds} = \frac{\partial H_0}{\partial p}$$

$$\frac{\partial p}{ds} = -\frac{\partial H_0}{\partial q}$$

So we restart from:

$$\frac{\partial q}{\partial K_1} \cdot \frac{\partial K_1}{\partial s} + \frac{\partial q}{\partial K_2} \cdot \frac{\partial K_2}{\partial s} = \frac{\partial \tilde{\mathcal{H}}}{\partial p}$$

$$\frac{\partial p}{\partial K_1} \cdot \frac{\partial K_1}{\partial s} + \frac{\partial p}{\partial K_2} \cdot \frac{\partial K_2}{\partial s} = -\frac{\partial \tilde{\mathcal{H}}}{\partial q}$$

Let D be the determinant

$$D = \begin{vmatrix} \frac{\partial q}{\partial K_1} & \frac{\partial q}{\partial K_2} \\ \frac{\partial p}{\partial K_1} & \frac{\partial p}{\partial K_2} \end{vmatrix}$$

So:

$$\begin{bmatrix} \frac{\partial K_1}{\partial s} \\ \frac{\partial K_2}{\partial s} \end{bmatrix} = \frac{1}{D} \cdot \begin{bmatrix} \frac{\partial p}{\partial K_2} & \frac{\partial q}{\partial K_2} \\ -\frac{\partial p}{\partial K_1} & -\frac{\partial q}{\partial K_1} \end{bmatrix} \cdot \begin{bmatrix} \frac{\partial \tilde{\mathcal{H}}}{\partial p} \\ \frac{\partial \tilde{\mathcal{H}}}{\partial q} \end{bmatrix}$$

Finally:

$$\begin{cases} \frac{dK_1}{ds} = \frac{1}{D} \cdot \frac{\partial \bar{\mathcal{H}}}{\partial p} \\ \frac{dK_2}{ds} = -\frac{1}{D} \cdot \frac{\partial \bar{\mathcal{H}}}{\partial q} \end{cases} \tag{2.37}$$

where $\bar{\mathcal{H}}$ is obtained by replacing in $\tilde{\mathcal{H}}$ the expressions of q and p by the ones of the non perturbed system.

2.3 Spin dynamics

Spinors formalism

When it comes to rotation matrices, spinors have the advantage to use only 4 coefficients instead of 9 for 3D rotations. This formalism also allows us to have an explicit expression of the angles and precession axis in the matrix and to inverse it more easily.

In spherical coordinates, on the unitary sphere, we can express:

$$\begin{cases} S_x = \cos(\theta)\sin(\phi) \\ S_y = \sin(\theta)\sin(\phi) \\ S_z = \cos(\phi) \end{cases} \tag{2.38}$$

To (x, y, z) we can associate a spinor (defined up to a phase A):

$$\vec{S} = \begin{cases} \cos(\frac{\phi}{2})\exp\left(-i\frac{\theta}{2} + iA\right) \\ \sin(\frac{\phi}{2})\exp\left(i\frac{\theta}{2} + iA\right) \end{cases} = \begin{cases} \Psi_1 \\ \Psi_2 \end{cases} \tag{2.39}$$

and its inverse mapping:

$$\begin{cases} S_x = 2\mathcal{R}(\Psi_1\bar{\Psi}_2) \\ S_y = -2\mathcal{I}(\Psi_1\bar{\Psi}_2) \\ S_z = |\Psi_1|^2 - |\Psi_2|^2 \end{cases} \tag{2.40}$$

Numerically, this spinor can be written in the form of a 2x2 chart: two components composed each by a real and an imaginary part.

A rotation with a θ angle is expressed as:

$$R(\theta) = \begin{bmatrix} \cos\left(\frac{\theta}{2}\right) - iu_z.\sin\left(\frac{\theta}{2}\right) & -(iu_x + u_y).\sin\left(\frac{\theta}{2}\right) \\ (-iu_x + u_y).\sin\left(\frac{\theta}{2}\right) & \cos\left(\frac{\theta}{2}\right) + iu_z.\sin\left(\frac{\theta}{2}\right) \end{bmatrix} \tag{2.41}$$

which is a rotation matrix where the θ rotation angle and the (u_x, u_y, u_z) unitary rotation axis appear explicitly. We can easily compare eq.(2.41) to the numerical rotation matrix to find the θ, u_x, u_y, u_z values if needed.

The matrix is always of the form:

$$R(\theta) = \begin{bmatrix} a & b \\ -\bar{b} & \bar{a} \end{bmatrix} \tag{2.42}$$

and is characterized by only two (complex) coefficients exclusively, which is extremely convenient as half of the coefficients have to be computed.

Whatever the evolution of the spin is, it can always be given by the rotation matrix from eq.(2.41). The main difficulty is to find this matrix.

Polarisation for a beam of particles (BMAD)

When it comes to represent a beam, i.e. several particles, one can still use the spinor formalism. The coordinates and operations remain the same. We only need to introduce the polarization of the beam P such as:

$$P = |\Psi_1|^2 + |\Psi_2|^2 \leq 1 \tag{2.43}$$

Equation (2.38) becomes:

$$\begin{cases} S_x = P \cdot \cos(\theta) sin(\phi) \\ S_y = P \cdot \sin(\theta) sin(\phi) \\ S_z = P \cdot \cos(\phi) \end{cases} \tag{2.44}$$

This is used by BMAD to represent the quantity of particles that have the polarisation given by the spinor. A beam perfectly polarised will have $P = 1$ and a beam totally unpolarized will have $P = 0$.

2.4 Mathematical tools developed

2.4.1 Differential equation solving

Spin and trajectories differential equation problematics

Locally, the spin evolution corresponds to a precession around the local unitary precession axis (u_x, u_y, u_z), with an angular velocity ω.

We can obtain these values directly from the T-BMT equation (eq 1.2 and 1.3):

$$\dot{S} = \frac{\omega}{2}. \begin{bmatrix} -i.u_z & -(iu_x + u_y) \\ (-iu_x + u_y) & iu_z \end{bmatrix} .S = \frac{\omega}{2}.A.S \tag{2.45}$$

where A is a matrix, S the spin vector and ω a function of time (or s in our case).

In the particular case where A is constant, the solution is:

$$S(L) = \exp\left(\frac{\phi(L)}{2}.A\right).S_0 \tag{2.46}$$

where

$$\phi(L) = \int_0^L \omega(t)dt \tag{2.47}$$

This is the case in the inner part of the deflector, with no fringe fields ($\vec{E} = [E_x, 0, 0]$) and when the momentum of the particle is fully longitudinal ($\vec{P} = [0, 0, P_z]$). At this moment, the precession axis remains constant ($\vec{u} = [0, u_y, 0]$) with a total angle of rotation ϕ.

In other cases – in practical all the cases – the axis of rotation varies with time, and the exponential is no longer a solution, because A does not commute with its primitive (from the mathematical point of view).

We will show later that the mathematical problem of the equations of motion remains the same as the equation to solve (in chapter 3.2.3) is also of the form:

$$\dot{X} = A(s) \cdot X \tag{2.48}$$

with a solution:

$$X = R \cdot X_0 \tag{2.49}$$

The solution of (2.48) can be expressed as:

$$R(L) = I + \int_0^L A(t)dt + \sum_{n=1}^{\infty} \int_0^L \left[A(t_n) \int_0^{t_n} \left[A(t_{n-1}) \cdots \int_0^{t_0} A(x)dx \right] dt_{n-1} \right] dt_n \tag{2.50}$$

where I is the identity matrix. This formula can not be used directly, as A should be small to have fast convergence. It needs to be used in a perturbative scheme.

This solution is based on a remark from Jean-Marie De Conto, and is linked to the Magnus expansion. See [13] for more details.

A perturbative solution both for spin and paraxial motion

In a general case, the equations (2.45) and (2.48) cannot be solved by using the simple exponential solution given by eq (2.46). Working with a perturbative method allows us to solve this equations up to an arbitrary order.

This paragraph gives a demonstration for the resolution of equation (2.45), but can be skipped by going directly to the solution given by equations (2.59) and (2.58) .

The equation

$$\dot{Y_0} = A_0.Y_0 \tag{2.51}$$

with A_0 constant gives from eq. (2.46):

$$Y_0 = \exp\left(\int_0^T A dt \right) .Y_{00} \tag{2.52}$$

where Y_{00} corresponds to the initial conditions $(\Psi_1, \Psi_2)|_0$.

Let us now consider the general equation:

$$\dot{Y} = AY \tag{2.53}$$

We can split the A matrix in two distinct parts, a constant axis part named A_0 and a non constant axis part named E (supposed small):

$$A = A_0 + E \tag{2.54}$$

We have also:

$$Y = Y_0(I + \epsilon).Y_{00} = Y_0\Delta.Y_{00} \tag{2.55}$$

where ϵ is small.

From eq (2.55) and eq (2.53), we can write:

$$\dot{Y} = AY = (\dot{Y_0}\Delta + Y_0\dot{\Delta}).Y_{00} \tag{2.56}$$

$$(Y_0\dot{\Delta}).Y_{00} = AY - (\dot{Y_0}\Delta).Y_{00} = [AY_0 - \dot{Y_0}]\Delta.Y_{00} = EY_0\Delta.Y_{00} \tag{2.57}$$

Finally:

$$\dot{\Delta} = Y_0^{-1}.E.Y_0.\Delta = U.\Delta \tag{2.58}$$

If the U matrix is small, the differential equation $\dot{\Delta} = U \cdot \Delta$ has the solution given by equation (2.50), and can be solved at any order with a fast convergence:

$$\Delta = I + \sum_1^\infty \int_0^{t_n} U(t_n)dt_n \int_0^{t_{n-1}} U(t_{n-1})dt_{n-1} ... \int_0^{t_0} U(t_0)dt_0$$

We have at the end the final solution:

$$Y = Y_0.\Delta.Y_{00} \tag{2.59}$$

2.4.2 Numerical resolution: integration by quadrature

In order to solve the previous equations with the solution (2.50), one needs to compute different integrals.

These integrals are particular integrals of the field and the equations of motion that needs to be computed only once, for a given position of the diaphragm.

These integrals will appear later in the manuscript and are of the form:

$$I_1 = \int_{-1}^{1} f(t) \cdot dt \tag{2.60}$$

$$I_2 = \int_{-1}^{1} \left[g(t) \cdot \int_{-1}^{t} f(x) \cdot dx \right] \cdot dt \tag{2.61}$$

$$I_3 = \int_{-1}^{1} dX \int_{-1}^{X} A(x) dx \int_{-1}^{x} dt \int_{-1}^{t} A(u) du \tag{2.62}$$

We can compute such integrals by using quadrature methods. We will in practice only need to compute the value of the field at specific points which represents a considerable gain of computation time.

The intervals of integration are obtained with a change of variable. These operations are quite fast as they are expressed as a sum of numerical values.

The quadrature method for the I_1 integral is well known and is given by:

$$I_1 = \int_{-1}^{1} f(t) \cdot dt \approx \sum_{j=1}^{Q} \lambda_j \cdot f_j \tag{2.63}$$

with

$$P_0 = 1, P_1 = 0$$

$$P_{n+1} = \frac{1}{n+1} \cdot [(2n+1) \cdot x \cdot P_n - n \cdot P_{n-1}]$$

the Legendre polynomials on [-1 ; + 1].

$$\lambda_i = \frac{2}{(1 - z_i^2) \cdot P_Q'^2}$$

are the associated Christoffel coefficients and $f_j = f(x_j)$ with x_j the zeros of P_Q.

We can extend method (2.63) to integral I_2 and show that we have:

$$I_2 = \int_{-1}^{1} \left[g(t) \cdot \int_{-1}^{t} f(x) \cdot dx \right] \cdot dt \approx \sum_{i,j=1}^{Q} \lambda_i \cdot g_i \cdot T_{ij} \cdot \lambda_j \cdot f_j \tag{2.64}$$

with

$$P_i(z_j) = P_{ij} \qquad P_Q(z_j) = 0$$

$$A^0_{ij} = P_{0i} \cdot [P_{0j} - P_{1j}]$$

$$A^k_{ij} = P_{ki} \cdot [P_{(k-1)j} - P_{(k+1)j}] \quad (k > 0)$$

$$T_{ij} = \frac{1}{2} \sum_{k=1}^{N} A^k_{ij}$$

which is exact for every polynomial function with a degree $\leq Q$.

By using the relation (see Jean-Marie De Conto [19]):

$$\int\int A = \int_{-1}^{1} dx \int_{-1}^{x} A(t)dt = \int_{-1}^{1} A(x) \cdot (1-x) \cdot dx$$

we can re-express the integral I_3 as:

$$I_3 = \int\int A \int\int A = \int_{-1}^{1} (1-x) \cdot A(x) \int_{-1}^{x} (x-t) \cdot A(t)dt \cdot dx \tag{2.65}$$

which can be computed with the method of eq.(2.64).

The list of the different integrals and the associated values are given in appendix A and A.2 respectively.

2.5 Méthodes et outils employés - Résumé en français

Ce chapitre présente les méthodes et outils qui ont été utilisés et/ou développés pendant ma thèse.

Ces outils concernent les calculs de champs, de trajectoires et de spin et sont utilisés à de multiples reprises dans le chapitre 3.

Outils de calcul de champs électriques

Il a été mentionné dans la partie 1.2.3 que les champs de fuite, par l'ajout de composantes de champs supplémentaires, peuvent s'avérer être une source de décohérence de spin. Plusieurs modèles de champs de fuite existent actuellement (comme le modèle hard-edge ou les fonctions de Enge).

Bien que ces modèles représentent une bonne approximation dans la majorité des cas, ils pourraient être insuffisants dans le cas des mesures d'EDM, nécessitant une extrême précision.

Cette partie fournit un rappel du formalisme des champs complexes et décrit la méthode employée utilisant les transformations conformes.

Une transformation conforme est une transformation du plan complexe qui conserve localement les angles (et en particulier les perpendiculaires).

Le potentiel $V(z)$ dans un système initial est exactement le même que le potentiel $V(Z)$ dans un système final où $Z = f(z)$ est l'image de z par la transformation conforme f.

Ainsi, si on connaît la transformation entre un système connu (à priori simple) et le système voulu (à priori plus complexe), il est possible de connaître le potentiel dans le deuxième système.

L'utilisation de transformations conformes a plusieurs avantages.

Ces transformations permettent de décrire analytiquement un système, permettant d'avoir des résultats précis et complets (connaissance des composantes multipolaires et longitudinales).

L'ajout de conditions aux limites se fait par l'ajout d'équipotentielles nulles dans le système initial.

De plus, nous avons montré qu'il est possible d'avoir des formules universelles pour un déflecteur cylindrique, dépendant uniquement du ratio Gap/Rayon du déflecteur.

Trajectoires des particules et formalisme des spineurs

Les trajectoires des particules doivent être calculées, à l'ordre 2, à la fois dans la partie centrale du déflecteur et dans les champs de fuite.

Cette partie donne l'expression de l'Hamiltonien en coordonnées curvilignes et définit les principales grandeurs propres au mouvement (quantité de mouvement, gamma de Lorentz...). La résolution des équations du mouvement se fait via la méthode

de la variation des constantes, qui est expliquée dans cette partie, et par la résolution d'une équation différentielle particulière, similaire à celle du spin, dont la résolution sera explicitée dans une prochaine partie.

Il est plus pratique de représenter les rotations de spin en utilisant le formalisme des spineurs. Ceci nous permet de n'utiliser que 4 coefficients (2 coefficients complexes) plutôt que 9 dans les matrices de rotation.

Je présente dans cette partie les bases du formalisme des spineurs et la forme générale de la matrice de rotation.

Outils mathématiques développés

La description de la dynamique des trajectoires et du spin se fait par la résolution d'une équation différentielle similaire aux deux cas.

Cette équation différentielle, de la forme :

$$\dot{X} = A(s) \cdot X$$

se résoud par perturbations avec pour solution :

$$X = R \cdot X_0$$

Et, où I est la matrice identité :

$$R = I + \sum_{1}^{\infty} \int_0^{t_n} A(t_n) dt_n \int_0^{t_{n-1}} A(t_{n-1}) dt_{n-1} ... \int_0^{t_0} A(t_0) dt_0$$

Cette partie décrit le processus général de résolution de l'équation différentielle par perturbation.

Méthodes de quadratures

La solution donnée précédemment nécessite le calcul de différentes intégrales. Ces intégrales sont des intégrales particulières du champ et des équations du mouvement, qui ne doivent être calculées qu'une seule fois pour une position donnée des conditions aux limites.

Ces intégrales ont une forme particulière et nous avons développé des méthodes d'intégration par quadrature spécifiques à ce problème. Seules quelques valeurs particulières du champ à des points spécifiques sont nécessaires, et cela représente un gain considérable de temps, comparé à la génération d'une carte de champs.

Ces intégrales sont calculées avec les méthodes décrites dans cette partie, et stockées dans un fichier séparé donné en annexe A.

Chapter 3

Results

Contents

This section presents the different analytic or semi-analytic results obtained in order to compute the spin dynamics in the whole deflector. Three different main results are presented:

- An analytic model for the electric fringe fields of the deflector. We use here conformal mapping, as presented in part (2.1.2). This model is composed by universal formulas allowing us to compute the exact fringe field of a curved or straight deflector given only two parameters (Gap G, radius ρ) for a given value of D (distance to the diaphragm).
- Two different models for trajectories in the deflector and trajectories in the fringe fields using the Hamiltonian presented in (2.2) and perturbation methods.
- Two models for spin dynamics in the internal part of the deflector and in the fringe fields. The model in the central part is using the T-BMT equation and the trajectories calculated before and is giving analytic transfer functions for spin at the second order of perturbation. The model for the fringe field is a semi-analytic model using the T-BMT equation, trajectories and a list of multiple different integrals of the electric field that can easily been extracted in BMAD. These integrals are long to compute but need to be calculated only once for a given value of D (distance between the electrodes and the diaphragm/vacuum pipe).

These models have the advantages of being (semi-)analytic and faster in terms of computation time. They also allow the user to understand deeper the spin dynamics as we can easily get the spin transfer matrices and there dependencies according to the phase-space parameters $(x, p_x, y, p_y, dz, \Delta P/P_0)$.

3.1 Results of field computations

Describing the electric field in the deflector in an accurate and complete way is a critical task to know the spin dynamics. The final results, whether they are simulation results or analytical formulas will rely on the field values.

The following section presents the analytical results and formulas we developed in order to compute in the most accurate and realistic way the electrostatic fringe field of a cylindrical deflector.

These are the result of a long research work and multiple improvements done by the LPSC during more than one year.

We give here the results in the natural order of the transformations (i.e. from the starting system to the final system). In practical, we only knew at the beginning the final system and tried to find an initial system and transformations to obtain it (see fig 3.1).

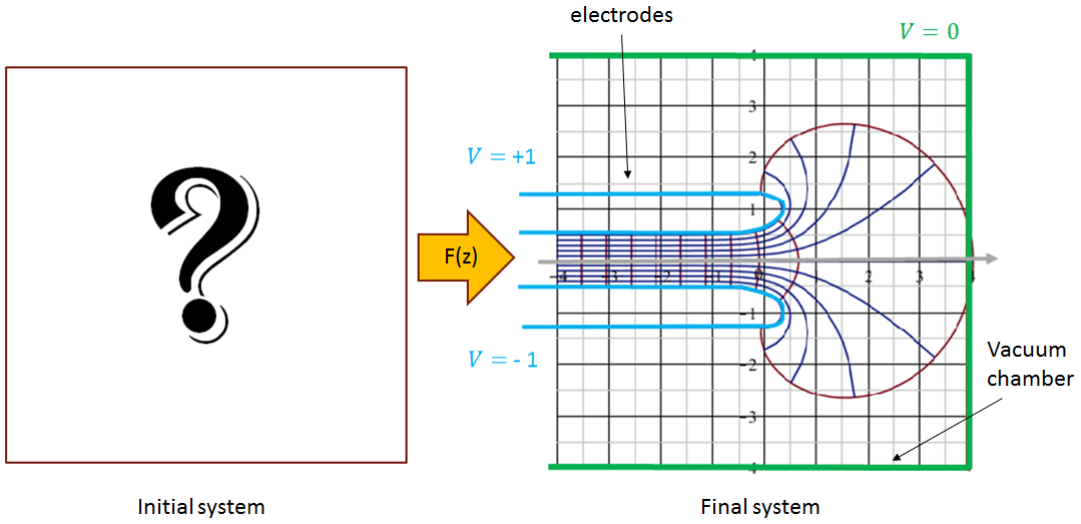

Figure 3.1: Known final and realistic system, including two parallel electrodes ($\pm V_0$), vacuum chamber and a diaphragm ($V = 0$). Field lines are not realistic and for illustration only.

Electric field of a cylindrical deflector

When we are inside the inner part of the deflector, we consider no fringe fields and a linear potential in the case of a straight deflector or a logarithmic potential for a curved (cylindrical) deflector.

The electrostatic potential in a cylindrical electrostatic deflector can be written:

$$V = -\mathcal{E}_0 \cdot \rho_0 \cdot ln(1 + \frac{x}{\rho_0}) \rightarrow \mathcal{E} = \frac{\mathcal{E}_0}{1 + \frac{x}{\rho}} \tag{3.1}$$

In the case of protons and deuterons, by using (3.1) and the electric rigidity, we have for the electrostatic field:

$$\mathcal{E} = -\frac{\gamma_0 \cdot m \cdot c^2 \cdot \beta_0^2}{q(1 + \frac{x}{\rho_0})} \tag{3.2}$$

The field given in eq (3.2) is the field used in parts (3.2.2) and (3.3.2) to compute the trajectories and spin dynamics in the inner part of the deflector.

The field in a straight deflector is given with the limit $\rho_0 \rightarrow \infty$.

3.1.1 Semi-infinite box potential

We start the transformations from an initial known system. We consider a semi-infinite box as shown in fig (3.2):

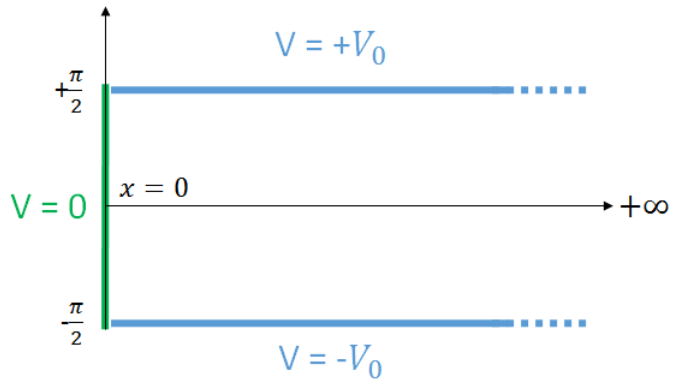

Figure 3.2: Semi-infinite box with two opposite potentials on electrodes and zero potential vertical end.

The potential in such a system is known. For $(x, y) \in [0, +\infty] \times [-\frac{\pi}{2}, \frac{\pi}{2}]$, we have:

$$V(x, y) = \frac{1}{\pi} \cdot V_0 \cdot \int_{-\infty}^{\infty} \frac{\sinh(2\omega y/\pi) \cdot \sin(2\omega x/x)}{\omega \cdot \sinh(\omega)} \cdot d\omega \tag{3.3}$$

This formula is complicated, and takes a long time to integrate, leading to difficulties with the final model.

This function takes for value $\pm V_0$ on the electrodes.

A detailed demonstration is given in appendix B and is summarized here:

We can find the corresponding complex potential:

$$\underline{\mathrm{V}}(z) = -\int \underline{\mathrm{E}}(z) \cdot dz = i \cdot \frac{V_0}{\pi} \cdot ln[th^2(z) - 1] + C = i \cdot \frac{V_0}{\pi} \cdot ln\left[\frac{1}{\cosh^2(z)}\right] + C \quad (3.4)$$

$$\underline{\mathrm{V}}(z) = -2 \cdot i \cdot \frac{V_0}{\pi} \cdot \ln[\cosh(z)] \quad (3.5)$$

And the associated electric field:

$$\underline{\mathrm{E}}(z) = i \cdot \frac{2}{\pi} \cdot V_0 \cdot \tanh[z] \quad (3.6)$$

We now have an analytic formula for the potential in a know system, with two opposite potentials and a boundary condition at $V = 0$.

We can prove (see Jean-Marie De Conto [14]) that eq (3.3) can be rewritten as:

$$V(x, y) = \frac{2}{\pi} \cdot V_0 \cdot \arctan[\tanh(x) \cdot \tan(y)] \quad (3.7)$$

3.1.2 Realistic profile for the electrodes

The double transformation T:

$$\left[-\frac{\pi}{2} \leq \Im(z) \leq \frac{\pi}{2}\right] \vdots T : z \to Z_1 = [1 + z + e^z] \to Z_2 = \frac{1}{\pi} \cdot [\alpha^* + Z_1 + e^{Z_1}] \quad (3.8)$$

transforms the infinite planar capacitor in a semi-infinite planar capacitor with curved electrodes:

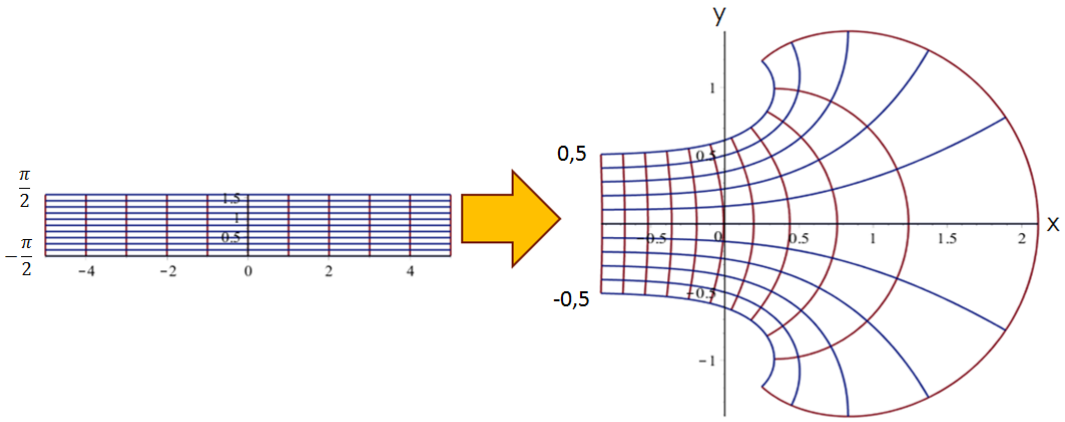

Figure 3.3: Double conformal transformation changing an infinite planar capacitor (with $z = x + i \cdot y$) into a semi-infinite planar capacitor (with $Z_2 = X_2 + i \cdot Y_2$).

This double transformation is actually the transformation (2.8) applied twice with a correction factor α^*. The α^* factor is a horizontal offset to place the exit of the deflector at the right position.

While the electrodes for the single transformation are going to infinity, inducing a non-vanishing field, the electrodes obtained with the double transformation are closed at the exit of the capacitor. In this sense, this model is a more realistic model than the previous one with a single transformation.

This model has been validated by comparison with this profile designed in Aachen within the JEDI collaboration (see fig (3.4)):
This model have been found independently from the design model and agreed almost perfectly with it.

We now have a realistic shape for the electrodes. However, the model is still not complete as we need to include boundary conditions.

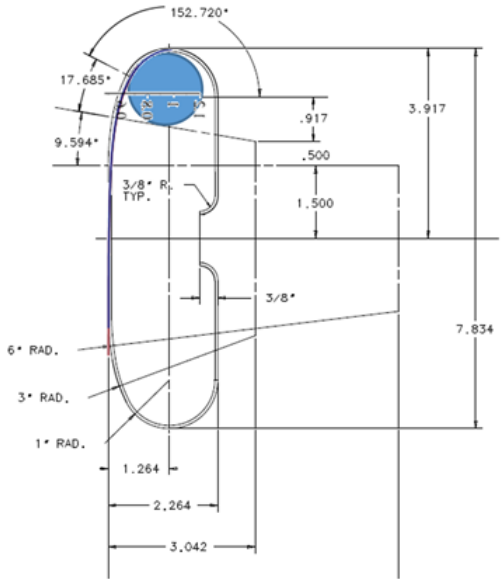

Figure 3.4: Comparison of the analytical model (the curved part of the analytical model is the blue circle) with the model of electrodes developed at Aachen within the JEDI collaboration. The shape of the electrodes are superposed with a really good agreement.

3.1.3 Boundary conditions

If we apply the reciprocal of transformation T given by eq.(3.8) to the final system, we obtain:

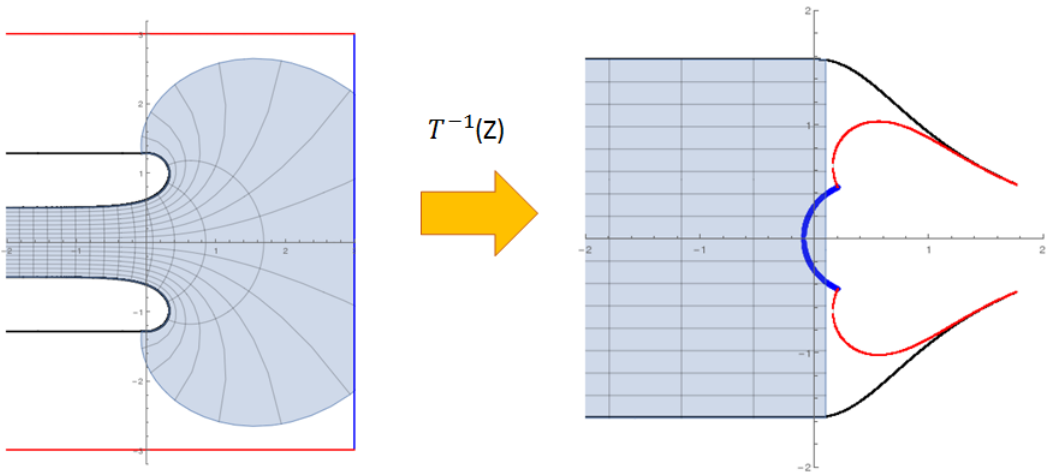

Figure 3.5: Inverse of the double transformation applied to the final system. The blue curve corresponds to the diaphragm, the red curves stand for the vacuum chamber and the black lines represent the electrodes.

The internal contours are the boundary conditions (blue and red lines) while the external black lines are the electrodes.

We can approximate the external envelope with a straight line of slope $\pi/5.5$ that crosses the axis $y = \pi/2$ in $x = 0.25$.

We now consider the Schwartz transformation:

$$g_1(z) = \int_0^z \frac{dt}{t^{\frac{35}{55}} \cdot (t^2-1)^{\frac{10}{55}}} = \frac{11}{4} \cdot e^{i \cdot \frac{2\pi}{11}} \cdot z^{\frac{4}{11}} \cdot H_{\frac{2}{11},\frac{2}{11},\frac{13}{11}}(z^2) \tag{3.9}$$

This transformation transforms the real straight line into a contour close to the researched one.

We can obtain the straight line from the semi-infinite box by using the transformation:

$$Z = i \cdot e^z \tag{3.10}$$

At the end, we consider:

$$G(Z) = \beta^* - \frac{11}{4} \cdot e^{\frac{4z}{11}} \cdot H_{\frac{2}{11},\frac{2}{11},\frac{13}{11}}(-e^{2z}) \tag{3.11}$$

That transforms the semi-infinite box in a system close to the one obtained in fig(3.5):

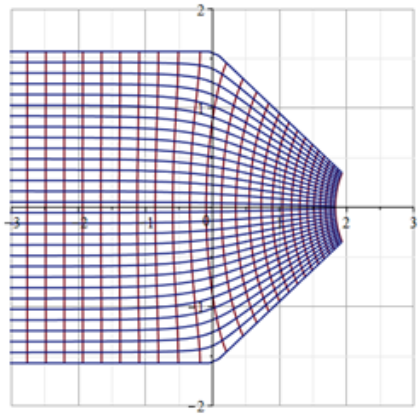

Figure 3.6: Profile obtained from the semi-infinite box after applying the eq(3.11) transformation. The boundary conditions are approximated by a circle.

The boundary conditions are approximated here by a unique circle which still remains a really good approximation as we show in part 3.1.4 with the finite elements validation of the model.

Summary of the different transformations

From $z \in [0, +\infty] \times \left[-\frac{\pi}{2}, \frac{\pi}{2}\right]$ we start from a semi-infinite box whose potential is:

$$\underline{V}(z) = -2 \cdot i \cdot \frac{V_0}{\pi} \cdot \ln[\cosh(z)] \tag{3.12}$$

To this system we apply the Schwartz-like transformation:

$$z \to z_1 = \beta^* - \frac{11}{4} \cdot e^{\frac{4z}{11}} \cdot H_{\frac{2}{11},\frac{2}{11},\frac{13}{11}}(-e^{2z}) \tag{3.13}$$

Finally, the shape of the electrodes is given by the double transformation:

$$z_1 \to z_2 = [1 + z_1 + e^{z_1}] \to Z = \frac{1}{\pi} \cdot [\alpha^* + z_2 + e^{z_2}] \tag{3.14}$$

with $\alpha^* = 0.3303665906$ and $\beta^* = 2.6899133724$.

By applying all the transformation, we obtain at the end a profile close to the wanted one:

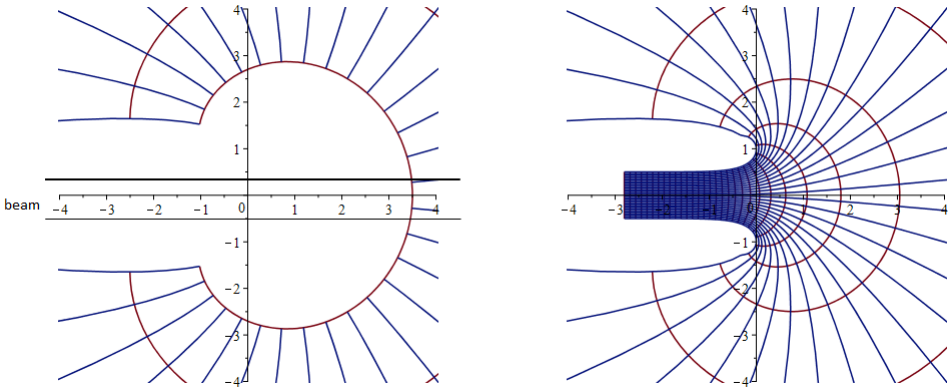

Figure 3.7: Left: Representation of the zero equipotential for a diaphragm and vacuum chamber chosen to be at a 3.5G distance from the exit of the deflector. Right: Shape of the electrodes and different boundary conditions configurations (the red lines stand for the different positions of the diaphragm or vacuum chamber and the blue lines are the electrodes). This figure does not include the formula for the potential of the semi-infinite box.

At the end, we obtain a final system close to the real system (fig 3.1). We do not have a square structure as the Joukowski transformation is not perfect. We will discuss in the next part these results and there accuracy.

Inverse mapping and derivatives

In order to get the potential in the starting system, one needs to inverse the mapping.

As we showed in eq(2.11), we can find for the inverse transformations:

$$z_2 = \pi \cdot Z - \alpha^* - W\left[e^{\pi \cdot Z - \alpha^*}\right] \tag{3.15}$$

$$z_1 = z_2 - 1 - W\left[e^{z_2 - 1}\right] \tag{3.16}$$

$$z = G^{-1}(z_1) \tag{3.17}$$

where G^{-1} is computed numerically (Mapple).

One needs to be careful with the (3.15) and (3.16) inverse equations as the Lambert W function is multi-valuated, and the right branch has to be selected when using computing software (such as Mathematica or Mapple).

All the computations are done numerically by a short code (≈ 50 lines, Jean-Marie De Conto: Mapple), for a straight deflector with a gap $G = 1$, and for a boundary condition $V = 0$ at n Gaps from the deflector.

We can compute the electric field by doing the product of the derivatives:

$$\underline{\mathrm{E}}(Z) = \frac{d\underline{\mathrm{V}}(z)}{dZ} = \frac{dV}{dz} \cdot \frac{dz}{dz_1} \cdot \frac{dz_1}{dz_2} \cdot \frac{dz_2}{dZ} \tag{3.18}$$

where equation (2.16) give us:

$$\frac{dz_2}{dZ} = \frac{\pi}{1 + W\left[\exp(\pi Z - 1)\right]} \tag{3.19}$$

and

$$\frac{dz_1}{dz_2} = \frac{1}{1 + W\left[\exp(Z_2 - 1)\right]} \tag{3.20}$$

The derivation of V is given by eq.(3.6):

$$\frac{dV}{dz} = i \cdot \frac{2}{\pi} \cdot V_0 \cdot \tanh[z] \tag{3.21}$$

3.1.4 Electrostatic fringe field components and field validation

A universal formula for the fringe fields

By using the previous formulas, one can compute the dipolar, quadrupolar, hexapolar (etc) components of the field along the reference trajectory.

The following picture shows the dipolar (called k_0) and hexapolar (called k_2) components of the field along the reference trajectory (for $x = y = 0$), for a **straight deflector**:

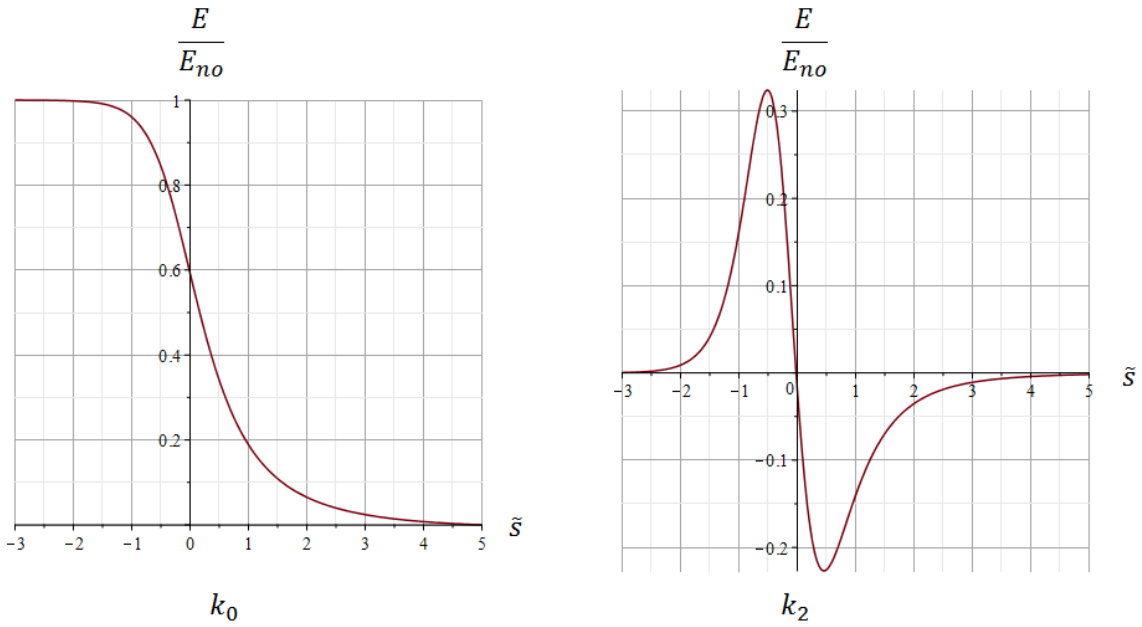

Figure 3.8: Dipolar (left) and sextupolar (right) components of the normalized electrostatic fringe field along the reference trajectory. The longitudinal coordinate is given in gap unit where $\tilde{s} = s/G$.

In the case of a straight deflector the quadrupolar component of the field is equal to zero ($k_1 = 0$). We pass from the straight to the cylindrical deflector by using the exponential (2.17) formula.

The potential or field in any cylindrical deflector can be expressed as a function of the potential in the straight deflector.

At order 2, the transverse electric field in a **cylindrical deflector** fringe field is:

$$E_x(s) = \frac{E_{no}}{\rho_0} \cdot \left[K_0 - K_0 \cdot \frac{x}{\rho_0} + K_2 \cdot \left(\frac{x}{\rho_0} \right)^2 \right] = \frac{E_{no}}{\rho_0} \cdot \mathcal{E}_x \tag{3.22}$$

where $E_{no} = \frac{mc^2 \gamma_0 \beta_0^2}{q}$ is the norm of the electric field, $K_0(s) = k_0\left(\frac{s}{G}\right)$ the dipolar component of the field.

The quadrupolar component of the field is the opposite of the dipolar one: $K_1(s) = -K_0(s)$.

$K_2(s)$ is the hexapolar component and is expressed as:

$$K_2(s) = k_0\left(\frac{s}{G}\right) - k_2\left(\frac{s}{G}\right) \cdot \left(\frac{\rho_0}{G}\right)^2 \tag{3.23}$$

The longitudinal field, coming from $\Delta V = 0$, is given by:

$$E_s(s) = \frac{E_{no}}{G} \cdot \dot{k}_0\left(\frac{s}{G}\right) \cdot \left[\frac{x}{\rho_0} - \frac{1}{2} \cdot \left(\frac{x}{\rho_0} \right)^2 \right] = \frac{E_{no}}{\rho_0 G} \cdot \mathcal{E}_s \tag{3.24}$$

where $\dot{k}_0$ is the longitudinal field in the straight deflector and is the derivative along the normalized variable $\tilde{s} = s/G$. These results come directly from the exponential transform and the $\Delta V = 0$ condition (for the longitudinal part).

Equations (3.22) and (3.24) are universal formulas depending only of the Gap/Radius ratio for a given configuration of the boundary conditions. We define for the following the factor α such that:

$$\alpha = \frac{G}{\rho} \tag{3.25}$$

In the studied case (see chapter 4), this factor is equal to:

$$\alpha \approx \frac{0.03\text{m}}{30\text{m}} \approx \frac{1}{1000}$$

Hence, the electrostatic fringe field can be given in any configuration of deflector (straight or cylindrical, with different radii and gaps), by using only two functions: k_0 and k_2, for different α values.

Verification of the model

This model has been validated with finite elements computations, using the ANSYS software.

In order to model a deflector with realistic values, I created a simplified model during my master internship by solving the Poisson equation without charge ($\Delta V = 0$) in a periodic system.

We agreed on the following dimensions:

- The vacuum chamber must be at a minimum distance of 1.5*Gap of the electrodes.
- The height of the electrodes should be at least 4*Gap.

The shape of the electrode was done with CATIA using the double transformation of eq.(3.8).

An analysis with the finite elements software ANSYS (see fig. 3.9) showed a really good accuracy for a squared shape of the boundary conditions (the vacuum chamber and diaphragm should be at the same distance of the electrodes).

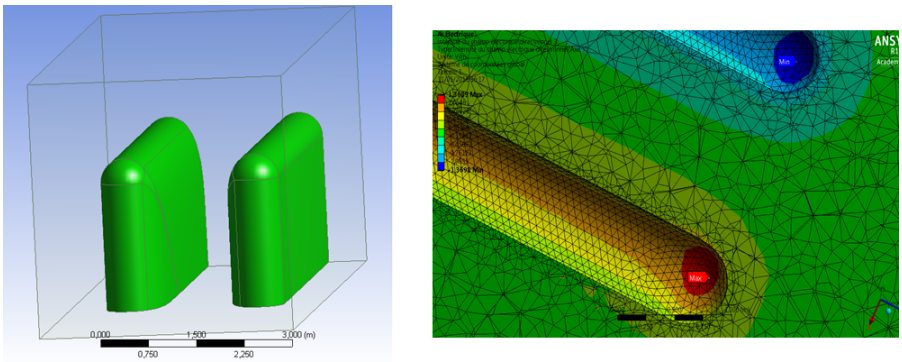

Figure 3.9: Left: Shape of the electrodes used in the ANSYS simulation. Right: Meshing and peak field with finite elements computation.

Figure 3.10 show a comparison between the analytic field and the numerical field.

We see an agreement up to a relative difference of 10^{-5} on the entire range of field values, even for small field values. Considering the used meshing and ANSYS parameters, we evaluated the accuracy of the software to be around $\approx 10^{-5}$.

Using finite elements to compute the electric field can give good values of field, but is also quite limited to give more information like multipolar components of the field.

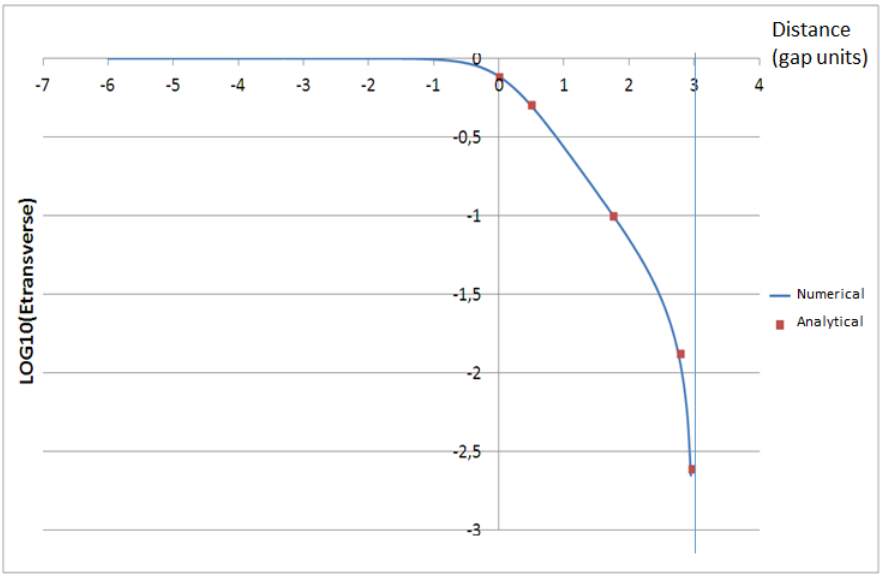

Figure 3.10: Comparison between the analytic field profile (red dots) and the numerical profile (blue curve) of the fringe field along the reference trajectory.

3.2 Computation of the particles trajectories

3.2.1 Use of normalized coordinates

We define in this part the coordinates and values that will be used in the following.

We will use the space coordinates expressed in gap units:

$$\tilde{x} = \frac{x}{G} \quad ; \quad \tilde{y} = \frac{y}{G} \quad ; \quad \tilde{s} = \frac{s}{G} \tag{3.26}$$

as well as the normalized momenta:

$$\bar{p}_x = \frac{p_x}{p_0} \quad ; \quad \bar{p}_y = \frac{p_y}{p_0} \quad ; \quad \bar{p}_s = \frac{p_s}{p_0} \tag{3.27}$$

where p_0 is the reference momentum.

These quantities are linked by the following relations, according to the Hamiltonian presented in part 2.2.1:

$$x' = \frac{\partial \mathcal{H}}{\partial \bar{p}_x} = -\left(1 + \frac{x}{\rho_0}\right) \cdot \frac{\bar{p}_x}{\sqrt{\frac{\gamma^2-1}{\gamma_0^2-1} - (\bar{p}_x^2 + \bar{p}_y^2)}} \tag{3.28}$$

$$y' = \frac{\partial \mathcal{H}}{\partial \bar{p}_y} = -\left(1 + \frac{x}{\rho_0}\right) \cdot \frac{\bar{p}_y}{\sqrt{\frac{\gamma^2-1}{\gamma_0^2-1} - (\bar{p}_x^2 + \bar{p}_y^2)}} \tag{3.29}$$

If we develop these values at first order, we have:

$$x' \approx \bar{p}_x \cdot \left[1 - \delta + \frac{x}{\rho_0} \cdot (1 + K_0)\right] \tag{3.30}$$

$$y' \approx \bar{p}_y \cdot \left[1 - \delta + \frac{x}{\rho_0} \cdot (1 + K_0)\right] \tag{3.31}$$

where $\delta = \frac{\Delta p}{p_0}$.

We recall the expression of $\bar{p}_s$:

$$\bar{p_s} = \frac{p_s}{p_0} = \left(1 + \frac{x}{\rho}\right) \cdot \sqrt{\frac{\gamma^2 - 1}{\gamma_0^2 \beta_0^2} - (\bar{p_x^2} + \bar{p_y^2})}$$

which is, at first order:

$$\bar{p_s} \approx 1 - \frac{x}{\rho_0} \cdot (K_0 - 1) + \delta \tag{3.32}$$

We now have the tools to compute the trajectories of the particles both in the inner part of the deflector, and in the fringe fields, as a function of the field k_0 and k_2 computed for the straight deflector.

3.2.2 Trajectories in the internal part of the deflector

3.2.2.1 First order trajectories

This short section presents the first order transfer matrix for the inner part of the deflector. The Hamilton equations give us the paraxial equation of motion:

$$x'' + \frac{\gamma_0^2 + 1}{\gamma_0^2} \cdot x = \frac{\gamma_0^2 + 1}{\gamma_0^2} \cdot \frac{1}{\rho} \cdot \frac{\Delta P}{P_0} \tag{3.33}$$

Let be:

$$k^2 = \frac{1}{\rho^2} \tag{3.34}$$

Equation 3.33 becomes:

$$x'' + k^2 \cdot x = k^2 \cdot \rho \cdot \frac{\Delta P}{P_0} \tag{3.35}$$

The transfer matrix in the horizontal plan is then:

$$M = \begin{bmatrix} C & S \\ C' & S' \end{bmatrix} = \begin{bmatrix} \cos(k \cdot L) & \frac{\sin(k \cdot L)}{k} \\ -k \cdot \sin(k \cdot L) & \cos(k \cdot L) \end{bmatrix} \tag{3.36}$$

The dispersion is given by:

$$\eta = k^2 \cdot \rho \cdot \left[S \int C - S \int S\right] = \rho \cdot (1 - \cos(kL)) \tag{3.37}$$

$$\eta' = \rho \cdot k \cdot \sin(kL) \tag{3.38}$$

We define the radius of curvature as a function of the field $\mathcal{E}$:

$$\mathcal{E} = \frac{V_0 \cdot \gamma \cdot \beta^2}{\rho} = \frac{\mathcal{E}_0}{1 + \frac{x}{\rho_0}} \rightarrow \frac{1}{\rho} = \frac{\gamma_0 \cdot \beta_0^2}{\gamma \cdot \beta^2} \cdot \frac{1}{\rho_0 \cdot \left(1 + \frac{x}{\rho}\right)} \tag{3.39}$$

Let σ be the curvilinear abscissa along the reference trajectory, at nominal radius and velocity. s is the abscissa at radius $\rho = \rho_0 + x$.

$$ds = v \cdot dt = \frac{v}{v_0} \dot{d\sigma} \tag{3.40}$$

The difference of trajectory, back to the central trajectory is:

$$ds = \left[\frac{\beta(x)}{\beta_0 \cdot \left(1 + \frac{x}{\rho_0}\right)} - 1 \right] \cdot d\sigma = \left[\frac{v}{v_0 \cdot \left(1 + \frac{x}{\rho_0}\right)} - 1 \right] \cdot d\sigma \tag{3.41}$$

We have

$$x = x_0 \cdot \cos(k\sigma) + x_0' \cdot \frac{\sin(k\sigma)}{k} + \eta \cdot \frac{\Delta P}{P_0} \tag{3.42}$$

We obtain the terms M_{16} and M_{26} by developping ds along x at order 1, then replacing x by $cos(k\sigma)$ or $sin(k\sigma)/k$ respectively, then integrating the result from zero to L.

We obtain the term M_{56} by developping ds along $\frac{\Delta P}{P_0}$ at order 1, then replacing x by $\eta \cdot \frac{\Delta P}{P_0}$, then integrating the result from zero to L.

Finally we get:

$$M_{51} = \frac{\gamma_0^2 + 1}{\gamma_0^2} \cdot \frac{\sin(kL)}{k \cdot \rho_0} \tag{3.43}$$

$$M_{52} = \frac{\gamma_0^2 + 1}{\gamma_0^2} \cdot \frac{1 - \cos(kL)}{k^2 \cdot \rho_0} \tag{3.44}$$

$$M_{56} = \frac{\gamma_0^2 + 1}{\gamma_0^2} \cdot \frac{kL - \sin(kL)}{k} \tag{3.45}$$

By using this matrix, we can obtain, in a very fast and easy way, the value of the phase-space coordinates vector at the exit of the deflector such that $X_{exit} = M \cdot X_{start}$.

The M matrix is:

$$M = \begin{bmatrix} \cos(k \cdot L) & \frac{\sin(k \cdot L)}{k} & 0 & 0 & 0 & \rho_0 \cdot (1 - \cos(k \cdot L)) \\ -k \cdot \sin(k \cdot L) & \cos(k \cdot L) & 0 & 0 & 0 & k \cdot \rho_0 \cdot \sin(k \cdot L) \\ 0 & 0 & 1 & L & 0 & 0 \\ 0 & 0 & 0 & 1 & 0 & 0 \\ k \cdot \rho_0 \cdot \sin(k \cdot L) & \rho_0 \cdot [1 - \cos(k \cdot L)] & 0 & 0 & 1 & 2 \cdot k^2 \cdot \rho_0^2 \cdot \left(L - \frac{\sin(k \cdot L)}{k}\right) \\ 0 & 0 & 0 & 0 & 0 & 1 \end{bmatrix} \tag{3.46}$$

where $k^2 = \frac{\gamma_0^2 + 1}{\gamma_0^2 \cdot \rho_0^2}$ and L is the length of the deflector.

This method is a first order tracking method and should not be used for precise particles tracking. However, it is useful to use it in a first approach or to study global effects. One can for example compute the 1-turn transfer matrix of the whole machine using this formula.

3.2.2.2 Second order trajectories

The second order transfer functions are obtained from the Hamiltonian presented in part 2.2.1 and by using the variation of constants methods presented in part 2.2.2.

At first order, the equations of motion are:

$$x = x_0 \cdot \cos(ks) + \frac{p_0}{k} \cdot \sin(ks) + \delta \cdot \rho_0 \cdot (1 - \cos(ks)) \tag{3.47}$$

$$p_x = -x_0 \cdot k \cdot \sin(ks) + p_0 \cdot \cos(ks) + \delta \cdot \rho_0 \cdot k \cdot \sin(ks) \tag{3.48}$$

At second order, we have:

$$x = K_1(s) \cdot \cos(ks) + \frac{K_2(s)}{k} \cdot \sin(ks) + \delta \cdot \rho_0 \cdot (1 - \cos(ks)) \tag{3.49}$$

$$p_x = -K_1(s) \cdot k \cdot \sin(ks) + K_2(s) \cdot \cos(ks) + \delta \cdot \rho_0 \cdot k \cdot \sin(ks) \tag{3.50}$$

where $K_1(s)$ and $K_2(s)$ are the functions determined with eq (2.36).

The analytical calculations of the equation of motion are done with computation software (Maple and Mathematica in our case).

Trajectory length

We can express the difference in the length of the trajectory of the particle in the deflector compared to the reference particle as:

$$d\Delta L = ds - ds_0 = \frac{v_s - v_0}{v_0} \dot{ds}_0 \tag{3.51}$$

$$\frac{d\Delta L}{ds_0} = \frac{\gamma}{\gamma_0} \cdot \frac{\rho_0^2}{\rho^2} \cdot \bar{p}_s - 1 = \frac{\gamma}{\gamma_0} \cdot \frac{\rho_0^2}{\rho^2} \cdot \mathcal{H} - 1 \tag{3.52}$$

where $\mathcal{H}$ is the spatial hamiltonian and $\rho = \rho_0 + x$.

Finally:

$$\Delta L = \int_0^L \left(\frac{\gamma}{\gamma_0} \cdot \frac{\rho_0^2}{\rho^2} \cdot \mathcal{H} - 1 \right) \cdot ds_0 \tag{3.53}$$

For the second order we have:

$$\begin{aligned} \frac{d\Delta L}{ds_0} = &- \frac{(\gamma_0^2 + 1)}{\gamma_0^2 \cdot \rho_0} \cdot x + \frac{1}{\gamma_0^2} \cdot \delta + \frac{\gamma_0^4 + 1}{\gamma_0^4 \cdot \rho_0^2} \cdot x^2 - \frac{1}{2} \cdot p_x^2 \\ &+ \frac{2(\gamma_0^2 - 1)}{\gamma_0^4 \cdot \rho_0} \cdot x\delta - \frac{(3\gamma_0^2 - 2) \cdot (\gamma_0^2 - 1)^2}{2 \cdot (\gamma 0^2 - 1)^2 \cdot \gamma_0^4)} \cdot \delta^2 \end{aligned} \tag{3.54}$$

where δ is the normalised difference of momentum with respect to the reference particle ($\frac{\Delta P}{P_0}$) at the entrance of the deflector. Its evolution in the deflector is directly included in the equations.

The equation (3.54) has to be integrated, after inserting the second order transfer functions.

Remark: Note that the relative energy $\Delta E/E_0$ is the same at the entrance and the exit of the deflector, so we have:

$$\left. \frac{\Delta E}{E_0} \right|_{exit} = \left. \frac{\Delta E}{E_0} \right|_0 \tag{3.55}$$

3.2.3 Perturbation method for trajectories in the fringe field

The equation of motion in the fringe field (as a function of the curvilinear coordinate s) can be obtained from the Hamilton equations, with respect to the reference circle:

$$x'' + \frac{(k_0 + k_0^2 - 1) \cdot \gamma_0 + k_0}{\gamma_0^2} \cdot \frac{x}{\rho_0^2} = \frac{1}{\rho_0} \cdot (1 - k_0) + \frac{\gamma_0^2 + 1}{\gamma_0^2} \cdot \frac{k_0}{\rho_0} \cdot \delta \tag{3.56}$$

where x is the transverse position with respect to the reference circle. The reference particle does not belong to the reference circle anymore. We compute its trajectory in a separate paragraph.

We can rewrite this equation as a function of $\tilde{s} = s/G$ and x in gap units:

$$\ddot{\tilde{x}} + \frac{(k_0 + k_0^2 - 1) \cdot \gamma_0 + k_0}{\gamma_0^2} \cdot \left(\frac{G}{\rho_0}\right)^2 \cdot \tilde{x} = \frac{G}{\rho_0} \cdot \left[1 - k_0 \cdot \left(1 + \frac{\gamma_0^2 + 1}{\gamma_0^2} \cdot \delta\right)\right] \tag{3.57}$$

or also:

$$\ddot{\tilde{x}} + \omega \cdot \alpha^2 \cdot \tilde{x} = \alpha \cdot \phi \tag{3.58}$$

where the dot is the derivative with respect to $\tilde{s}$.

By using the resolution method presented before in chapter (2.4.1), we deduce the transverse motion functions, that are the cos-like and sin-like usual functions:

$$C = 1 - \left(\frac{G}{\rho}\right)^2 \cdot \int\int \omega + \left(\frac{G}{\rho}\right)^4 \cdot \int\int \omega \int\int \omega \tag{3.59}$$

$$S = \tilde{s} - \left(\frac{G}{\rho}\right)^2 \cdot \int\int \omega\tilde{s} + \left(\frac{G}{\rho}\right)^4 \cdot \int\int \omega \int\int \omega\tilde{s} \tag{3.60}$$

$$C' = - \left(\frac{G}{\rho}\right)^2 \cdot \int \omega + \left(\frac{G}{\rho}\right)^4 \cdot \int \omega \int\int \omega \tag{3.61}$$

$$S' = 1 - \left(\frac{G}{\rho}\right)^2 \cdot \int \omega\tilde{s} + \left(\frac{G}{\rho}\right)^4 \cdot \int \omega \int\int \omega\tilde{s} \tag{3.62}$$

where the boundaries of the integrals have been removed to simplify reading.
The particular solution, corresponding to the reference particle's trajectory is:

$$\eta = C \int S\phi - S \int C\phi \tag{3.63}$$

and the transverse position with respect to the reference particle is $x - \eta$.
Finally, at order 3 in $\alpha = G/\rho$:

$$\eta = \frac{G}{\rho} \cdot [I_1 - \tilde{s} \cdot I_3] - \left(\frac{G}{\rho}\right)^3 \cdot [A_1 \cdot I_1 + I_2 - A_2 \cdot I_3 - \tilde{s} \cdot I_4] \tag{3.64}$$

where $I_1, I_3, A_1, A_2...$ are integrals of the field given in appendix (A). All these integrals are computed by quadrature using the methods presented in chapter (2.4.2).

3.3 Spin dynamics in a cylindrical deflector: universal formulas

We now have an analytical and universal description of the electric field in a cylindrical deflector. We know the trajectories transfer functions in the deflector and in the fringe fields, as functions of integrals of the field that have been calculated once and for all, and stored in a proper file.

This part shows how we compute the spin dynamics of the particles in the inner part and in the fringe fields of the deflector.

The solution for the fringe field is again, expressed as a function of the different integrals.

3.3.1 Equation of motion

In the particular case of a purely electrostatic deflector and no EDM, the Thomas-BMT equation gives for the omega vector $\vec{\Omega}$:

$$\vec{\Omega} = \frac{q}{mc^2}\left(G - \frac{1}{\gamma^2 - 1}\right)\vec{v} \times \vec{E} \tag{3.65}$$

where, as a reminder:

$$\frac{d\vec{S}}{dt} = \vec{\Omega} \times \vec{S}$$

This expression can be rewritten in longitudinal coordinates as:

$$\begin{aligned}\vec{\Omega_s} = &\left[1 - \frac{(\bar{p}_x^2 + \bar{p}_y^2)}{2} \cdot \left(\frac{\beta_0\gamma_0}{\beta\gamma}\right)^2\right] \cdot \left(1 + \frac{x}{\rho_0}\right) \cdot \frac{\beta_0^3\gamma_0^2}{\beta\gamma\rho_0} \\ &\cdot \left(G_m - \frac{1}{\gamma^2 - 1}\right) \cdot \begin{bmatrix} -\bar{p}_y \cdot \mathcal{E}_s \\ -\tilde{p}_s \cdot \mathcal{E}_x + \bar{p}_x \cdot \mathcal{E}_s \\ \bar{p}_y \cdot \mathcal{E}_x \end{bmatrix}\end{aligned} \tag{3.66}$$

where $\mathcal{E}_x$ and $\mathcal{E}_s$ are the fields defined in eq. (3.22) and eq. (3.24).

Equation (3.66) can be rewritten into:

$$\Omega = F(s) \cdot \begin{bmatrix} -\bar{p}_y \cdot \mathcal{E}_s \\ -\tilde{p}_s \cdot \mathcal{E}_x + \bar{p}_x \cdot \mathcal{E}_s \\ \bar{p}_y \cdot \mathcal{E}_x \end{bmatrix} \tag{3.67}$$

where $F(s)$ can be interpreted as the angular velocity and the vector as the axis of rotation. For symmetry reasons, $\vec{E_y}$ is assumed to be zero. It is not the case for a tilted or non perfect deflector.

We remind the general formula for the transverse electrostatic field:

$$E_x(s) = \frac{E_{no}}{\rho_0} \cdot \left[K_0 - K_0 \cdot \frac{x}{\rho_0} + K_2 \cdot \left(\frac{x}{\rho_0} \right)^2 \right] = \frac{E_{no}}{\rho_0} \cdot \mathcal{E}_x$$

In the case of the inner part of the deflector, with no fringe fields, the angular precession velocity given in eq. (3.66) can be expressed as:

$$\Omega = F_2(s) \cdot \begin{bmatrix} 0 \\ -\tilde{p}_s \\ \bar{p}_y \end{bmatrix} \tag{3.68}$$

where the only component of the field (E_x) is contained in the $F_2(s)$ function. We can deduce:

$$S' = \Omega \times S = F(s) \begin{pmatrix} (\tilde{p}_s \cdot \mathcal{E}_x - \bar{p}_x \cdot \mathcal{E}_s) \cdot S_z + (\bar{p}_y \cdot \mathcal{E}_x) \cdot S_y \\ -(\bar{p}_y \cdot \mathcal{E}_x) \cdot S_x - (\bar{p}_y \cdot \mathcal{E}_s) \cdot S_z \\ (\bar{p}_y \cdot \mathcal{E}_s) \cdot S_y - (\tilde{p}_s \cdot \mathcal{E}_x - \bar{p}_x \cdot \mathcal{E}_s) \cdot S_x \end{pmatrix} \tag{3.69}$$

$$S' = F(s) \begin{bmatrix} 0 & \bar{p}_y \cdot \mathcal{E}_x & \tilde{p}_s \cdot \mathcal{E}_x - \bar{p}_x \cdot \mathcal{E}_z \\ -\bar{p}_y \cdot \mathcal{E}_x & 0 & -\bar{p}_y \cdot \mathcal{E}_s \\ -\tilde{p}_s \cdot \mathcal{E}_x + \bar{p}_x \cdot \mathcal{E}_z & \bar{p}_y \cdot \mathcal{E}_s & 0 \end{bmatrix} \cdot \begin{pmatrix} S_x \\ S_y \\ S_z \end{pmatrix} \tag{3.70}$$

We can obtain the equivalent of this 3x3 matrix in complex 2x2 dimension:

$$M = \begin{bmatrix} -iu_z & -(iu_x + u_y) \\ -iu_x + u_y & +iu_z \end{bmatrix} \tag{3.71}$$

to get finally:

$$S' = \frac{F(s)}{2} \begin{bmatrix} i \cdot \bar{p}_y \cdot \mathcal{E}_x & -i \cdot \bar{p}_y \cdot \mathcal{E}_s - \tilde{p}_s \cdot \mathcal{E}_x + \bar{p}_x \cdot \mathcal{E}_s \\ -i \cdot \bar{p}_y \cdot \mathcal{E}_s + \tilde{p}_s \cdot \mathcal{E}_x - \bar{p}_x \cdot \mathcal{E}_s & -i\bar{p}_y \cdot \mathcal{E}_x \end{bmatrix} .S \tag{3.72}$$

The equivalent of eq. (3.72) in the central part of the deflector gives:

$$S' = \frac{F_2(s)}{2} \begin{bmatrix} -i\bar{p}_y & \tilde{p}_s \\ -\tilde{p}_s & i\bar{p}_y \end{bmatrix} .S = MS \tag{3.73}$$

3.3.2 Spin motion in the central part of the deflector

We want to solve the equation:

$$S' = MS \tag{3.74}$$

with:

$$M = \frac{1}{2} \cdot F_2(s) \cdot \begin{bmatrix} -i \cdot p_y & \tilde{p_s} \\ -\tilde{p_s} & i \cdot p_y \end{bmatrix} \tag{3.75}$$

For symmetry reasons, we assume that the vertical component of the electric field is equal to zero. Thus p_y is constant all over the deflector.

In the case of the central part of the deflector, the potential is a logarithm and the field has only one component $\vec{E} = (E_x, 0, 0)$. Due to this reason, it can be included in the $F_2(s)$ function and simplify the calculation. This is not the case for the fringe field, where the field has many components and is not included in the F function.

We can develop $\tilde{p_s}$ at first order:

$$\tilde{p_s} = \frac{p_s}{1 + \frac{x}{\rho}} = 1 - \frac{x}{\rho} + \delta \tag{3.76}$$

At the second order, we have for $\tilde{p_s}$:

$$\tilde{p_s} = \frac{p_s}{1 + \frac{x}{\rho}} = 1 - \frac{x}{\rho} + \delta - \frac{p_x^2}{2} - \frac{p_y^2}{2} - \frac{\delta^2}{2\gamma_0^2} + \frac{x^2 \cdot (\gamma_0^2 - 1)}{2\gamma_0^2 \rho^2} + \frac{x \cdot \delta}{\gamma_0^2 \rho} \tag{3.77}$$

where x and p_x are respectively the position and the momentum calculated in part (2.2), up to second order.

In the following calculations, we will use ϵ_p, defined as the small variation of the longitudinal momentum around the momentum of the reference particle:

$$\tilde{p_s} = 1 - \epsilon_p \tag{3.78}$$

The value of ϵ_p is then:

$$\epsilon_p = -\left(-\frac{x}{\rho} + \delta - \frac{p_x^2}{2} - \frac{p_y^2}{2} - \frac{\delta^2}{2\gamma_0^2} + \frac{x^2 \cdot (\gamma_0^2 - 1)}{2\gamma_0^2 \rho^2} + \frac{x \cdot \delta}{\gamma_0^2 \rho} \right) \tag{3.79}$$

We can rewrite the matrix M:

$$M = \frac{1}{2} \cdot F_2(s) \cdot \begin{bmatrix} -i \cdot p_y & 1 - \epsilon_p \\ -1 + \epsilon_p & i \cdot p_y \end{bmatrix} \tag{3.80}$$

This form is more convenient as it allows us to split the M matrix in two different matrices. One matrix that is constant and corresponds to a rotation of 90 degrees, and another varying matrix with small components, corresponding to a perturbation:

$$M = \frac{1}{2} \cdot F_2(s) \cdot \left(\begin{bmatrix} 0 & 1 \\ -1 & 0 \end{bmatrix} + \begin{bmatrix} -i \cdot p_y & -\epsilon_p \\ \epsilon_p & i \cdot p_y \end{bmatrix} \right) \tag{3.81}$$

We define the perturbation matrix E (eq 3.82) and the principal solution matrix as Y_0 (eq 3.83):

$$E = \frac{1}{2} \cdot F \cdot \begin{bmatrix} -i \cdot p_y & -\epsilon_p \\ \epsilon_p & i \cdot p_y \end{bmatrix} \tag{3.82}$$

$$Y_0 = \begin{bmatrix} \cos\left(\frac{\phi}{2}\right) & \sin\left(\frac{\phi}{2}\right) \\ -\sin\left(\frac{\phi}{2}\right) & \cos\left(\frac{\phi}{2}\right) \end{bmatrix} \tag{3.83}$$

with ϕ the angle of rotation along a deflector of lenght L:

$$\phi = \int_0^L F_2(s) ds \tag{3.84}$$

We use the method described in part (2.4.1) to solve the differential equation (3.74). We define the matrix U:

$$U = Y_0^{-1} \cdot E \cdot Y_0 = \frac{1}{2} \cdot \dot{\phi} \cdot \begin{bmatrix} i \cdot p_y \cdot (\sin\left(\frac{\phi}{2}\right)^2 - \cos\left(\frac{\phi}{2}\right)^2) & -2\sin\left(\frac{\phi}{2}\right) \cdot \cos\left(\frac{\phi}{2}\right) \cdot i \cdot p_y - \epsilon_p \\ -\bar{U}_{12} & \bar{U}_{11} \end{bmatrix}$$

Or also:

$$U = Y_0^{-1} \cdot E \cdot Y_0 = \frac{1}{2} \cdot \dot{\phi} \cdot \begin{bmatrix} -i \cdot p_y \cdot \cos(\phi) & -\sin(\phi) \cdot i \cdot p_y - \epsilon_p \\ -\bar{U}_{12} & \bar{U}_{11} \end{bmatrix} \tag{3.85}$$

We define the matrix R as the solution of the perturbation, and remind its general form:

$$R = I + \int_0^L U ds + \int_0^L \left[U \int_0^s U dt \right] ds + ...$$

At order zero, we have $R^0 = I$ where I is the identity matrix.
The first order solution R^1 is given by:

$$R^1 = \begin{bmatrix} R^1_{11} & R^1_{12} \\ R^1_{21} & R^1_{22} \end{bmatrix} = \int_0^L U ds \tag{3.86}$$

The second order is:

$$R^2 = \begin{bmatrix} R^2_{11} & R^2_{12} \\ R^2_{21} & R^2_{22} \end{bmatrix} = \int_0^L \left[U \int_0^s U dt \right] ds \tag{3.87}$$

Or also, if we omit the boundaries for simplify reading:

$$R^2 = \int \begin{bmatrix} U_{11} \int U_{11} - U_{12} \int \bar{U_{12}} & U_{11} \int U_{12} + U_{12} \int \bar{U_{11}} \\ -\bar{U_{12}} \int U_{11} - \bar{U_{11}} \int \bar{U_{12}} & -\bar{U_{12}} \int U_{12} + \bar{U_{11}} \int \bar{U_{11}} \end{bmatrix} \tag{3.88}$$

Note: R^2 is not the square of R, it stand for the second order part of R.

First order solution computation

The first order solution consists to find two integrals. The first term is:

$$R^1_{11} = \int_0^L U_{11} ds = -\frac{i}{2} \cdot p_y \cdot \sin(\phi) \tag{3.89}$$

and the second:

$$R^1_{12} = \int_0^L U_{12} ds = \frac{1}{2} \cdot [\cos(\phi) - 1] \cdot i \cdot p_y - \frac{1}{2} \int_0^L \dot{\phi} \cdot \epsilon_p \cdot ds \tag{3.90}$$

If we define I as:

$$I = \frac{1}{2} \int_0^L \dot{\phi} \cdot \epsilon_p \cdot ds \tag{3.91}$$

We finally have:

$$R^1_{12} = \frac{i}{2} \cdot p_y \cdot [\cos(\phi) - 1] - I \tag{3.92}$$

The two remaining terms R_{21} and R_{22} are respectively $-\bar{R}_{12}$ and $\bar{R}_{11}$. These terms can be mathematically calculated by computation softwares such as Mathematica or Maple, up to second order.

Second order solution computation

We now have to compute the second order solution matrix R^2. These computations represent a huge amount of analytical calculations and verification. As they are a consistent part of my work, I decided to include them directly in this thesis. If wanted, **the reader can move directly to the summary** of the results at page (76), eq(3.111).

The first term can be written as:

$$R^2_{11} = \int_0^L \left[U_{11} \int_0^S U_{11} ds \right] dS - \int_0^L \left[U_{12} \int_0^S \bar{U}_{12} ds \right] dS \tag{3.93}$$

The first part gives:

$$\int U_{11} \int U_{11} = \frac{1}{2} \cdot \left[\int U_{11} \right]^2 = -\frac{1}{4} \cdot P_y^2 \cdot \sin^2(\phi) \tag{3.94}$$

The second part, not integrated:

$$U_{12} \int \bar{U}_{12} = \frac{1}{2} \cdot \dot{\phi} \cdot (\sin(\phi) \cdot i \cdot p_y + \epsilon_p) \cdot \left(\frac{1}{2} [\cos(\phi) - 1] \cdot i \cdot p_y + I \right) \tag{3.95}$$

By integrating, we have for the real part:

$$-\Re \left(\int U_{12} \int \bar{U}_{12} \right) = -\left[\frac{1}{2} \cdot I^2 + \frac{1}{8} \cdot [\cos(\phi) - 1]^2 \cdot p_y^2 \right] \tag{3.96}$$

The imaginary part is:

$$\Im[U_{12}\int \bar{U}_{12}] = \frac{1}{2}\cdot\dot{\phi}\cdot\epsilon_p\cdot\frac{1}{2}[\cos(\phi)-1]\cdot i\cdot p_y + \frac{I}{2}\cdot\dot{\phi}\cdot\sin(\phi)\cdot i\cdot p_y \tag{3.97}$$

$$-\Im\int[U_{12}\int\bar{U}_{12}] = -\int\left[\frac{i\cdot p_y}{2}[\dot{I}\cdot\cos(\phi)+I\cdot\dot{\phi}\cdot\sin(\phi)-\dot{I}]\right] \tag{3.98}$$

If we stay at the second order, considering ϵ varies slowly, we can write:

$$C^* = \dot{I}\cos(\phi)+\dot{\phi}I\sin(\phi)\sim\dot{I}+\dot{\phi}\phi\int\frac{\epsilon\dot{\phi}}{2} \tag{3.99}$$

$$\int C^* = I+\frac{\phi^2}{2}I-\int\frac{\phi^2}{2}\epsilon\dot{\phi}\sim I\left(1+\frac{\phi^2}{2}\right)-\frac{\epsilon\cdot\phi^3}{6} \tag{3.100}$$

The second term of the second order solution is:

$$R_{12}^2 = \int_0^L\left[U_{11}\int_0^S U_{12}ds\right]dS+\int_0^L\left[U_{12}\int_0^S\bar{U}_{11}ds\right]dS \tag{3.101}$$

We first write:

$$U_{11}\int U_{12} = -\frac{1}{2}\cdot\dot{\phi}\cdot i\cdot p_y\cdot\cos(\phi)\cdot\left[\frac{1}{2}(\cos(\phi)-1)\cdot i\cdot p_y - I\right]$$

$$U_{11}\int U_{12} = \frac{1}{4}\cdot\dot{\phi}\cdot\cos(\phi)\cdot(\cos(\phi)-1)\cdot p_y^2+\frac{1}{2}\cdot i\cdot p_y\cdot I\cdot\dot{\phi}\cdot\cos(\phi) \tag{3.102}$$

By integrating respectively real and imaginary parts:

$$\Re\int_0^S\left[U_{11}\int_0^s U_{12}\right] = \frac{P_y^2}{8}\left(\frac{\sin(2\phi)}{2}+\phi\right)-\frac{P_y^2}{4}\sin(\phi) \tag{3.103}$$

$$\Im\int_0^S\left[U_{11}\int_0^s U_{12}\right] = \int_0^S i\frac{P_y}{2}\dot{\phi}I\cos(\phi) \tag{3.104}$$

Secondly, we care about:

$$U_{12}\int\bar{U}_{11} = -\frac{i\cdot p_y}{2}\cdot\sin(\phi)\cdot\frac{1}{2}\cdot\dot{\phi}\cdot(\sin(\phi)\cdot i\cdot p_y+\epsilon_p) \tag{3.105}$$

Or also:

$$U_{12}\int\bar{U}_{11} = \frac{1}{4}\cdot p_y^2\cdot\dot{\phi}\cdot\sin^2(\phi)-\frac{i\cdot p_y}{2}\cdot\dot{I}\cdot\sin(\phi) \tag{3.106}$$

By integrating:

$$\Re\int_0^S\left[U_{12}\int\bar{U_{11}}\right] = \frac{P_y^2}{8}\phi-\frac{P_y^2}{16}\sin(2\phi) \tag{3.107}$$

$$\Im \int_0^S \left[U_{12} \int \bar{U_{11}} \right] = -i \frac{P_y}{2} \int_0^S \dot{I} \sin(\phi) \tag{3.108}$$

As we did for eq (3.100) by assuming small variations for ϵ and second order calculations we can write:

$$D^* = \dot{\phi} I \cos(\phi) - \dot{I} \sin(\phi) \sim I\dot{\phi} + \dot{I}\phi = \dot{\phi} \int \frac{\epsilon\dot{\phi}}{2} - \frac{\phi\dot{\phi}\epsilon}{2} \tag{3.109}$$

$$\int D^* = \phi I - \int \phi\dot{\phi}\epsilon \sim I\phi - \frac{\phi^2\epsilon}{2} \tag{3.110}$$

Summary: spin perturbative solution for the internal part

Summing the solutions up to second order gives the final matrix $R = R^0 + R^1 + R^2$:

$$R = R^0 + R^1 + R^2 = \begin{bmatrix} 1 & 0 \\ 0 & 1 \end{bmatrix} + \begin{bmatrix} A & B \\ -\bar{B} & \bar{A} \end{bmatrix} \tag{3.111}$$

with

$$\begin{aligned} A = &-\frac{i}{2} \cdot p_y \cdot \sin(\phi) - \frac{1}{8} \cdot P_y^2 \cdot \sin^2(\phi) - \left[\frac{1}{2} \cdot I^2 + \frac{1}{8} \cdot [\cos(\phi) - 1]^2 \cdot p_y^2 \right] \\ &+ i \cdot \frac{P_y}{2} \cdot I + I \left(1 + \frac{\phi^2}{2} \right) - \frac{\epsilon \cdot \phi^3}{6} \end{aligned} \tag{3.112}$$

$$B = \frac{i}{2} \cdot p_y \cdot [\cos(\phi) - 1] - I - \frac{P_y^2}{4} \sin(\phi) + \frac{P_y^2}{4}\phi + I\phi - \frac{\phi^2\epsilon}{2} \tag{3.113}$$

We recall

$$\phi = \int_0^L F(s) ds$$

$$I = \frac{1}{2} \int_0^L \dot{\phi} \cdot \epsilon_p \cdot ds$$

Spin dynamics in the internal part of the deflector

According to eq. (2.59) the final rotation matrix is expressed as:

$$M = Y_0 \cdot R \tag{3.114}$$

with, as a reminder:

$$Y_0 = \begin{bmatrix} \cos\left(\frac{\phi}{2}\right) & \sin\left(\frac{\phi}{2}\right) \\ -\sin\left(\frac{\phi}{2}\right) & \cos\left(\frac{\phi}{2}\right) \end{bmatrix}$$

The transfer matrix for spin can then be computed mathematically by using computation softwares. I used, in my case, Mathematica (see annex C for more details). The different functions $\phi, I, \epsilon...$ as well as the trajectories have to be implemented and developed as series of $(x_0, p_{x0}, y_0, p_{y0}, d_z, \frac{\Delta P}{P_0})$.

The final transfer matrix, i.e. the one implemented in the tracking code is a 2×2 transfer matrix for spin depending of the phase space vector of the particle.

As an example, figure 3.11 shows the dependencies in $(x_0, p_{x0}, y_0, p_{y0}, d_z, \frac{\Delta P}{P_0})$ of real and imaginary parts of the two M_{11} and M_{12} components of the transfer matrix. This matrix is extracted from BMAD for a standard electrostatic machine and has only to be computed once each time the code runs.

	M11Re	M11Im	M12Re	M12Im
CSTE	1.0000000000000000	0.0000000000000000	0.0000000000000000	0.0000000000000000
x0	-8.5638697376555674E-020	0.0000000000000000	-2.4516127984766304E-003	0.0000000000000000
xp0	-1.3469863770053733E-019	0.0000000000000000	-3.8560710781479855E-003	0.0000000000000000
delta0	2.7404383160497816E-018	0.0000000000000000	7.8451609551252174E-002	0.0000000000000000
yp0	0.0000000000000000	0.0000000000000000	0.0000000000000000	0.0000000000000000
x0^2	-3.0003804917699099E-006	0.0000000000000000	-2.5330153724255393E-004	0.0000000000000000
xp0^2	-2.4663991535900451E-005	0.0000000000000000	-9.6219936975855717E-004	0.0000000000000000
delta0^2	-3.0975709831156288E-003	0.0000000000000000	-0.29713098993926579	0.0000000000000000
yp0^2	-0.0000000000000000	0.0000000000000000	-0.0000000000000000	0.0000000000000000
x0.xp0	-9.4535932070231901E-006	0.0000000000000000	-1.0371691396119376E-003	0.0000000000000000
x0.delta0	1.9233297003694124E-004	0.0000000000000000	1.8633006106527562E-002	0.0000000000000000
x0.yp0	0.0000000000000000	2.4516127984766300E-003	0.0000000000000000	-0.0000000000000000
xp0.delta	3.0251498262474214E-004	0.0000000000000000	4.0079377699588623E-002	0.0000000000000000
xp0.yp0	0.0000000000000000	3.8560710781478727E-003	0.0000000000000000	-0.0000000000000000
delta.yp0	0.0000000000000000	-7.8451609551252161E-002	0.0000000000000000	0.0000000000000000

Figure 3.11: An example of transfer matrix, showed by BMAD. In this example, lots of values are close or equal to zero due to the specific magic condition of the ring used. In this particular case, the CSTE part of the M11Re term is equal to 1 because the 0^{th} order rotation in a magic ring is the unitary matrix.

3.3.3 Spin motion in the fringe field

We proceed in this part in the same way that we did for the internal part of the deflector. The difference is that we cannot integrate analytically the equation as done in part 3.3.2, as the expression of the electric field is way more complicated. These integrals have been computed numerically.

All the results are expressed analytically up to the last possible point, and the numerical solutions are inserted at the very last moment, directly in the tracking code. In the same way as for the inner part of the deflector, these computations can be skipped directly to page(79), eq. (3.126).

We consider the function $F(s)$:

$$F(s) = \left[1 - \frac{(\vec{p}_x^2 + \vec{p}_y^2)}{2} \cdot \frac{\gamma_0^2 - 1}{\gamma - 1}\right] \cdot \left(1 + \frac{x}{\rho_0}\right) \cdot \frac{\beta_0^3 \gamma_0^2}{\sqrt{\gamma^2 - 1} \cdot \rho_0} \cdot \left(G_m - \frac{1}{\gamma^2 - 1}\right) \quad (3.115)$$

where the γ factor is the one defined in eq. (2.31). This function is not including the electric field, as we did for the internal part.

We now have to express the axis vector of rotation of eq. (3.67), including the new expression of the electric field:

$$V = \begin{bmatrix} -\dot{k}_0 \cdot x \cdot \frac{y'}{G} \\ -k_0 + k_0 \cdot (k_0 + 1) \cdot \frac{x}{\rho_0} - \delta \cdot k_0 + [2 \cdot k_0^2 + k_2] \cdot \left(\frac{x}{\rho_0}\right)^2 + 2 \cdot k_0 \cdot \delta \cdot \frac{x}{\rho_0} + \dot{k}_0 \cdot x \cdot \frac{x'}{G} \\ k_0 \cdot y' - k_0 \cdot (k_0 + 2) \cdot y' \cdot \frac{x}{\rho_0} + y' \cdot \delta \cdot k_0 \end{bmatrix} \quad (3.116)$$

or, expressed in gap units, which is more convenient:

$$V = \begin{bmatrix} -\dot{k}_0 \cdot \tilde{x} \cdot \dot{\tilde{y}} \\ -k_0 + k_0 \cdot (k_0 + 1) \cdot \frac{G}{\rho_0} \cdot \tilde{x} - \delta \cdot k_0 + [2 \cdot k_0^2 + k_2] \cdot \left(\frac{G}{\rho_0}\right)^2 \cdot \tilde{x}^2 + 2 \cdot k_0 \cdot \delta \cdot \frac{G}{\rho_0} \cdot \tilde{x} + \dot{k}_0 \cdot \tilde{x} \cdot \dot{\tilde{x}} \\ k_0 \cdot \dot{\tilde{y}} \cdot \left[1 - (k_0 + 2) \cdot \frac{G}{\rho_0} \cdot \tilde{x} + \delta\right] \end{bmatrix} \quad (3.117)$$

where $\tilde{x} = \frac{x}{G}$, $\tilde{y} = \frac{y}{G}$ and $\delta = \frac{\Delta P}{P_0}$.

The system to solve is:

$$\dot{S} = M \cdot S \quad (3.118)$$

with

$$M = \frac{1}{2} \cdot F(s) \cdot \begin{bmatrix} -i \cdot V_3 & -i \cdot V_1 - V_2 \\ -i \cdot V_1 + V_2 & iV_3 \end{bmatrix} \quad (3.119)$$

We set up the non-pertubative part of the V vector, which corresponds to the main horizontal rotation due to the dipolar component of the field, with a constant axis of rotation:

$$V_0 = \begin{bmatrix} 0 \\ -k_0 \\ 0 \end{bmatrix} \tag{3.120}$$

and the perturbative part W, with a varying axis of rotation:

$$W = \begin{bmatrix} -\dot{k}_0 \cdot \tilde{x} \cdot \dot{\tilde{y}} \\ k_0 \cdot (k_0+1) \cdot \frac{G}{\rho_0} \cdot \tilde{x} - \delta \cdot k_0 + [2 \cdot k_0^2 + k_2] \cdot \left(\frac{G}{\rho_0}\right)^2 \cdot \tilde{x}^2 + 2 \cdot k_0 \cdot \delta \cdot \frac{G}{\rho_0} \cdot \tilde{x} + \dot{k}_0 \cdot \tilde{x} \cdot \dot{\tilde{x}} \\ k_0 \cdot \dot{\tilde{y}} \cdot \left[1 - (k_0+2) \cdot \frac{G}{\rho_0} \cdot \tilde{x} + \delta\right] \end{bmatrix} \tag{3.121}$$

We define ϕ the non-perturbative angle of rotation, and the associated rotation matrix:

$$\phi = \int_0^L k_0 \cdot F(s) ds \tag{3.122}$$

$$Y_0 = \begin{bmatrix} \cos\left(\frac{\phi}{2}\right) & \sin\left(\frac{\phi}{2}\right) \\ -\sin\left(\frac{\phi}{2}\right) & \cos\left(\frac{\phi}{2}\right) \end{bmatrix} \tag{3.123}$$

We consider the perturbative E matrix (in the same way that the one of eq. (3.82) for the inner part of the deflector):

$$E = \frac{F(s)}{2} \cdot \begin{bmatrix} -i \cdot W_3 & -i \cdot W_1 - W_2 \\ -i \cdot W_1 + W_2 & i \cdot W_3 \end{bmatrix} \tag{3.124}$$

We compute the U matrix:

$$\begin{aligned} U &= Y_0^{-1} \cdot E \cdot Y_0 \\ &= \frac{F(s)}{2} \cdot \begin{bmatrix} -i \cdot (W_1 \cdot \sin(\phi) - W_3 \cdot \cos(\phi)) & -W_2 - i \cdot (W_3 \cdot \sin(\phi) + W_1 \cdot \cos(\phi)) \\ -\bar{W}_{12} & \bar{W}_{11} \end{bmatrix} \end{aligned} \tag{3.125}$$

We compute the first order solution matrix:

$$R_{11}^1 = i \cdot \int_0^L F(s) \cdot (W_1(s) \cdot \sin[\phi(s)] - W_3(s) \cdot \cos[\phi(s)]) \cdot ds \tag{3.126}$$

$$R_{12}^1 = \int_0^L F(s) \cdot [-W_2 - i \cdot (W_3(s) \cdot \sin([\phi(s)] + W_1(s) \cdot \cos[\phi(s)])] \cdot ds \tag{3.127}$$

and knowing that $R_{21}^1 = -\bar{R}_{12}^1$ and $R_{22}^1 = \bar{R}_{11}^1$.

We also compute the second order of the perturbative method:

$$R_{11}^2 = \int_0^L \left[U_{11} \int_0^S U_{11} ds \right] dS - \int_0^L \left[U_{12} \int_0^S \bar{U}_{12} ds \right] dS \tag{3.128}$$

$$R_{12}^2 = \int_0^L \left[U_{11} \int_0^S U_{12} ds \right] dS - \int_0^L \left[U_{12} \int_0^S \bar{U}_{11} ds \right] dS \tag{3.129}$$

and knowing that $R_{21}^2 = -\bar{R}_{12}^2$ and $R_{22}^2 = \bar{R}_{11}^2$.

All these integrals are determined by quadrature with the methods given in part (2.4.2) and their values are stored in a separate file.

An example of resolution

We obtain the final analytic solution by substituting x by its analytical expression in equations (3.126, 3.127, 3.128, 3.129):

$$x = C(s) \cdot x_0 + S(s) \cdot x_0' + \alpha \cdot \eta_1 + \alpha \cdot \eta_2 \cdot \delta \tag{3.130}$$

where $C(s)$ and $S(s)$ are the equations of motion determined previously in equations (3.59) and (3.60) and η_1, η_2 the particular solutions of the reference trajectory.

As the field is no more the nominal field anywhere, the reference particle deviates from the reference circle: the trajectory of the reference particle is no more a circle, nor a straight line. This correction is made with the η_1 factor.

We define F_{00} that is equal to zero when the ring is magic and F_{01}:

$$F_{00} = \frac{\gamma_0^2 - \gamma_m^2}{\gamma_0 \cdot (\gamma_m^2 - 1)} \tag{3.131}$$

$$F_{01} = \frac{\gamma_0^2 - 3\gamma_m^2 + 2}{\gamma_0 \cdot (\gamma_m^2 - 1)} \tag{3.132}$$

where γ_m is the magic energy corresponding to the frozen-spin condition:

$$\gamma_m = \sqrt{1 + \frac{1}{G_m}} \tag{3.133}$$

As an example, the dependence in x_0 of the R_{12} term of the transfer matrix is given by taking the derivative of R_{12} with respect to x_0 (here up to the second order in $\alpha \approx 0.001$):

$$\frac{\partial R_{12}}{\partial x_0} = \alpha^2 \cdot \left(F_{00} \int_0^L C + F_{01} \int_0^L C k_0 - F_{00} \cdot \left(\int_0^L C \cdot (k_0 \cdot k_2) + \int_0^L \dot{k}_0 (\dot{S}\eta_1 + S\dot{\eta}_1) \right) \right) \tag{3.134}$$

All the integrals contained in equation (3.134) are calculated by quadrature and are given in appendix A.2. This formula is an universal formula and only depends on the $\alpha = G/\rho_0$ ratio of the deflector.

The integrals of the field and the motion equations are always the same and only need to be computed once for each position of the diaphragm.

Remark: The integrals are not the same for the entrance and exit fringe fields. We have to integrate in one case from the maximum field to E = 0, and the inverse for the other case. Two integral files have to be considered.

We can, by this method, compute all the terms of the final transfer matrix, at any order. My thesis provides all the terms and crossed-terms up to the second order. These terms are given in appendix C.

Conclusion on the model

This chapter provides a complete model for field, trajectories and spin both in the internal part and in the fringe field part of an electrostatic deflector. The whole way to get the formulas, from the field computation to the final spin transfer matrix expression, has been done with a lot of checks and rigor by a local team of three persons.

Many iterations, and time, have been necessary before getting the last results. The principal advantages of the model are recalled in the following paragraphs.

Analytic and realistic model

The electrostatic field of the deflector is computed by conformal mapping, which allows us to have an analytic description of the field. Boundary conditions are included in the model as well as realistic electrode shapes.

From a semi-infinite box (which we showed the resolution for the potential), we can express to potential and field in the wanted system.

The precision of the analytical field has been verified with a finite elements simulation and validated to be better than 10^-5 relatively to the nominal field.

As we know the analytical form of the field, we can by derivation extract its different components, as the dipolar, quadrupolar, hexapolar, longitudinal components.

Universal functions

All the field functions are given for a straight deflector. This can easily be extended to a curved deflector as a function of the gap/radius ratio.

All the remaining results, including trajectories and spin, are functions of the gap/radius ratio and can be applied to every size of deflector.

This allows the user to gain plenty of time while changing the deflector size in a lattice.

Understand the spin precessing phenomenon

The spin transfer matrix is given as a function of the initial conditions before entering the deflector. All the dependencies up to order two can be explicitly separated.

As an example, the effect of energy spread can be studied separately from the effect of the position of the particle, which can allow us to apply specific corrections.

Analytical analysis and machine design

For a further analytical analysis of the beam behavior or for machine design optimization, all the calculations given here can exhibit the role of any parameter.

As an example: a remaining question is the role of $(\Delta p/p_0)^2$. The corresponding term can be isolated analytically (to see the amplitude of the G-factor, or dispersion etc.) and numerically (to compare the amplitudes of the different effects for example).

3.4 Résultats - Résumé en français

Ce chapitre présente les différents résultats analytiques ou semi-analytiques obtenus dans le but de calculer la dynamique de spin dans le déflecteur total. Trois principaux résultats sont présentés :

- Un modèle analytique et universel pour les champs de fuites d'un déflecteur. Nous utilisons ici les transformations conformes.
- Deux modèles de trajectoires distincts pour le déflecteur et les champs de fuite respectivement, utilisant les équations d'Hamilton et la variation des constantes.
- Deux modèles distincts pour la dynamique de spin dans la partie centrale du déflecteur et pour les champs de fuite. Le modèle pour la partie centrale utilise l'équation de Thomas-BMT et des équations du mouvement calculées précedemment pour donner des formules complètement analytiques jusqu'à l'ordre 2 de perturbation. Le modèle de champs de fuite est un modèle semi-analytique faisant intervenir des intégrales universelles, qui n'ont besoin d'être calculées qu'une seule et unique fois.

Modèle de champ de fuite Une transformation conforme est une transformation du plan complexe qui conserve localement les angles.

En connaissant le potentiel d'un système initial (idéalement simple) et en connaissant la transformation entre ce système et le système voulu, il est possible de connaître le potentiel dans ce dernier.

Le système que nous avons cherché à modéliser est un système réaliste comprenant des éléctrodes réalistes (courbées) et des conditions aux limites (voir fig 3.12).

Nous sommes partis d'une boite semi-infinie dont nous avons montré que le potentiel s'écrit :

$$V(x,y) = \frac{2}{\pi} \cdot V_0 \cdot \arctan[th(x) \cdot \tan(y)]$$

Un profile réaliste pour les électrodes est donné par la formule :

$$\left[-\frac{\pi}{2} \leq \Im(z) \leq \frac{\pi}{2}\right] \vdots T : z \to Z_1 = [1 + z + e^z] \to Z_2 = \frac{1}{\pi} \cdot [\alpha^* + Z_1 + e^{Z_1}]$$

Enfin, il est possible de transformer la boite semi-infinie en un système réaliste comprenant des conditions aux limites par la transformation :

$$G(Z) = \beta^* - \frac{11}{4} \cdot e^{\frac{4z}{11}} \cdot H_{\frac{2}{11},\frac{2}{11},\frac{13}{11}}(-e^{2z})$$

La liste des transformations inverses, nécessaires à l'obtention du champ est donnée en page 60. Le champ électrique a été validé par éléments finis avec une précision de l'ordre de 10^{-5} sur toute la gamme de champ.

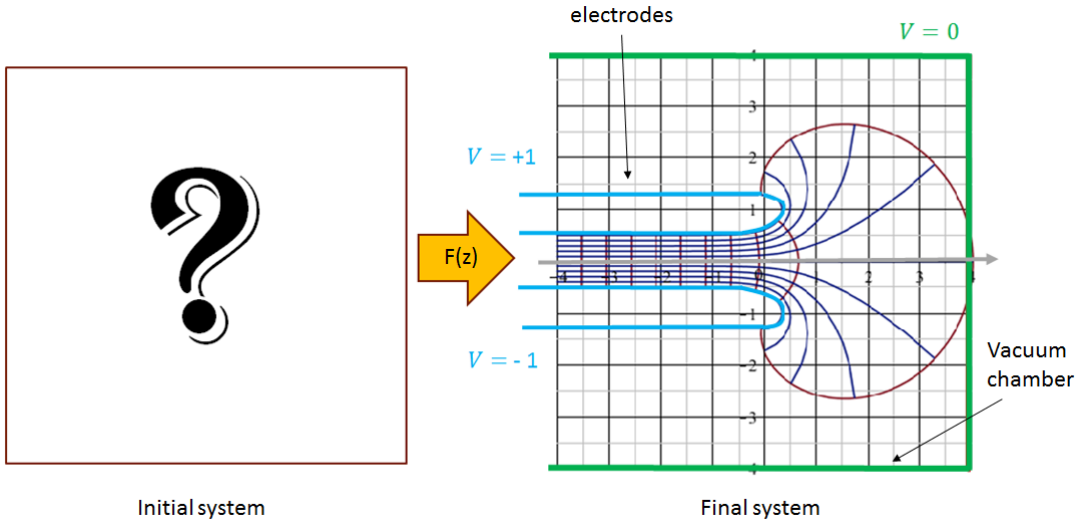

Figure 3.12: Système final, connu et réaliste, incluant deux électrodes parallèles ($\pm V_0$) ,une chambre à vide et un diaphragme (V = 0). Les lignes de champ sont ici uniquement pour illustration

Trajectoires Les trajectoires sont calculées au second ordre à partir des équations d'Hamilton par les méthodes présentées dans le chapitre précédent.

Dans la partie centrale :

$$x = K_1(s) \cdot \cos(ks) + \frac{K_2(s)}{k} \cdot \sin(ks) + \delta \cdot \rho_0 \cdot (1 - \cos(ks))$$

$$p_x = -K_1(s) \cdot k \cdot \sin(ks) + K_2(s) \cdot \cos(ks) + \delta \cdot \rho_0 \cdot k \cdot \sin(ks)$$

où $K_1(s)$ et $K_2(s)$ sont les fonctions déterminées avec l'eq (2.36).

Dans les champs de fuite :

$$C = 1 - \left(\frac{G}{\rho}\right)^2 \cdot \int\int \omega + \left(\frac{G}{\rho}\right)^4 \cdot \int\int \omega \int\int \omega$$

$$S = \tilde{s} - \left(\frac{G}{\rho}\right)^2 \cdot \int\int \omega\tilde{s} + \left(\frac{G}{\rho}\right)^4 \cdot \int\int \omega \int\int \omega\tilde{s}$$

$$C' = -\left(\frac{G}{\rho}\right)^2 \cdot \int \omega + \left(\frac{G}{\rho}\right)^4 \cdot \int \omega \int\int \omega$$

$$S' = 1 - \left(\frac{G}{\rho}\right)^2 \cdot \int \omega\tilde{s} + \left(\frac{G}{\rho}\right)^4 \cdot \int \omega \int\int \omega\tilde{s}$$

où les bornes d'intégration ont été retirées pour simplifier la lecture. Ces intégrales sont calculées indépendemment par quadrature et ne dépendent que du ratio G/ρ.

Dynamique du spin La dynamique du spin est obtenue par la résolution de l'équation de Thomas-BMT avec une méthode perturbative. L'équation de précession du spin peut être réécrite comme :

$$S' = \frac{F(s)}{2} \begin{bmatrix} i \cdot \bar{p}_y \cdot \mathcal{E}_x & -i \cdot \bar{p}_y \cdot \mathcal{E}_s - \tilde{p}_s \cdot \mathcal{E}_x + \bar{p}_x \cdot \mathcal{E}_s \\ -i \cdot \bar{p}_y \cdot \mathcal{E}_s + \tilde{p}_s \cdot \mathcal{E}_x - \bar{p}_x \cdot \mathcal{E}_s & -i\bar{p}_y \cdot \mathcal{E}_x \end{bmatrix} .S$$

où les $\bar{p_i}$ sont les moments conjugués normalisés, $\mathcal{E}_i$ les champs électriques et S le spin.

Les résultats de la résolution sont données en page 76 pour la partie centrale et en page 80 pour les champs de fuite.

Chapter 4

Analysis and implementation in the BMAD code

Contents

4.1 Implementation

4.1.1 Description of BMAD

Bmad (Otherwise known as "Baby MAD" or "Better MAD" or just plain "Be MAD!") is a subroutine library for relativistic charged–particle and X-Ray simulations in high energy accelerators and storage rings.

More information about BMAD can be found in [24]. It has been developed by David Sagan at Cornell University's Laboratory for Elementary Particle Physics.

As a library, BMAD is a code requiring a lot of practice to be well used. It presents many advantages, as its versatility and the possibility to modify it easily.

BMAD is using a ".bmad" input lattice file, whose syntax was developed from the MAD standard syntax with some evolutions. The species of particles as well as the energy should be specified in the lattice file.

It proposes plenty of routines that can be used and modified at will. These routines should be called in the main program, written in FORTRAN90 by the user.

What is already included in BMAD, what has been implemented

BMAD contains all the routines necessary to create/parse a lattice (in our case a storage ring), create a beam of particles and track it through the lattice.

The user can chose between many different tracking methods as linear (with transfer matrices), bmad_standard (with paraxial approximation), MAD, runge_kutta... and also a custom tracking routine, which is the one I am interested in. Both the trajectories and the spin can be tracked.

BMAD does already include spin tracking methods. These methods use tracking with field maps or numerical integrations (Romberg integration) and are generally slow.

I implemented a custom spin tracking routine based on transfer functions with complex elements. This matrix is created during the code initialisation by separated custom routines (one for the internal part of the deflector and one for the fringe fields) and is depending on the initial phase space coordinates before entering the deflector.

Also phase space tracking through the deflector and the fringe field has been implemented in a custom routine, whose transfer functions (up to order 2) are computed with custom routines.

4.1.2 Transfer functions creation routines

I implemented five transfer functions creation routines:

- **make_mat6_custom**: This is a simple routine creating the 1st order transfer matrix for the internal part of the deflector with the matrix given in part 3.2.2.1 equation (3.46). This is used to make faster computations for qualitative or design purposes.

- **make_traj_defl**: This routine uses the equations given in part 3.2.2.2 to compute the 2nd order trajectories transfer functions for the inner part of the deflector. Transfer functions are created only once per code run during the initialisation phase and used each time a particle goes through the deflector.

- **make_mat_defl**: In the same way, this routine computes the spin transfer matrix (2x2 complex matrix) depending on the initial phase space before entering the deflector. This matrix is computed only once per code run but needs to be filled with the initial coordinates at each passage through the deflector. This is using all the results presented in part 3.3.2 developed and integrated with Mathematica.

- **make_traj_FF**: Routine to create the trajectory transfer function up to order 2 by using the solutions given in part 3.2.3. This routine is called twice when the code runs: once for the entrance fringe field, and once for the exit. This uses the list of integrals given in appendix A computed upstream by quadrature.

- **make_mat_FF**: The routine that creates the spin transfer matrix for the fringe field. In the same way as for the inner part, this matrix is computed only once (once for entrance, once for exit) and needs to be filled with the initial coordinates before entering the deflector. This routine also uses the list of integrals in appendix A.

4.1.3 Tracking routines

The tracking routines are using the transfer functions shown in the previous part. The operation is quite straightforward.

- **track1_custom**: Multiply the terms of the transfer functions by the associated phase space coordinate, up to 2nd order. Example:

$$x_{exit} = a \cdot x_0 + b \cdot p_{x0} + c \cdot \left.\frac{\Delta P}{P_0}\right|_0 + d \cdot x_0^2 + e \cdot x_0 \cdot p_{x0} + ...$$

- **track1_spin_custom**: Fill in the transfer matrix with the initial coordinates such as:

$$R(\theta) = \begin{bmatrix} A + i \cdot B & C + i \cdot D \\ -\bar{R_{12}} & \bar{R_{11}} \end{bmatrix}$$

with:

$$A = a_1 \cdot x_0 + b_1 \cdot p_{x0} + c_1 \cdot \left.\frac{\Delta P}{P_0}\right|_0 + d_1 \cdot x_0^2 + e_1 \cdot x_0 \cdot p_{x0} + ...$$

$$B = a_2 \cdot x_0 + b_2 \cdot p_{x0} + c_2 \cdot \left.\frac{\Delta P}{P_0}\right|_0 + d_2 \cdot x_0^2 + e_2 \cdot x_0 \cdot p_{x0} + ...$$

$$C = a_3 \cdot x_0 + b_3 \cdot p_{x0} + c_3 \cdot \left.\frac{\Delta P}{P_0}\right|_0 + d_3 \cdot x_0^2 + e_3 \cdot x_0 \cdot p_{x0} + ...$$

$$D = a_4 \cdot x_0 + b_4 \cdot p_{x0} + c_4 \cdot \left.\frac{\Delta P}{P_0}\right|_0 + d_4 \cdot x_0^2 + e_4 \cdot x_0 \cdot p_{x0} + ...$$

Then apply the rotation:

$$\begin{bmatrix} \Psi_1 \\ \Psi_2 \end{bmatrix}_{exit} = \begin{bmatrix} A + i \cdot B & C + i \cdot D \\ -\bar{R_{12}} & \bar{R_{11}} \end{bmatrix} \cdot \begin{bmatrix} \Psi_1 \\ \Psi_2 \end{bmatrix}_{init} \tag{4.1}$$

All the coefficients $a_i, b_i, c_i...$ are computed during the initialisation phase and are given in appendix C. They do not change while the code is running and only depends of the input parameters of the lattice file (ρ_0, γ_0, Gap, length ...) and the particular integrals list.

4.2 The storage ring

4.2.1 Ring specifications

The machine used in this analysis is a simplified design of the final storage ring that should be used by the JEDI collaboration to measure the proton EDM.

The ring is composed of 64 electrostatic deflectors divided in sixteen parts. It is composed of a periodic FODO structure with two families of quadrupoles:

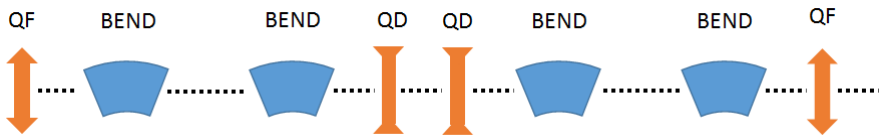

Figure 4.1: One sixteenth of the ring. Each fraction is composed by a FODO structure. The BEND elements are the electrostatic deflectors while QF and QD stands for focusing quadrupole and defocusing quadrupole respectively. Black dots are the drifts.

Because the ring has only electric bending, one can totally freeze the spin if the particles have a particular "magic" energy. This can only be done with protons.

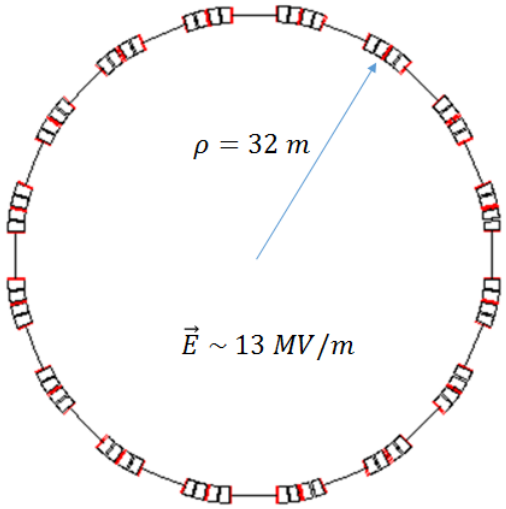

Figure 4.2: Final ring simplified lattice. The ring is a fully electric 500m long storage ring.

The following table shows the principal parameters used in the ring and the deflectors:

Ring specifications						
Particles	Length	Nbend	Energy	Gamma	Q_x	Q_y
Protons	500 m	64	232 MeV	1.2481	0.40	0.45

Deflector specifications				
Length	Radius	Angle	Gap	Field
3.14 m	32 m	$\pi/32$	0.03 m	13 MV/m

Fringe fields specifications				
Starting	End	Length	Diaphragm	G
- 3 · G	+ 5 · G	8 · G	5 · G	0.03 m

As BMAD is not providing electrostatic quadrupoles, the focusing is done with magnetic quadrupoles, but their effect on spin is turned off to zero. The transfer matrix for spin is forced to be the identity matrix.

4.2.2 Use of the RF cavity

Using a RF cavity is mandatory to reach more than a few milliseconds of spin coherence time [25] due to momentum spread of the beam.

Even if the energies of the particles in the beam are not the same, the synchrotron oscillations(see fig(4.3)) induced by the cavity will mix the energies around an average value of zero.

To get this effect, the cavity should be tuned with respect to the synchronous particle (i.e tuned at the zero phase).

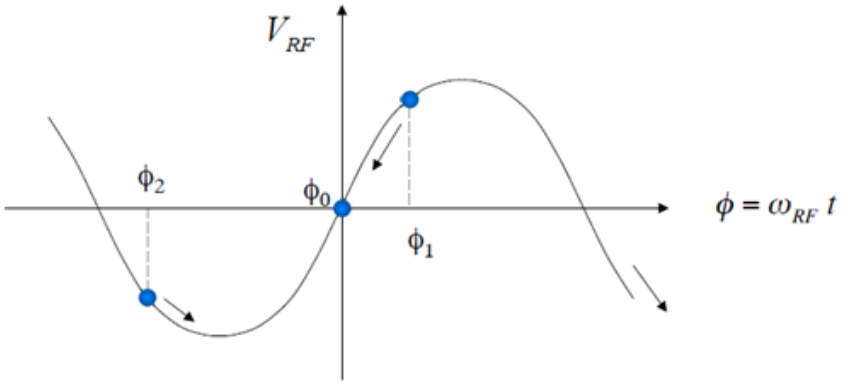

Figure 4.3: Effect of the RF Cavity on a non-synchronous particle. A particle with more energy than the reference particle arrives in advance and sees a decelerating field, and vice versa [26].

As my analysis only concerns the effect of the electrostatic deflectors, a zero length RF cavity, working as a "kick" in energy is a sufficient approximation.

The energy kick given by the cavity is proportional to the synchrotron phase:

$$\Delta E = -e \cdot V \cdot sin(2\pi \cdot (\phi_t - \phi_{ref}))$$

where e is the charge of the electron, V the voltage of the cavity, ϕ_t the phase of the particle and ϕ_{ref} the phase of the reference (also synchronous) particle.

I used in my case a voltage of -10 000 V which is close to the minimum value necessary to eliminate the off-momentum effect on the spin (see fig (4.4).

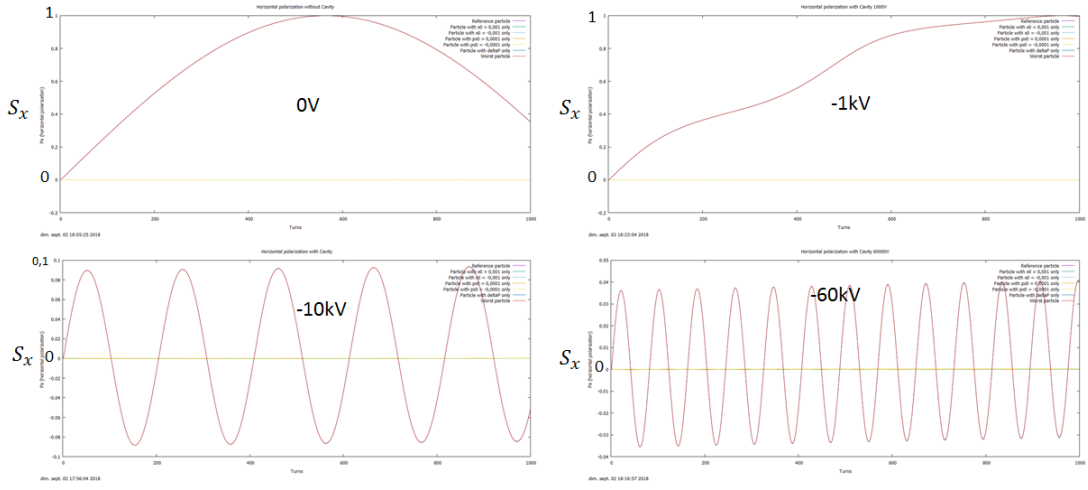

Figure 4.4: Evolution of the horizontal spin polarisation of an off-momentum particle for different voltages of the cavity over 1000 turns. The spin starts to oscillate around zero for a certain value, which is the minimum required for the RF cavity.

4.2.3 Implementation of the fringe fields

The objective with the fringe fields is to quantify their effect on the spin coherence time.

The most intuitive way is to simulate two different lattices, one with and one without the fringe fields.

The fringe field starts inside the "physical" deflector (we estimated it to start at -3 Gap inside the deflector) and stops after the deflector at an arbitrary distance D.

Including the fringe field as a new element implies to change the length of the deflectors and drifts in a manner that the lattice length and the total angle of the deflector are not changed, in the simple way shown in figure (4.5).

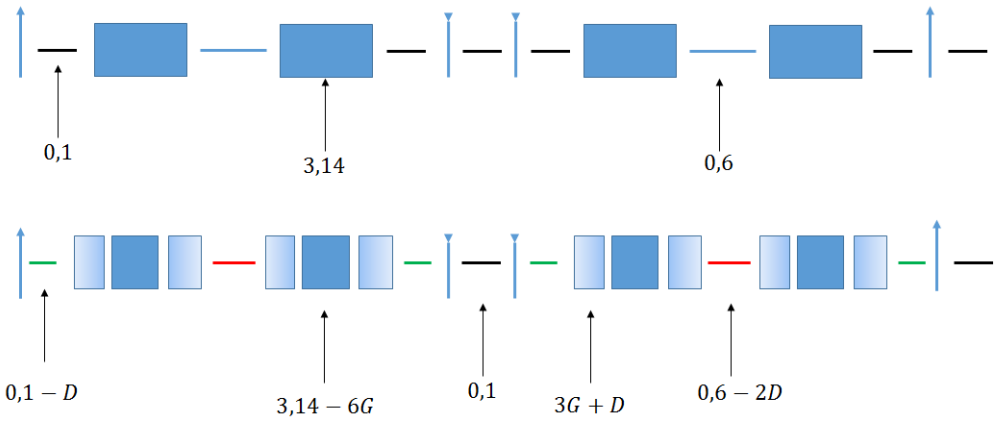

Figure 4.5: Inserting a new element as fringe fields changes some dimensions of others elements.

Additionally, the betatron oscillations have a non negligible effect on the spin dynamics. One must re-tune the new lattice so that the vertical and horizontal tunes (i.e the number of betatron oscillations per turn) are the same for the lattice with and without fringe fields. Betatron and dispersion functions are shown in figure (4.6).

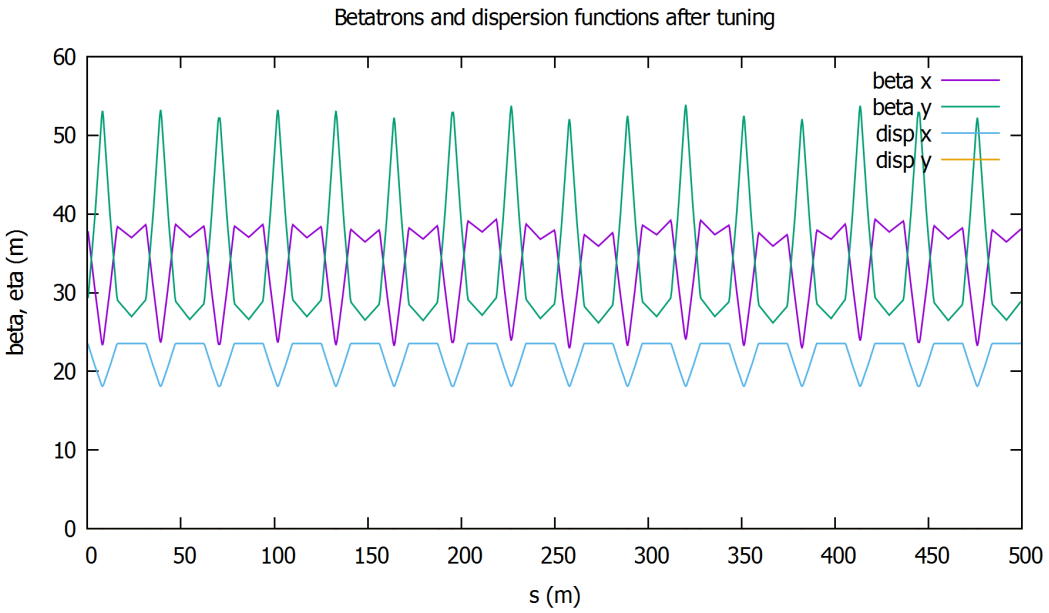

Figure 4.6: Betatron functions and dispersion along the lattice with fringe fields.

As the clockwise and counter-clockwise method requires to measure a difference in the vertical position of the two beams, very large betatron functions for the transverse vertical plan are needed, so the vertical tune should be as small as possible.

4.3 Results, analysis, discussion

4.3.1 Observation of standard spin motion effects

Many effects on spin dynamics are well known and can be easily detected. I used such effects to benchmark the model (both for trajectories and spin) of the deflector.

4.3.1.1 On a quasi-frozen spin (QFS) lattice

I first applied the spin dynamics model for the deflectors and fringe fields on a quasi-frozen spin lattice (See [27]).

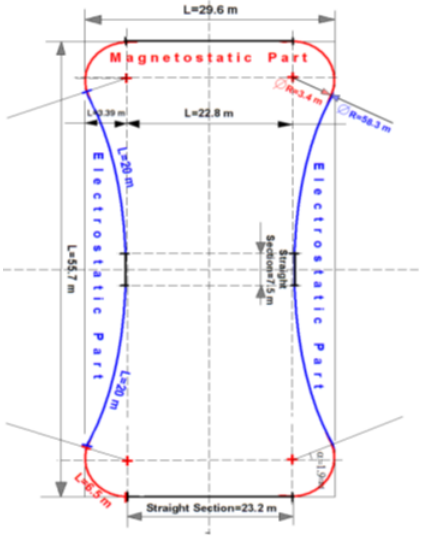

Figure 4.7: Quasi-frozen spin lattice with successive magnetic and electric fields with bone-shape. The stored particles are deuterons with an energy of 270 MeV. The electrostatic deflectors have a radius of 42m, a length of 3.6m and an electric field of 12MV/m.

The quasi-frozen spin scenario uses both electric and magnetic bending. With no EDM, the spin of the reference particle should oscillate horizontally around a fully longitudinal polarisation (i.e. around $S_x = 0, S_y = 0, S_z = 1$).

By using the BMAD standard spin tracking method for the magnetic elements and the model developed in this thesis for the electric elements, one can qualitatively check the behavior of the model.

Figure (4.8) shows the evolution of the polarisation of the reference particle along one turn of the QFS lattice.

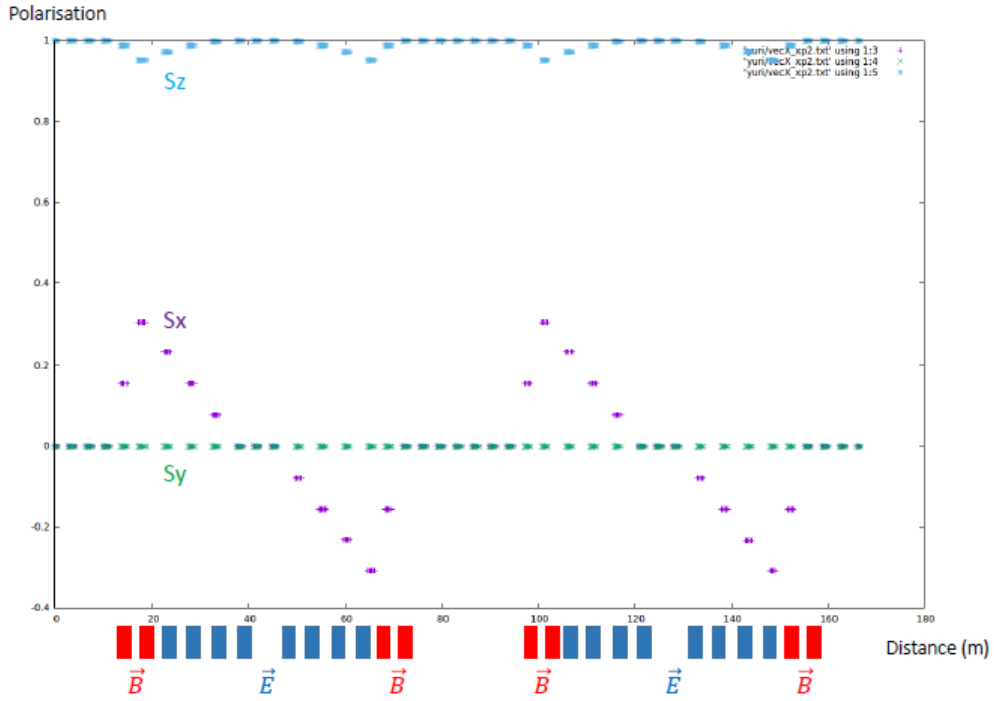

Figure 4.8: Spin evolution of the reference particle along one turn of a quasi-frozen spin lattice. The spin is oscillating around a fully longitudinal polarisation with opposite contributions for the magnetic and electric elements, as expected.

4.3.1.2 Effect of the synchrotron oscillations - RF cavity

Adding a RF cavity to the machine allows to mix the momentum of the off-momentum particles. The direct consequence is that the average energy of each particle is the same as the reference particle on many turns.

This is a fundamental step as all the particles must be at the magic energy to freeze the horizontal polarisation.

Figures 4.9 and 4.10 shows the evolution of the particles' spin without and with the RF cavity.

One can, with this method, totally cancel the first order contribution of $\frac{\Delta P}{P_0}$ on the spin decoherence.

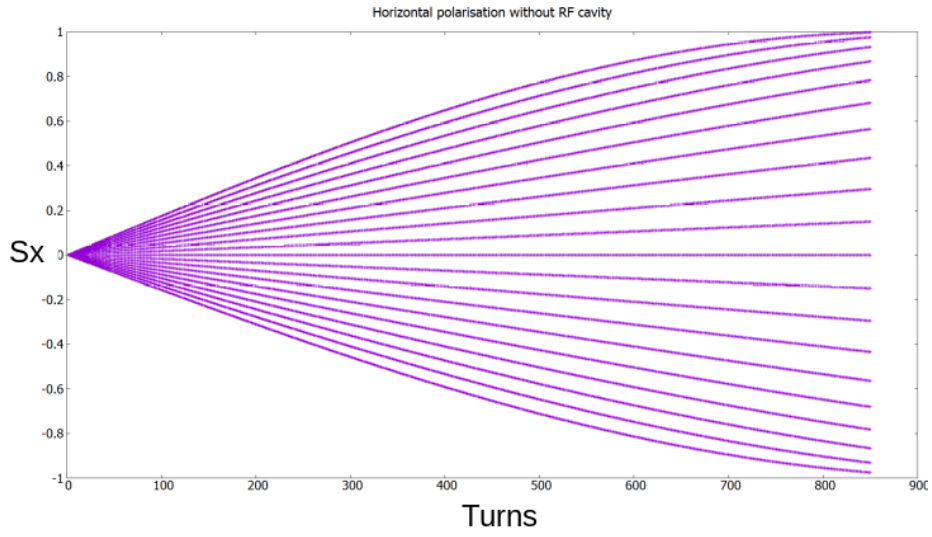

Figure 4.9: Evolution of the spins of a beam of particles without the RF cavity. The particles are distributed uniformly in energy in the range $\frac{\Delta P}{P_0} \in [-5 \cdot 10^{-4}; 5 \cdot 10^{-4}]$. The spin of the worst particles (i.e. having the most energy) is rotating horizontally by around $\pi/2$ radian after less than a thousand turns. In this case, the spin coherence time is only a few milliseconds.

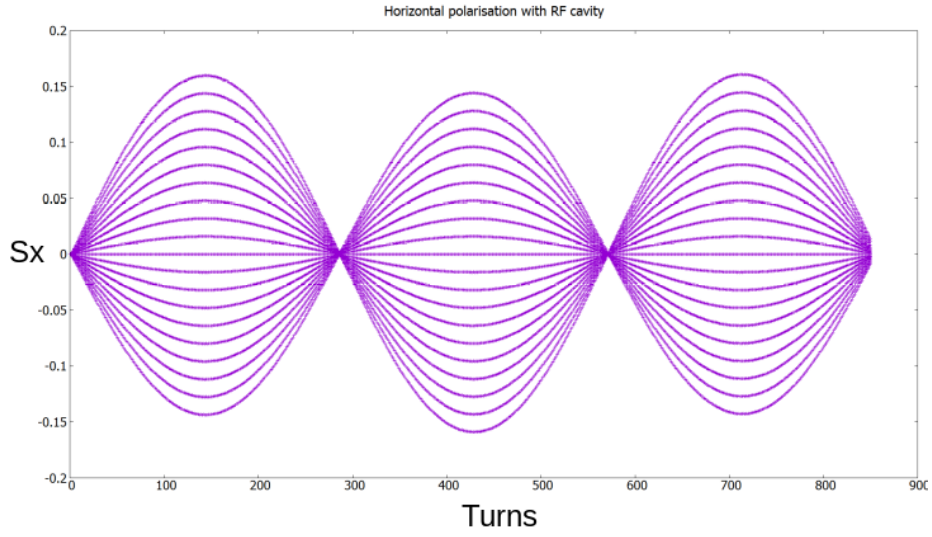

Figure 4.10: Evolution of the spins of a beam of particles with the RF cavity. The particles are distributed uniformly in energy in the range $\frac{\Delta P}{P_0} \in [-5 \cdot 10^{-4}; 5 \cdot 10^{-4}]$. Due to synchrotron oscillations, the spins stay in the range $S_x \in [-0.15; 0.15]$ and the beam spin coherence time can be extended by many orders of magnitude (up to few seconds).

4.3.2 First and second order effects

This model has the particularity to explicit the different contributions of the phase space coordinates on the spin dynamics.

One can first observe a zero order contribution to the spin rotation for the deflector:

$$R_{11cste} = 1 - \frac{L^2 \cdot F_{00}^2}{8 \cdot \rho_0^2} \tag{4.2}$$

$$R_{12cste} = \frac{1}{2} \cdot \frac{L \cdot F_{00}}{\rho_0} \tag{4.3}$$

with

$$F_{00} = \frac{\gamma_0^2 - \gamma_m^2}{\gamma_m^2 - 1}$$

The component (4.2) is strictly one for a frozen-spin lattice as $F_{00} = 0$ if γ_0 is the magic energy, which means no rotation.

In the case of a non frozen-spin lattice, as the previous quasi frozen-spin lattice shown in part 4.3.1.1, this component is not zero and corresponds to a constant rotation of the spin each time a particle goes through a deflector.

Additionally to this zeroth order rotation, one can observe first order and second order rotations, whose behaviors are totally different.

4.3.2.1 Linear effects

First order effects include the effect of $x_0, p_{x0}, p_{y0}, \frac{\Delta P}{P_0}$ for the inner part and the fringe fields of the deflector. As the electrostatic potential only depends on the x position, y_0 and z_0 have no effects on the spin dynamics.

Each effect is represented by four components in the spin transfer matrix, corresponding to the A, B, C, D values of equation (4.1). They correspond to the real ($\mathcal{R}$) and imaginary ($\mathcal{I}$) parts of the R_{11} and R_{12} components of the rotation matrix.

Tables (4.3.2.1) and (4.3.2.1) shows the values of the first order effects for the machine scenario presented in part 4.2:

Deflector				
/	$\mathcal{R}[R_{11}]$	$\mathcal{I}[R_{11}]$	$\mathcal{R}[R_{12}]$	$\mathcal{I}[R_{12}]$
x_0	0	0	-2.45E-3	0
p_{x0}	0	0	-3.85E-3	0
p_{y0}	0	0	0	0
$\frac{\Delta P}{P_0}$	0	0	7.85E-2	0

Exit fringe field				
/	$\mathcal{R}[R_{11}]$	$\mathcal{I}[R_{11}]$	$\mathcal{R}[R_{12}]$	$\mathcal{I}[R_{12}]$
x_0	0	0	-6.61E-5	0
p_{x0}	0	0	-2.93E-6	0
p_{y0}	0	0	0	$< 10^{-9}$
$\frac{\Delta P}{P_0}$	0	0	2.5E-3	0

Only the exit fringe field is shown here as the value slightly differs from the entrance fringe field. Most of the values are equal to zero in this case as the ring works at the magic energy (i.e F00 = 0).

The first order effects are strong effects and can lead to a fast spin decoherence.

Fortunately, first order effects can be averaged to zero after multiple turns by averaging the associated coordinate to zero with the use of betatron and synchrotron oscillations (see part 4.3.1.2 on the cavity for the example of the energy). By this method, spin coherence time can be increased from a few milliseconds to a few seconds.

4.3.2.2 Quadratic and crossed terms

Second order effects include all the quadratic and crossed-term effects. There amplitude is few orders of magnitude lower than the 1st order effects.

However, unlike linear effects, quadratic effects (and sometimes crossed-terms) cannot be averaged to zero on multiple turns. Even if these effects have lower amplitudes, they become non negligible on a long time scale (> 1 s).

A particular attention should be pay to these effects.

The following tables show the values of the 2nd order terms in the rotation matrix for the studied ring:

Deflector				
/	$\mathcal{R}[R_{11}]$	$\mathcal{I}[R_{11}]$	$\mathcal{R}[R_{12}]$	$\mathcal{I}[R_{12}]$
x_0^2	-2.66E-6	0	-9.48E-5	0
p_{x0}^2	-1.48E-6	0	-3.84E-4	0
p_{y0}^2	-1.84E-10	0	0	0
$\frac{\Delta P}{P_0}^2$	-2.77E-3	0	-0.133	0
$x_0 \cdot px_0$	-7.65E-6	0	-4.95E-4	0
$x_0 \cdot \frac{\Delta P}{P_0}$	1.71E-4	0	8.36E-3	0
$x_0 \cdot p_{y0}$	0	2.31E-3	0	0
$p_{x0} \cdot \frac{\Delta P}{P_0}$	2.53E-4	0	2.20E-2	0
$p_{x0} \cdot p_{y0}$	0	3.43E-3	0	0
$\frac{\Delta P}{P_0} \cdot p_{y0}$	0	-7.40E-2	0	0

This time again, many values are equal to zero as they depend on the $F - 00$ factor, which is zero for a magic ring.

All the computations have been done up to α^3 with $\alpha = \frac{G}{\rho} \approx 10^{-3}$. Effects $< 10^{-9}$ are higher order effects and have been neglected for now.

Fringe Field				
/	$\mathcal{R}[R_{11}]$	$\mathcal{I}[R_{11}]$	$\mathcal{R}[R_{12}]$	$\mathcal{I}[R_{12}]$
x_0^2	$< 10^{-9}$	0	$< 10^{-9}$	0
p_{x0}^2	$< 10^{-9}$	0	$< 10^{-9}$	0
p_{y0}^2	$< 10^{-9}$	0	0	0
$\frac{\Delta P}{P_0}^2$	-1.90E-5	0	-9.58E-3	0
$x_0 \cdot px_0$	$< 10^{-9}$	0	$< 10^{-9}$	0
$x_0 \cdot \frac{\Delta P}{P_0}$	0	0	1.01E-3	0
$x_0 \cdot p_{y0}$	0	3.31E-5	0	$< 10^{-9}$
$p_{x0} \cdot \frac{\Delta P}{P_0}$	0	0	3.09E-5	0
$p_{x0} \cdot p_{y0}$	0	4.88E-5	0	$< 10^{-9}$
$\frac{\Delta P}{P_0} \cdot p_{y0}$	0	2.51E-3	0	2.07E-4

The case of $\frac{\Delta P}{P_0}^2$

The most noticeable quadratic effect is the $\frac{\Delta P}{P_0}^2$ effect. Even with the use of synchrotron oscillations, this effect cannot be averaged to zero and induce a slow but linear increase of the horizontal spin component of the off-momentum particle.

Figure (4.11) shows the evolution of the spin of an off-momentum particle due to $\frac{\Delta P}{P_0}$ effects.

The $\frac{\Delta P}{P_0}^2$ effect has an important effect on the horizontal polarisation as it induces a constant rotation of the spin over time, not cancelled by synchrotron oscillations.

The effect on the total beam polarisation is that all the off-momentum particles will undergo a different slope (with zero rotation for the reference particle), leading to a slow beam decoherence.

Figure (4.12) shows the decoherence effect for a beam of a few particles.

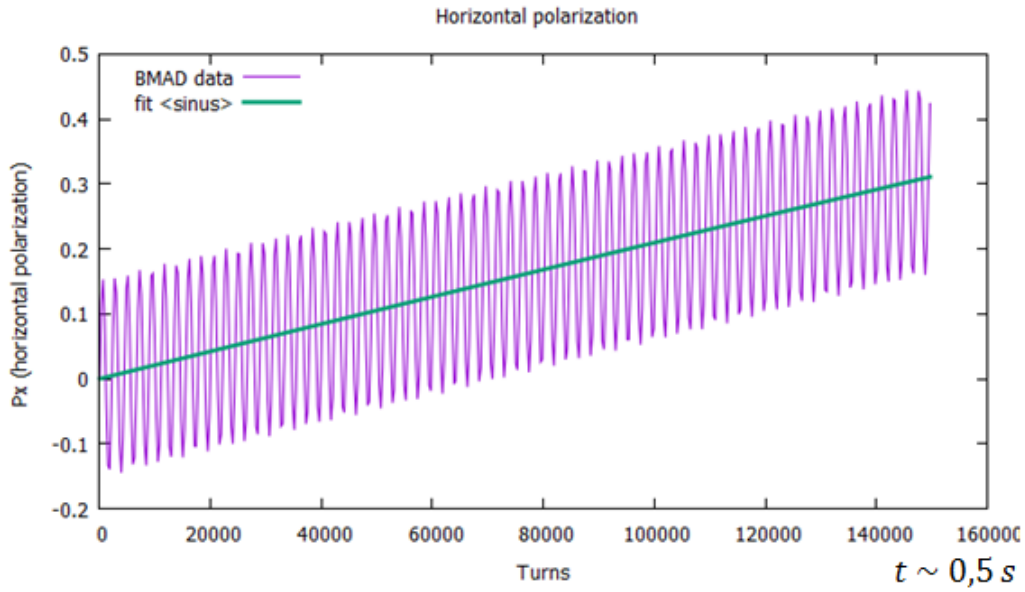

Figure 4.11: Evolution of the spin of an off-momentum particle on 150 000 turns, corresponding to approximately 0.5 seconds. The particle initially has no position and transverse momentum offset, but only a longitudinal momentum difference with respect to the reference particle. We can observe both the effect of 1st and 2nd order terms. The first order term makes the spin oscillate quickly and averaged to zero. The second order component induces a slope in the oscillations.

By looking at figure (4.12), a beam with a reference particle and a particle with $\frac{\Delta P}{P_0}$ will have approximately a spin coherence time of 10 seconds.

As this effect has a square dependence in $\frac{\Delta P}{P_0}$, decreasing the energy difference by a factor 10 (i.e from $\frac{\Delta P}{P_0} = 5.10^{-4}$ to $\frac{\Delta P}{P_0} = 5.10^{-5}$ for example) will decrease this effect by a factor 100.

These are preliminary results, and a mistake (from simulation or analytical computations) cannot be excluded. More investigations on this point are needed.

The analytical model allows us to isolate this effect and study it independently. Moreover, this machine is a simplified machine and is not totally optimised. No sextupoles are implemented and they can allow us to correct many effects.

Other quadratic effects

The other quadratic effects present the same behavior as the one for $\frac{\Delta P}{P_0}^2$. Figure (4.13) shows the evolution of the spin of a particle for different initial conditions.

We still observe a (small) oscillating behavior due to first order effects and the quadratic effects for the other components that add up. However the energy dependence remains dominant.

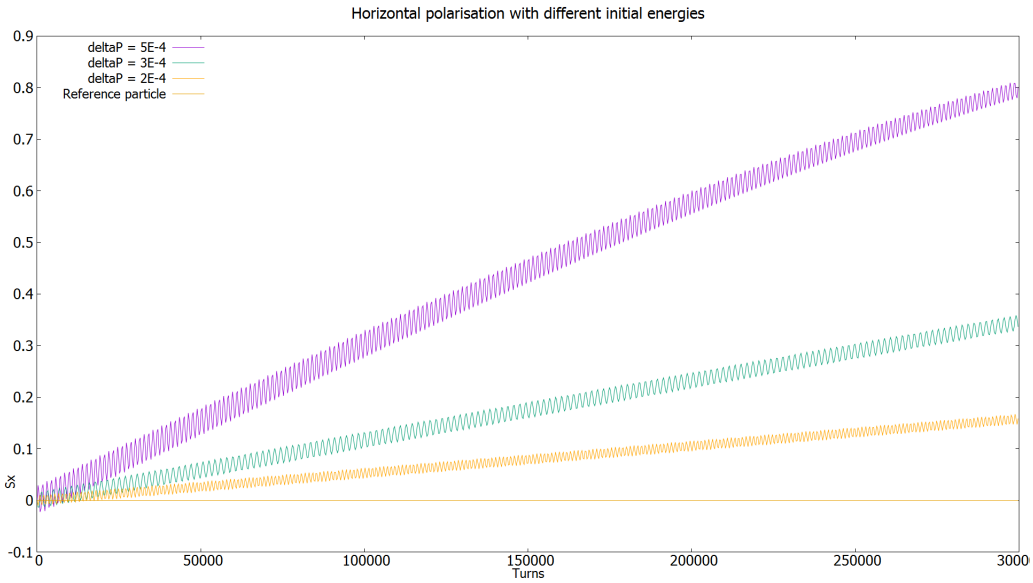

Figure 4.12: Spin decoherence induced by the second order energy component for a beam of particles. The reference particle stays at zero horizontal spin component while other particles undergo different precession frequencies.

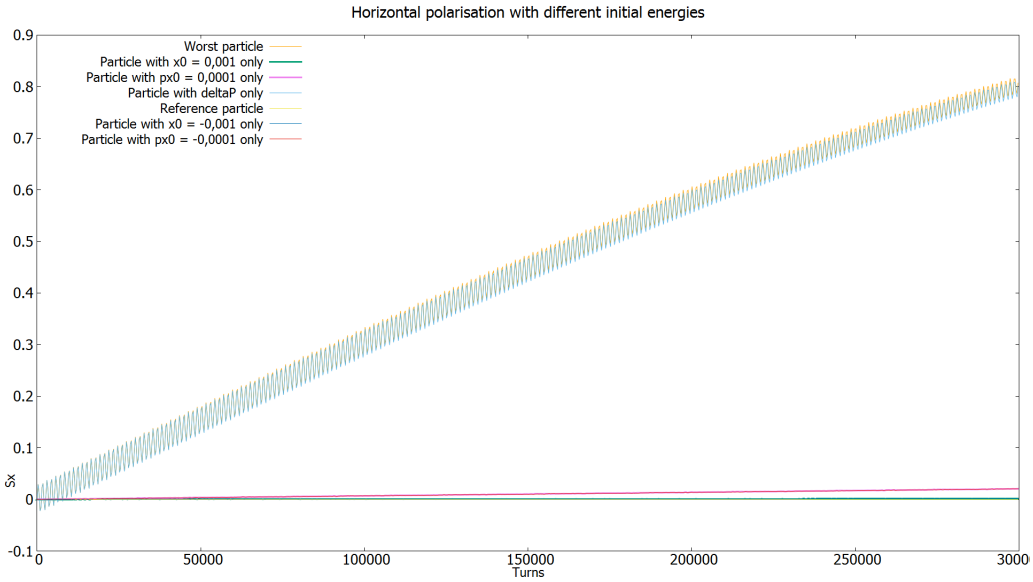

Figure 4.13: Evolution of the horizontal spin component of a particle with different initial conditions: x_0 only, p_{x0} only, $\frac{\Delta P}{P_0}$ only and a particle with x_0, p_{x0} and $\frac{\Delta P}{P_0}$ called the "worst particle".

Effect of crossed-terms

Crossed terms surprisingly appear to have a non negligible effect on the spin dynamics. Especially, the $x_0 \cdot \frac{\Delta P}{P_0}$ and $p_{x0} \cdot \frac{\Delta P}{P_0}$ components have a non-zero average value on

multiple turns.

The effect of the $x_0 \cdot \frac{\Delta P}{P_0}$ and $p_{x0} \cdot \frac{\Delta P}{P_0}$ crossed components has an opposite amplitude as compared to the quadratic effects (see table 4.3.2.2) and creates a compensating rotation of the spin.

Hypothesis: This could be due to the sign difference in the energy gamma factor: $V - \frac{\Delta P}{P_0}$ *as* V *depends mainly of* x*.*

Figure (4.14) shows the total rotation of the spin on 1 second tracking with all components enabled.

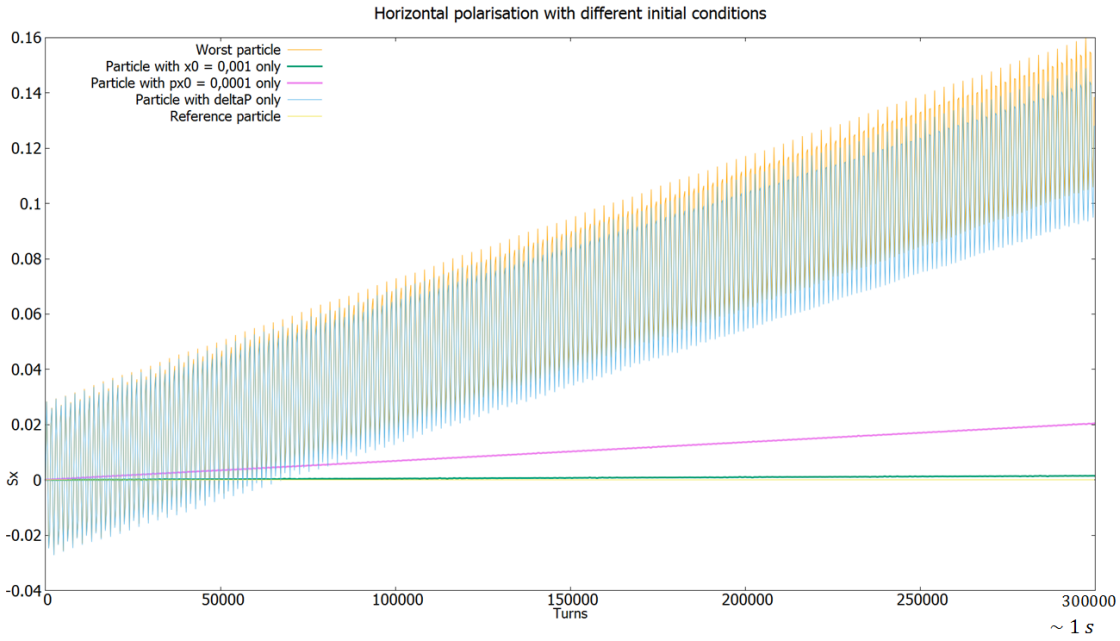

Figure 4.14: Evolution of the horizontal spin component of a particle with different initial conditions: x_0 only, p_{x0} only, $\frac{\Delta P}{P_0}$ only and a particle with x_0, p_{x0} and $\frac{\Delta P}{P_0}$ called the "worst particle".

Average energy issue: ***still under investigation***

Actually, the average value of the energy is not exactly zero, even with the RF cavity (see figure (4.15)).

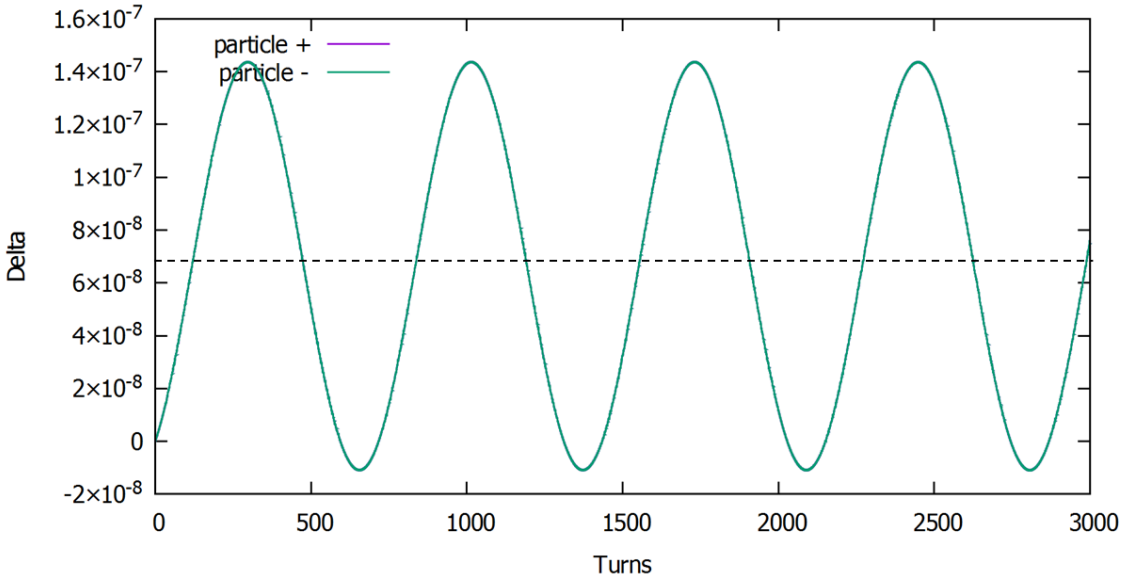

Figure 4.15: Average value of $\Delta P/P_0$ for a particle with no initial $\Delta P/P_0$ and other initial conditions. The value oscillates around an average value that is not exactly zero. This value depends on the initial conditions of the particle and does not depend on the initial $\Delta P/P_0$.

This issue has also been observed on an other lattice (COSY magnetic lattice) with BMAD using different tracking methods. This creates a linear depolarisation in time and adds up to other effects. Many leads have been proposed, including a core code issue and this is still under investigation.

A fast estimate

One can get a first estimate on the spin coherence time by looking at the transfer matrix amplitudes and the average values of the coordinates.

/	Average	$\mathcal{R}[R_{12}]$	$\mathcal{R}[R_{12}]$·Average	Sum	Sum·$N_{defl} \cdot N_{turns}$
$\frac{\Delta P}{P_0}$	$7.3 \cdot 10^{-8}$	$7.85 \cdot 10^{-2}$	$5.73 \cdot 10^{-9}$	$7.88 \cdot 10^{-9}$	$S_x = 0.15$
$\frac{\Delta P}{P_0}^2$	$7.5 \cdot 10^{-8}$	-0.14	$-1.05 \cdot 10^{-8}$		
x_0^2	$1.5 \cdot 10^{-6}$	$8.4 \cdot 10^{-3}$	$1.26 \cdot 10^{-8}$		
p_{x0}^2	$2.1 \cdot 10^{-9}$	$2.2 \cdot 10^{-2}$	$4.6 \cdot 10^{-11}$		

By multiplying the average value of a component by its associated value in the transfer matrix, one can have an estimate of the average effect on the spin dynamics at each passage through a deflector.

If we sum the main contributions and multiply them by the number of deflectors in the lattice and by the number of turns done by the particle, we can have a really fast estimate of the final angle of rotation.

Remark: the $\mathcal{R}[R_{12}]$ term is the one leading to an horizontal rotation of the spin.

4.3.3 Effect of fringe fields on the SCT

Adding the fringe fields leads to the presence of additional components in the spin rotation matrix, and a perturbation in the particles trajectories.

Effect on horizontal polarisation

Figure (4.16) shows the evolution of the spin of a particle in a lattice including fringe fields. The lattice has been re-tuned for the horizontal and vertical tunes to correspond to the lattice without fringe fields.

By comparing figure (4.16) with fringe fields, to figure (4.14) without fringe fields we observe a different final horizontal polarisation of the "worst particle".

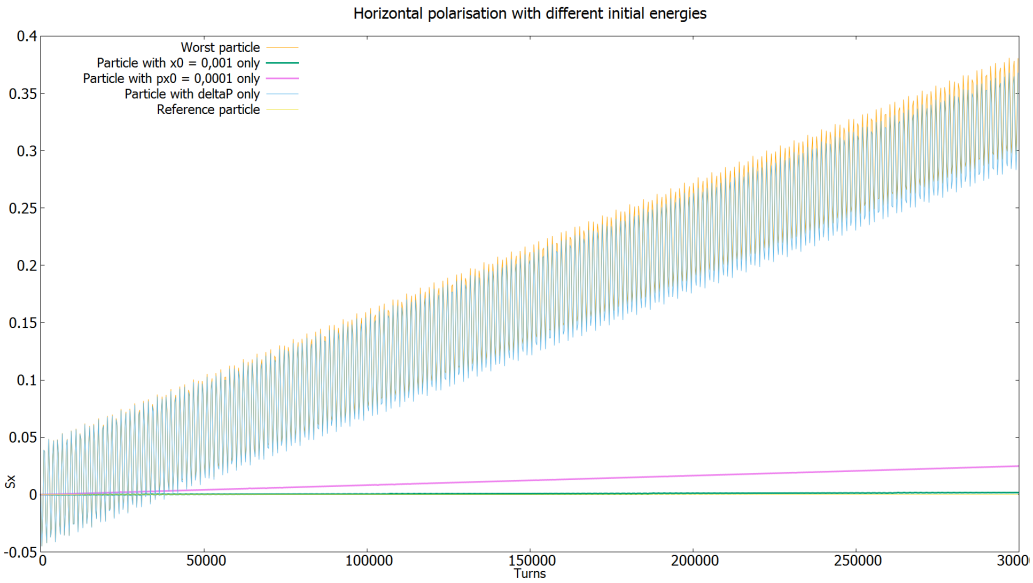

Figure 4.16: Evolution of the horizontal spin component of a particle with different initial conditions: x_0 only, px_0 only, $\frac{\Delta P}{P_0}$ only and a particle with x_0, px_0 and $\frac{\Delta P}{P_0}$ called the "worst particle". Fringe fields are this time included.

This final polarisation is bigger with a factor ≈ 2.5 when fringe fields are included. However, this plot has been obtained while the average energy issue presented few paragraphs earlier is not solved. More investigations are needed.

Effect on vertical polarisation

No vertical polarisation is created when adding the fringe field model ($S_y < 10^{-17}$). As mentioned before with the table of the fringe field components, higher order effects should be taken into account.

4.4 Analyse et implémentation avec le code BMAD - Résumé en français

Je présente dans ce chapitre les premiers résultats obtenus par le modèle décrit dans les chapitres précédents. Ce modèle a été complètement implémenté dans le code de calcul BMAD.

BMAD est une librairie de subroutines de simulations pour des accélérateurs de hautes énergies et les anneaux de stockage.

J'ai implémenté des routines personalisées pour le calcul des trajectoires et du spin des particules à la fois dans la partie centre et aussi pour les champs de fuites d'un déflecteur électrostatique.

La routine de tracking de spin créée une matrice de transfert :

$$R(\theta) = \begin{bmatrix} A + i \cdot B & C + i \cdot D \\ -\bar{R_{12}} & \bar{R_{11}} \end{bmatrix}$$

avec :

$$A = a_1 \cdot x_0 + b_1 \cdot p_{x0} + c_1 \cdot \left.\frac{\Delta P}{P_0}\right|_0 + d_1 \cdot x_0^2 + e_1 \cdot x_0 \cdot p_{x0} + ...$$

$$B = a_2 \cdot x_0 + b_2 \cdot p_{x0} + c_2 \cdot \left.\frac{\Delta P}{P_0}\right|_0 + d_2 \cdot x_0^2 + e_2 \cdot x_0 \cdot p_{x0} + ...$$

$$C = a_3 \cdot x_0 + b_3 \cdot p_{x0} + c_3 \cdot \left.\frac{\Delta P}{P_0}\right|_0 + d_3 \cdot x_0^2 + e_3 \cdot x_0 \cdot p_{x0} + ...$$

$$D = a_4 \cdot x_0 + b_4 \cdot p_{x0} + c_4 \cdot \left.\frac{\Delta P}{P_0}\right|_0 + d_4 \cdot x_0^2 + e_4 \cdot x_0 \cdot p_{x0} + ...$$

puis applique la rotation :

$$\begin{bmatrix} \Psi_1 \\ \Psi_2 \end{bmatrix}_{exit} = \begin{bmatrix} A + i \cdot B & C + i \cdot D \\ -\bar{R_{12}} & \bar{R_{11}} \end{bmatrix} \cdot \begin{bmatrix} \Psi_1 \\ \Psi_2 \end{bmatrix}_{init} \tag{4.4}$$

Tous les coefficients $a_i, b_i, c_i...$ sont calculés pendant la phase d'initialisation et sont donnés en annexe. Ils ne changent jamais de valeur pendant la simulation et ne dépendent que des paramètres d'entrée ($\rho, G, longeur...$).

L'anneau de stockage étudié est un anneau complètement électrostatique. Il est composé de 64 déflecteurs divisés dans 16 mailles FODO. Cette machine s'inscrit dans un scénario de type "frozen spin".

Plusieurs effets d'ordre 1 émergent du modèle comme l'annulation de l'effet du à $\Delta P/P$ par la cavité RF.

Premiers résultats Les premiers résultats montrent que les effets d'ordre 1 sont nuls en moyenne. Cela est dû aux oscillations betatron et synchrotron qui forcent les composantes d'ordre 1 (x, p_x, $\Delta P/P$) à être nulles en moyenne.

Les effets d'ordre deux, et en particulier les effets quadratiques semblent, quant à eux, être non négligeables car non nuls en moyenne. L'effet lié à $(\Delta P/P)^2$ semble contraindre le temps de cohérence de spin à rester en dessous de 10 secondes, pour un $\Delta P/P$ initial de 5.10^{-4}.

Cependant, ces anomalies peuvent toujours être liées à des erreurs externes comme une erreur résiduelle dans les calculs, ou une erreur de code.

De plus, la machine étudiée n'est pas optimisée et elle ne contient pas de sextupoles, qui sont en général nécessaires pour augmenter le temps de cohérence de spin.

Conclusion

As mentioned in the introduction, one needs accurate models for the deflectors and fringe fields to perform an EDM measurement in a storage ring.

Tools developed My thesis provides all the tools necessary to compute the electrostatic field, trajectories and spin dynamics in an entire deflector, including fringe fields.

All the work has been done from scratch and asked a lot of rigor and verification. The BMAD code does not include analytical models for an electrostatic deflector or fringe fields. Also other codes like COSY Infinity work as a black box and do not allow deeper investigations.

We developed specific (i.e. for our needs) methods for differential equation solving and for numerical integrals computation.

Field computations have been done using conformal mapping, and we now have an analytical, universal and realistic model for the fringe field of an electrostatic deflector.

Equations of motion have been solved using the Hamilton equations, and trajectories are given up to order two in both the inner and fringe field part of the deflector.

Finally, spin dynamics can be described up to order two for the entire deflector.

Universal and analytical model The model developed in this thesis is a universal model depending only on the ratio between the gap and the radius of the deflector, for a given position of the boundary conditions.

This is very useful as no field map has to be recomputed if one changes the dimensions of the deflector. This can be for example convenient for lattice design.

Also, we give an analytical model for spin dynamics up to the second order. This allows us to analyse independently the effects on spin dynamics by two methods:

- By the analytical formula directly.
- In the tracing code by enabling/disabling the different terms acting on spin.

Analysis The test and analysis phase are still preliminary. The model has been tested at order one by the visualisation of known effects. More investigations have to be done at second order to provide a final conclusion. The anomalies linked to $\Delta P/P_0$ emerging from the model could be due to:

- A residual error in the calculations. However, many crossed-checks and verification have already been done.
- As the anomalies are induced by very small numbers (generally $< 10^{-}7$), it could be due to a code issue, machine precision...
- Also, the machine is not yet optimised. Sextupoles will be necessary to reach a better spin coherence time.

Conclusion - Français

Il a été précisé en introduction de cette thèse qu'une grande compréhension et maîtrise de la dynamique de spin dans un anneau de stockage est essentielle pour la mesure précise de la valeur d'un EDM. Les déflecteurs électrostatiques sont la partie centrale de l'expérience et des modèles plus justes et précis peuvent aider à mieux contrôler leurs effets sur le spin.

Ma thèse fournit un modèle universel et réaliste pour le champ, les trajectoires et la dynamique de spin dans un déflecteur, incluant champs de fuite. Le code BMAD ne possède pas de modèle analytique pour un déflecteur électrostatique et le travail a du être mené entièrement, du calcul de champ, à la dynamique de spin.

Nous avons développé des méthodes spécifiques à notre problème, pour la résolution d'équations différentielles et le calcul numérique d'intégrales.

Le champ de fuite a été calculé par transformations conformes et inclut des électrodes réalistes et des conditions aux limites.

Les équations du mouvement sont calculées à l'ordre 2 à partir des équations d'Hamilton et dépendent des intégrales du champ calculé précédemment dans le cas des champs de fuite.

Enfin, la dynamique du spin est décrite à l'ordre deux dans le déflecteur complet.

Les fonctions de transfert de spin sont des fonctions des coordonnées de l'espace des phases avant l'entrée dans le déflecteur. Ces fonctions sont aussi, dans le cas des champs de fuite, dépendantes d'intégrales de champs calculées en amont, et qui restent fixées lors de la simulation.

Le modèle final est un modèle universel, ne dépendant que du ratio gap/rayon. Cela permet des calculs plus rapides pour du développement de machine par exemple, puisque aucune carte de champs n'a à être recalculée.

De plus, le caractère analytique du modèle nous permet d'étudier indépendemment les effets sur la dynamique de spin par :

- l'étude directe des formules analytiques.
- l'étude via le code de simulation en choisissant d'activer ou non les différentes composantes.

Les résultats et tests provenant du modèle sont pour l'instant au stade préliminaire.

Le modèle a été testé à l'ordre 1 par la visualisation de plusieurs effets connus. Une analyse plus poussée est cependant nécessaire pour les effets d'ordre deux.

Les anomalies liées au terme en $\Delta P/P$ émergeant du modèle peuvent être dues à plusieurs aspects :

- Une erreur résiduelle dans les calculs. Cependant, le modèle a été vérifié de manière indépendante à de multiples reprises par trois personnes.
- Les anomalies apparaissent à de très faibles ordres de grandeur ($< 10^{-7}$), et peuvent être liées à un problème interne au code de calcul ou à la précision de l'ordinateur.
- La machine n'est pas optimisée. L'ajout de sextupoles peut, par exemple, améliorer grandement le temps de cohérence de spin.

Bibliography

[1] V. Bargmann, L. Michel, and V.L. Telegdi, "Precession of the polarization of the particles moving in a homogeneous electromagnetic field" , Phys. Rev. Lett. 2, 435 (1959).

[2] Planck Collaboration et al. "Planck 2013 results. XVI. Cosmological parameters". In: A&A 571 (2014), A16. doi: 10.1051/0004-6361/201321591. url: https://doi.org/10.1051/0004-6361/201321591.

[3] J. Pretz: "Measurement of Permanent Electric Dipole Moments of Proton, Deuteron and Light Nuclei in Storage Rings", 5th International Symposium on Symmetries in Subatomic Physics - June 18 - 22, 2012. KVI, Groningen, Netherlands

[4] J. H. Christenson, J. W. Cronin, V. L. Fitch and R. Turlay, "Evidence for the 2π Decay of the K_2^0 Meson," Phys. Rev. Lett. **13** (1964) 138. doi:10.1103/PhysRevLett.13.138

[5] F. Abusaif *et al.*, "Feasibility Study for an EDM Storage Ring," arXiv:1812.08535 [physics.acc-ph].

[6] Y. Senichev*:* "Frozen and Quasi-frozen spin lattices", CERN Kickoff Meeting - March 13 - 14, 2017. CERN

[7] E. Durand*:* "Electrostatique et magnétostatique", Paris Masson 1953, cop. 1953

[8] D. Zyuzin, R. Maier, Yu. Senichev*:* "High order non-linear motion in electrostatic rings", Institute for Nuclear Physics, Forschungszentrum Juelich, D-52425 Juelich, Germany

[9] Jorg Pretz.*:* "Measurement of permanent electric dipole moment of charged hadrons in storage rings". In: Hyperfine Interactions 214.1 (2013) http://dx.doi.org/10.1007/s10751-013-0799-4.

[10] T. Zolkin*:* B"MT Equation Analysis and Spin in Accelerator Physics", The University of Chicago, Department of Physics

[11] Laurent Nadolski.*:* "Application de l'Analyse en Fréquence à l'Etude de la Dynamique des Sources de Lumière". Physique [physics]. Université Paris Sud - Paris XI, 2001. Français.

[12] Alex J. Dragt and Etienne Forest*:* "Computation of nonlinear behavior of Hamiltonian systems using Lie algebraic methods". Journal of Mathematical Physics 24, 2734 (1983); https://doi.org/10.1063/1.525671

[13] Blanes, Sergio & Casas, Fernando & Oteo, J.A. & Ros, J. (2008). textit: "The Magnus expansion and some of its applications". Physics Reports, 470(5-6), 151-238. Physics Reports. 470. 151-238. 10.1016/j.physrep.2008.11.001.

[14] Jean-Marie De Conto*:* Internal note: "Semi-infinite box potential"

[15] Yu. Senichev*:* "INVESTIGATION OF LATTICE FOR DEUTERON EDM RING", Proceedings of ICAP2015, Shanghai, China

[16] Yu. Senichev, A. Lehrach, R. Maier, D. Zyuzin*:* "THE SPIN ABERRATION OF POLARIZED BEAM IN ELECTROSTATIC RINGS", Institute for Nuclear Physics, Forschungszentrum Juelich, D-52425 Juelich, Germany

[17] E. M. Metodiev, K. L. Huang, Y. K. Semertzdis and W. M. Morse*:* "Fringe electric fields of flat and cylindrical deflectors in electrostatic charged particle storage ring", Brookhaven National Laboratory, Physical Review Special Topics - Accelerators and Beams, 2014

[18] Riley Molloy and Sam Blitz*:* "Fringe Field Effects on Bending Magnets, Derived for TRANSPORT/TURTLE", Fermilab, Chicago, August 5, 2013

[19] J.M. De Conto*:* Internal note "Formules de quadrature/intégration. Méthodes numériques". Feb 2018.

[20] B. D. Muratori, J. K. Jones and A. Wolski, "Analytical expressions for fringe fields in multipole magnets," Phys. Rev. ST Accel. Beams **18** (2015) no.6, 064001 doi:10.1103/PhysRevSTAB.18.064001 [arXiv:1404.1762 [physics.acc-ph]].

[21] Gautschi, Walter. (2011). The Lambert W-functions and some of their integrals: A case study of high-precision computation. Numerical Algorithms. 57. 27-34. 10.1007/s11075-010-9409-6.

[22] Corless, Robert & Gonnet, Gaston & E. G. Hare, D & Jeffrey, David & E. Knuth, D. (1996). On the Lambert W Function. Advances in Computational Mathematics. 5. 329-359. 10.1007/BF02124750.

[23] A. Lehrach [JEDI Collaboration], "Beam and Spin Dynamics for Storage Ring Based EDM Search," doi:10.18429/JACoW-IPAC2015-WEAB2

[24] The Bmad web site: http://www.lepp.cornell.edu/~dcs/bmad

[25] V. Anastassopoulos *et al.*, "A Storage Ring Experiment to Detect a Proton Electric Dipole Moment," Rev. Sci. Instrum. **87** (2016) no.11, 115116 doi:10.1063/1.4967465 [arXiv:1502.04317 [physics.acc-ph]].

[26] Elias Metral, JUAS course: Longitudinal dynamics

[27] Y. Senichev *et al.*, "Quasi-frozen Spin Method for EDM Deuteron Search," doi:10.18429/JACoW-IPAC2015-MOPWA044

Appendix A

Exhaustive list of integrals used in the code

This appendix gives the exhaustive list of the integrals necessary to run the spin dynamics model in a tracking code. These are the integrals computed by quadrature and are integrals of the field and motion equations in the fringe field.

The five first pages stand for the analytic expression for the integrals and the associated names. All the integrals are integrated over the curvilinear coordinate normalised to the gap ($\tilde{s} = s/G$ from $-3 \cdot G$ to $D \cdot G$ where D is the position of the diaphragm.

Page 123 stands for the integrals of the **entrance** fringe field.

Page 124 stands for the integrals of the **exit** fringe field.

The integrals are given here up to order 2 in α but are fully calculated in a Mathematica separate file.

A.1 List of analytic integrals

$$\beta = \left(\frac{G}{\rho}\right)^2 \cdot \left(\frac{b-a}{2}\right)^2$$

$$I0 = \int k_0$$

$$I01 = \int k_0^2$$

$$I_2 = \int k_2$$

$$I_3 = \int k_2 \cdot \hat{s}^2$$

$$I03 = \int k_0 \hat{s}$$

$$I04 = \int k_0^2 \hat{s}$$

$$I05 = \int k_0 \hat{s}^2$$

$$I06 = \int \dot{k}_0 k_0 \hat{s}$$

$$I07 = \int \dot{k}_0 \hat{s}^2$$

$$I11 = \iint k_0$$

$$K11 = \iint k_0 \cdot \hat{s}$$

$$I12 = \iint k_0^2$$

$$K12 = \iint k_0^2 \cdot \hat{s}$$

$$I00 = \int k_0 \int k_0 = \frac{I_{11}^2}{2}$$

$$J1p1 = -I01$$

$$J41 = \iint \iint k_0$$

$$Js42 = \iint \iint k_0 \cdot \hat{s}$$

$$J42 = \iint \iint k_0^2$$

$$Js41 = \iint \iint k_0^2 \cdot \hat{s}$$

$$J11 = \iint k_0 \iint k_0$$

$$L11 = \iint k_0 \iint k_0 \cdot \hat{s}$$

$$J22 = \iint k_0^2 \iint k_0^2$$

$$L22 = \iint k_0^2 \iint k_0^2 \cdot \hat{s}$$

$$J12 = \iint k_0^2 \iint k_0 + \iint k_0 \iint k_0^2$$

$$L12 = \iint k_0^2 \iint k_0 \cdot \hat{s} + \iint k_0 \iint k_0^2 \cdot \hat{s}$$

$$J0 = \iint \frac{(s-a)^2}{2} \cdot k_0$$

$$L2 = \iint \frac{(s-a)^2}{2} \cdot k_0^2$$

$$L0 = \iint \frac{(s-a)^3}{6} \cdot k_0$$

$$L1 = \iint \frac{(s-a)^3}{6} \cdot k_0^2$$

$$C(X) = 1 - \beta \cdot [A \cdot C_{11} + B \cdot C_{12}] + \beta^2 \cdot [A^2 \cdot C_{11} + A \cdot B \cdot C_{23} + B^2 \cdot C_{22}]$$

$$S(X) = X - a - \beta \cdot [A \cdot S_{11} + B \cdot S_{12}] + \beta^2 \cdot [A^2 \cdot S_{21} + A \cdot B \cdot S_{23} + B^2 \cdot S_{22}]$$

$$C'(X) = -\beta \cdot [A \cdot M_0 + B \cdot M_1] + \beta^2 \cdot [A^2 M_{11} + AB \cdot M_{12} + B^2 M_{12}]$$

$$S'(X) = 1 - \beta \cdot [A \cdot N_0 + B \cdot N_1] + \beta^2 \cdot [A^2 N_{11} + AB \cdot N_{12} + B^2 N_{12}]$$

$$A = \frac{1}{\gamma_0^2} + \frac{1}{\gamma_0}$$

$$B = \frac{1}{\gamma_0}$$

$$CK = I_0 - \beta \cdot [A \cdot P_{11} + B \cdot P_{12}]$$

$$CK2 = I_{01} - \beta \cdot [A \cdot P_{21} + B \cdot P_{22}]$$

$$C1Kp = -1 - \beta \cdot [A \cdot P_{31} + B \cdot P_{32}]$$

$$C2Kp = -1 - 2\beta \cdot [A \cdot P_{31} + B \cdot P_{32}]$$

$$C2KpK == -\frac{1}{2} - 2\beta \cdot [A \cdot P_{41} + B \cdot P_{42}]$$

$$P_{11} = \int C_{11} k_0$$

$$P_{12} = \int C_{12} k_0$$

$$P_{21} = \int C_{11} k_0^2$$

$$P_{22} = \int C_{12} k_0^2$$

$$P_{31} = \int C_{11} \dot{k}_0$$

$$P_{32} = \int C_{12} \dot{k}_0$$

$$P_{41} = \int C_{11} \dot{k}_0 k_0$$

$$P_{42} = \int C_{12} \dot{k}_0 k_0$$

$$CCpKp = \int C\dot{C}\dot{k}_0 = C1Kp$$

$$CKpE = I_{03} - \frac{I_{11}^2}{2} - 2I_{04}$$

$$CpKpE = \int \dot{C}\dot{k}_0 \eta_1 = 0$$

$$C3 = \int C\dot{k}_0 \int k_0 \sim J1p1 = -I_{01}$$

$$SK = \int Sk_0 = I_{03} - \beta \cdot \left[A \cdot Q_{11} + B \cdot Q_{12}\right]$$

$$SK2 = \int Sk_0^2 = I_{04} - \beta \cdot \left[A \cdot Q_{21} + B \cdot Q_{22}\right]$$

$$SKp = \int S\dot{k}_0 = -\frac{1}{2} I_{05} - \beta \cdot \left[A \cdot Q_{31} + B \cdot Q_{32}\right]$$

$$S2Kp = \int \dot{k}_0 S^2 = I_{07} - 2\beta \cdot \left[A \cdot Q_{31} + B \cdot Q_{32}\right]$$

$$S2KpK = \int \dot{k}_0 k_0 S^2 = I_{06} - 2\beta \cdot \left[A \cdot Q_{41} + B \cdot Q_{42}\right]$$

$$Q_{11} = \int S_{11} k_0$$

$$Q_{12} = \int S_{12} k_0$$

$$Q_{21} = \int S_{11} k_0^2$$

$$Q_{22} = \int S_{12} k_0^2$$

$$Q_{31} = \int S_{11} \dot{k}_0 \hat{s}$$

$$Q_{32} = \int S_{12} \dot{k}_0 \hat{s}$$

$$Q_{41} = \int S_{11} \dot{k}_0 k_0 \, \hat{s}$$

$$Q_{42} = \int S_{12} \dot{k}_0 k_0 \, \hat{s}$$

$$SSpKp = -\frac{1}{2} I_{05} - \beta \cdot [A \cdot (R_{11} + R_{12}) + B(R_{21} + R_{22})]$$

$$R_{11} = \int \dot{k}_0 \cdot S_{11}$$

$$R_{12} = \int \dot{k}_0 \cdot \hat{s} \cdot N_0$$

$$R_{21} = \int \dot{k}_0 \cdot S_{12}$$

$$R_{22} = \int \dot{k}_0 \cdot \hat{s} \cdot N_1$$

$$SkpE = \int S \dot{k}_0 \eta_1 \sim \int \dot{k}_0 \hat{s} \int (1 - k_0) \cdot \hat{s} - \int \dot{k}_0 \hat{s}^2 \int (1 - k_0)$$

$$SpKpE = \int \dot{S} \dot{k}_0 \eta_1 \sim CKpE$$

$$S3 = Q_{50} - \beta \cdot [A \cdot Q_{51} + B \cdot Q_{52}]$$

$$Q_{50} = \int \hat{s} \, \dot{k}_0 \int k_0$$

$$Q_{51} = \int \hat{s} \, \dot{k}_0 \cdot S_{11} \int k_0$$

$$Q_{52} = \int \hat{s} \, \dot{k}_0 \cdot S_{12} \int k_0$$

$$SCKp = \frac{I_{05}}{2} - \beta \cdot [A \cdot (Q_{31} + Q_{61}) + B \cdot (Q_{32} + Q_{62})]$$

$$Q_{31} = \int \dot{k}_0 S_{11}$$

$$Q_{32} = \int \dot{k}_0 S_{12}$$

$$Q_{61} = \int \dot{k}_0 \hat{s} C_{11}$$

$$Q_{62} = \int \dot{k}_0 \hat{s} C_{12}$$

$$SCKpK = I_{06} - \beta \cdot [A \cdot (Q_{73} + Q_{71}) + B \cdot (Q_{74} + Q_{72})]$$

$$I_{06} = \int \dot{k_0} k_0 \, \hat{s}$$

$$Q_{73} = \int k_0 \dot{k}_0 S_{11}$$

$$Q_{74} = \int k_0 \dot{k}_0 S_{12}$$

$$Q_{71} = \int k_0 \dot{k}_0 \hat{s} C_{11}$$

$$Q_{72} = \int k_0 \dot{k}_0 \hat{s} C_{12}$$

$$SCCS = -\beta \cdot [A \cdot R_{12} + B \cdot R_{22}]$$

$$KpE1 = CKpE$$

$$KpE2 = 0$$

$$Q1 = I_0 - I_{01}$$

$$Q2 = -I_{01}$$

$$Q3 = \dot{k}_0(b) \cdot \left[\frac{(b-a)^2}{2} - I_{03} - (b-a) \cdot (b-a-I_0)\right] + \int \frac{\hat{s}^3 \ddot{k}_0}{2} + \int \ddot{k}_0 \hat{s} \int k_0 \hat{s} - \int \ddot{k}_0 \hat{s}^2 \int k_0$$

$$Q4 = \dot{k}_0(b) \cdot [-I_{03} + (b-a) \cdot I_0] + \int \ddot{k}_0 \hat{s} \int k_0 \hat{s} - \int \ddot{k}_0 \hat{s}^2 \int k_0$$

$$C2K2 = I_0 - 2\beta \cdot [A \cdot P_{11} + B \cdot P_{12}]$$

$$S2K2 = I_{05} - 2\beta \cdot [A \cdot R_{11} + B \cdot R_{12}]$$

$$C2K21 = I_2 - 2\beta \cdot [A \cdot R_{21} + B \cdot R_{22}]$$

$$S2K21 = I_3 - 2\beta \cdot [A \cdot R_{31} + B \cdot R_{32}]$$

$$\int S\varphi = \frac{G}{\rho} \cdot \int (1-k_0) \cdot \tilde{s} - \left(\frac{G}{\rho}\right)^2 \cdot \iint \omega\, \tilde{s} = \frac{G}{\rho} \cdot \int (1-k_0) \cdot \tilde{s} - - \left(\frac{G}{\rho}\right)^3 \cdot \int (1-k_0) \iint \omega\, \tilde{s}$$

$$\int C\varphi = \frac{G}{\rho} \cdot \int (1-k_0) - \left(\frac{G}{\rho}\right)^2 \cdot \iint \omega = \frac{G}{\rho} \int (1-k_0) - \int (1-k_0) - \left(\frac{G}{\rho}\right)^3 \cdot \int (1-k_0) \iint \omega$$

$$I_1 = \int (1-k_0) \cdot \tilde{s}$$

$$I_2 = \int (1-k_0) \iint \omega\, \tilde{s} = \int (1-k_0) \int (u-\tilde{s})\, \omega \tilde{s}$$

$$J_2 = \int k_0 \iint \omega\, \tilde{s} = \int k_0 \int (u-\tilde{s})\, \omega \tilde{s}$$

$$I_3 = \int (1-k_0)$$

$$I_4 = \int (1-k_0) \iint \omega = \int (1-k_0) \int (u-\tilde{s})\, \omega$$

$$J_4 = \int k_0 \iint \omega$$

$$A_1 = \iint \omega$$

$$A_2 = \iint \omega\, \tilde{s}$$

$$\begin{aligned} \eta = C \int S\varphi - S \int C\varphi \\ = \frac{G}{\rho} \cdot I_1 - \left(\frac{G}{\rho}\right)^3 \cdot [A_1 \cdot I_1 + I_2 + \alpha \cdot J_2 \cdot \delta] \\ - \left[\frac{G}{\rho} \cdot \tilde{s} \cdot I_3 - \left(\frac{G}{\rho}\right)^3 \cdot [A_2 \cdot I_3 + \tilde{s} \cdot (I_4 + \alpha \cdot \delta \cdot J_4)]\right] \end{aligned}$$

A.2 Input file for integrals with values

```
start = -3
 end = 5

 3.3388804045388098882498786512539124132970000 = M_0
 6.0653771361827688447739079831017104502950000 = N_0
 -5.1833776380395806607970896634026362110640000 = M_1
 -27.8373764743249965158074829423515525601500000 = N_1
 3.3388804045388098882498786512539124132970000 = I_0
 2.8166223619604193392029103365972531241330000 = I_01
  0.0024744473680336232227045631822451399370540 = I_2
  -3.1715768179596019000710904885089922129220000 = I_3
  6.0653771361827688447739079831017104502920000 = I_03
  4.1626235256750034841925170576480047806440000 = I_04
  16.0939499357170905456303063976226289561500000 = I_05
  -1.4083013857539600070410650166448290361560000 = I_06
  -12.1307590443656814245105955629110218822200000 = I_07
  20.6456661001277102612251212269295888560600000 = I_11
  32.4290671537450602125609574671911546462000000 = K_11
  18.3703553700083512294307656351300202124200000 = I_12
  24.7159927999893476829889995962705539080300000 = K_12
  213.1217643589812684108057847386217140836000000 = I_00
  146.3783111253229353980899234839581225124000000 = J_41
  154.4876822259752125756742314164440369307000000 = J_s42
  138.0095517537166658870831535842606219628000000 = J_42
  180.2033656540128709683260789916608011522000000 = J_s41
  36.6095549402917539847529328000298355642500000 = J_11
  32.3935904724464687332332522251064156774400000 = L_11
  23.4065921349206882977243984752929711889000000 = J_22
  17.1334384465092873489815396703917166636300000 = L_22
  59.5325178336861863500278283707711925446900000 = J_12
  48.1618642271433212536587323191721374629400000 = L_12
  37.9061554018425595355535550927655651937490000 = J_0
  11.9526129103987698916884785993922920714300000 = L_2
  36.4594781572258795572948042891181959568800000 = L_0
  18.3449634036757161351353407830755403364900000 = L_1
  7.6163406941031549289163213970076587111760000 = P_11
  -0.6297687956945185972460908084894218240592000 = P_12
  4.2318316307051984603337511116567190656280000 = P_21
  -0.1031194597116916030121639017023905891316000 = P_22
  -5.5740637385054712843175936146063456784600000 = P_31
  0.7060672459818850596187572091719171214144000 = P_32
  -2.0225178422329295533101374331926988585660000 = P_41
  0.0979722923094142680742946020199448598223600 = P_42
  7.3549981611586568897264307138384510761600000 = Q_11
  -2.0268524653260066356003483206007445502970000 = Q_12
  3.3163252925653823720919106647475091723680000 = Q_21
  -0.2627361170851370139319962627973055682528000 = Q_22
  -25.7494180996381983924580571514304072713000000 = Q_31
  12.5365549836132656678181860986588636528900000 = Q_32
  -6.3021443165194951236336543601418403665000000 = Q_41
  1.0168922066056069605393988879919408970440000 = Q_42
  -32.4264683582603663468827860264613562350800000 = R_11
  -20.2515667473094737451695935035343901347000000 = R_12
  -32.3909945199864827199838500631473667257200000 = R_21
  92.9456610994135492711324125708442571080800000 = R_22
  -9.7288556572743502652680596672154338293360000 = Q_50
  -80.0392814612867402090078511255935327514400000 = Q_51
  40.9547642154468886827730097351401274146600000 = Q_52
  -21.5503099909279225917414374859638792995900000 = Q_61
  3.6039470043872544645982094739986724168820000 = Q_62
  -1.9820491434242740540638678149811789265140000 = Q_73
  0.2624609259561023561853274591512890610872000 = Q_74
  -6.2138745173425281090386322766558802463440000 = Q_71
  0.3655806858322576075839282270255238393514000 = Q_72
  2.5898165217244645425517545175922395358740000 = SkpE
  -9.9314407148034717805910745723181981461760000 = R_31
  5.8146530203313687119794230352784622144360000 = R_32
  -14.062983216067720015681001126732737570170000 = Q_3
  -14.324372775158668317370691980331867961000000 = Q_4
```

```
start = -3
 end = 5

 3.33888040453880988824987865125391241329600 0 = M_0
 20.64566610012771026122512122692958885610000 0 = N_0
 -5.18337763803958066079708966340263621106800 0 = M_1
 -13.62964462999164877056923436486953712838000 0 = N_1
 3.33888040453880988824987865125391241329600 0 = I_0
 2.81662236196041933902029103365972531241320000 = I_01
  0.00247444736803362322270456318224513993572 3 = I_2
  4.65211971398349289768207934298006861580800 0 = I_3
  20.64566610012771026122512122692958885608000 0 = I_03
  18.37035537000835122943076563513002021242000 0 = I_04
  132.73626164727662187724001234824555620240000 0 = I_05
  2.59102918425446666770897448004034258539600 0 = I_06
  22.70354003487634827952762598480412582356000 0 = I_07
  6.06537713618276884477390798310171045029000 0 = I_11
  32.42906715374506021256095746719115464620000 0 = K_11
  4.16262352567500348419251705764800478063800 0 = I_12
  24.71599279998934768298899959627055390805000 0 = K_12
  18.39439990206434322028149679538298336342000 0 = I_00
  8.82321478034193421565589155427818098249400 0 = J_41
  18.34496340367571613513534078307542219304000 0 = J_s42
  3.47825193361506032627586342028976434715000 0 = J_42
  36.45947815722587955729480428911827503128000 0 = J_s41
  7.34390585873589704642827598056973509268800 0 = J_11
  32.38661565287529096110775337235609058522000 0 = L_11
  3.19393368609625458121398101797931466111900 0 = J_22
  17.12155139218719867822432758959203468843000 0 = L_22
  10.08654718510658822534223843633943205221000 0 = J_12
  48.14552547563200121589604331608186359422000 0 = L_12
  91.81011321313768131469027894110896664730000 0 = J_0
  37.47937268957992547428952059314881574469000 0 = L_2
  180.20336565401287096832607899166036851640000 0 = L_0
  154.48768222597521257567423141644366659370000 0 = L_1
  7.61634132253688131300627966433534055672400 0 = P_11
  -62.13629669370129835299734516867511047096000 0 = P_12
  7.41720706163063740023642896195401674540800 0 = P_21
  -56.93404427907266528905297538950601028660000 0 = P_22
  0.49083305432145490310872508497107288793800 0 = P_31
  -11.23453185725300909949072831029293800400000 0 = P_32
  0.35255014500933366456920513769965597364150 0 = P_41
  -6.71457406439811107510166023853752414062400 0 = P_42
  36.62875686035226794818324416185459639290000 0 = Q_11
  -122.73639997783008470291301761089721040640000 0 = Q_12
  35.93863194752932765679873254926164474169400 0 = Q_21
  -114.56328473496957058025987375276632171850000 0 = Q_22
  9.66140811987137420745046714929109396133600 0 = Q_31
  -93.91970035339359934095225569560920853668000 0 = Q_32
  7.53780446584516044296815030973156005838800 0 = Q_41
  -62.50177925544778066511684103070570965876000 0 = Q_42
  32.42646819777232661412032160640177680019000 0 = R_11
  96.21866944031959876916749430196301493344000 0 = R_12
  32.38402009908434735754119175331836998896000 0 = R_21
  -63.52065682366534742067622901896402834060000 0 = R_22
  2.77885586439865393774698336668890382586400 0 = Q_50
  9.74278722447530143885069287885607151272800 0 = Q_51
  -71.25806461461700603736498858512563077568000 0 = Q_52
  2.62794258150022775739780034395610451190700 0 = Q_61
  -56.20495576579857848627391520117248137188000 0 = Q_62
  1.33460037315648640076189753670235612398800 0 = Q_73
  -11.63027038760022145440828827569713857063000 0 = Q_74
  1.96308835733991935439185961975874749461000 0 = Q_71
  -35.72396229540779060938311983489633063841000 0 = Q_72
  -54.26211638317599988980141062927642779776000 0 = SkpE
  6.97514941988447359852055640899697748302400 0 = R_31
  -34.58040420990565249949253244295069861842000 0 = R_32
  2.09942198189889125107978583326895787088700 0 = Q_3
  3.14897057504036089840949303664527979875600 0 = Q_4
```

Appendix B

Semi-infinite box potential (JMDC, French)

Un simple calcul de potentiel

JM De Conto, 26 octobre 2016

On est souvent amené à calculer (dans le cas des déflecteurs de JEDI par exemple), le potentiel créé par une boîte semi-infinie.

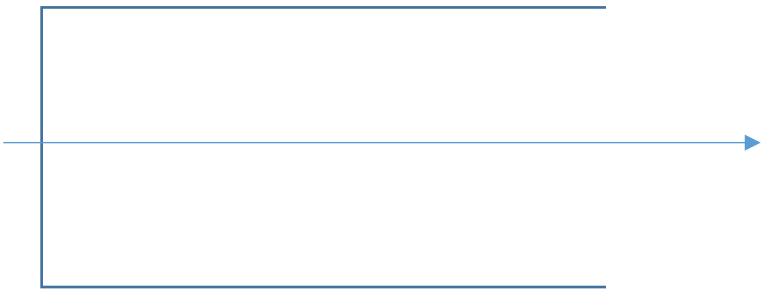

On suppose que les lignes supérieures sont à une position $y = \pm 1$ et portées à des potentiels respectifs $\pm\pi$. On suppose que la ligne verticale est en x=0 et au potentiel nul.

Questions : Que vaut le potentiel dans la boîte ? Comment le calculer de manière efficace ?

Réponses : Le potentiel est harmonique. Le problème est équivalent à un problème où l'on aurait deux lignes équipotentielles en miroir (donc de polarités opposées) symétriquement par rapport à l'axe vertical. Le potentiel en y=1 serait donc une fonction d'Heaviside décomposable en intégrale de Fourier soit, pour l'électrode :

$$\int_{-\infty}^{+\infty} \frac{\sin(\omega x)}{\omega} \cdot d\omega$$

Il faut une fonction impaire en x et y, harmonique, et par conséquent on devine aisément (et on vérifie) que la solution est :

$$V(x,y) = \int_{-\infty}^{+\infty} \frac{\mathrm{sh}(\omega y) \cdot \sin(\omega x)}{\mathrm{sh}(\omega) \cdot \omega} \cdot d\omega$$

***Nota** : à part deviner je ne sais pas faire, notamment je ne sais pas intégrer l'équation de Poisson. Désolé.*

On peut bien entendu déduire le champ et dérivant sous le signe somme selon x ou y.

La seconde question est naturellement le calcul numérique du champ ou du potentiel (quelques secondes par valeur sous Maple ou Mathematica !!!) pour une intégration type Runge-Kutta. Il faut une solution numérique rapide. L'idéal serait de pouvoir calculer cette intégrale analytiquement. Ceci est hors de ma portée, mais on peut toujours en calculer d'autres.

Remarque 1 : Le potentiel sur l'axe est nul et n'apporte aucune information. Par contre, le champ vertical sur l'axe est uniforme à $+\infty$ et nul à l'origine. Dit autrement, la connaissance du champ vertical sur l'axe tout entier permet de connaître le champ vertical dans tout l'espace (propriété des générales des fonctions analytiques donc des fonctions harmoniques). On peut d'ailleurs écrire cette relation qui est cependant sans intérêt (développement en série du champ).

Sur l'axe horizontal, en dérivant sous le signe somme selon y et en faisant y=0, on obtient :

$$E_{y0}(x) = \int_{-\infty}^{+\infty} \frac{\sin(\omega x)}{\mathrm{sh}(\omega)} \cdot d\omega$$

On peut par développer cette expression en série selon x, et chaque coefficient sur les puissances (impaires) de x s'avère valoir :

$$(-1)^n \cdot [4 + \alpha_i]$$

Où les α_i tendent vers zéro.

Ceci implique que, les coefficients étant sur les puissances impaires de x :

$$E_{y0}(x) = \frac{4x}{x^2+1} + \varphi(x)$$

Où $\varphi(x)$ est une fonction que nous allons estimer

Remarque 2 : On s'autorise à écrire l'intégrande sous une forme différente, plus explicite. On change les bornes pour avoir des fonctions qui tendent vers zéro à l'infini, sinon le calcul est impossible. C'est une petite astuce amusante mais indispensable.

$$E_{y0}(x) = \int_{-\infty}^{+\infty} \frac{2\sin(\omega x)}{1-e^{-2\omega}} \cdot e^{-\omega} d\omega = 2 \cdot \int_{0}^{+\infty} \frac{2\sin(\omega x)}{1-e^{-2\omega}} \cdot e^{-\omega} d\omega$$

Remarque 3 : On a la relation bien connue

$$\int_{0}^{+\infty} \sin(\omega x) \cdot e^{-\omega} d\omega = \frac{x}{x^2+1}$$

Et donc

$$\varphi(x) = 4 \cdot \int_0^{+\infty} \sin(\omega x) \cdot e^{-\omega} \cdot \left[\frac{1}{1-e^{-2\omega}} - 1\right] \cdot d\omega$$

$$\varphi(x) = 4 \cdot \int_0^{+\infty} \sin(\omega x) \cdot \frac{e^{-3\omega}}{1-e^{-2\omega}} \cdot d\omega$$

Remarque 4 : Cette dernière intégrale est connue (elle)

$$4 \cdot \int_0^{+\infty} \sin(\omega x) \cdot \frac{e^{-3\omega}}{1-e^{-2\omega}} \cdot d\omega = \pi \cdot th\left[\frac{\pi \cdot x}{2}\right] - \frac{4x}{x^2+1}$$

Par conséquent, les lois de l'addition étant ce qu'elles sont :

$$E_{y0}(x) = \pi \cdot th\left[\frac{\pi \cdot x}{2}\right]$$

Nous avons donc bien obtenu une expression analytique en calculant d'autres intégrales.

Remarque 5 : Le lecteur (ou la lectrice) grincheu(x ou euse) objectera que nous avons le champ selon y et pas selon x, pas plus que nous n'avons le potentiel. Nous lui ferons remarquer non sans ironie que le champ en y est l'opposé de la partie imaginaire du champ complexe.

Par conséquent, le champ complexe ne peut être que du type :

$$\underline{E}(z) = i \cdot \pi \cdot th\left[\frac{\pi \cdot z}{2}\right]$$

En intégrant formellement par rapport à z :

$$\underline{V}(z) = -\int \underline{E}(z) \cdot dz = i \cdot ln\left[th^2\left(\frac{\pi \cdot z}{2}\right) - 1\right] + C$$

La constante doit donner zéro sur l'axe et vaut simplement π

Remarque 6 : la fonction logarithme est multivaluée, et il y a en fait plusieurs cas (qui peuvent éventuellement varier selon le logiciel de calcul utilisé, et l'on commencera par vérifier numériquement ce que l'on fait). Ce qui suit n'est valable que pour x=Re(z)>0. On complète par symétrie

$$\underline{V}(z) = i \cdot ln\left[th^2\left(\frac{\pi \cdot z}{2}\right) - 1\right] + \pi \; quand \; Im(z) > 0$$

$$\underline{V}(z) = i \cdot ln\left[th^2\left(\frac{\pi \cdot z}{2}\right) - 1\right] - \pi \; quand \; Im(z) < 0$$

En définitive, les électrodes étant positionnées en $y = \pm 1$ et fixées au potentiel $\pm\pi$:

$$\underline{V}(z) = i \cdot ln\left[th^2\left(\frac{\pi \cdot z}{2}\right) - 1\right] + \pi \cdot signe(Im(z)) \quad \text{et } Re(z) \geq 0$$

$$\underline{E}(z) = i \cdot \pi \cdot th\left[\frac{\pi \cdot z}{2}\right]$$

Moralité : pour calculer une intégrale quand vous ne pouvez pas, calculez-en une autre. Et cela vous évitera des problèmes de calculs numériques longs et imprécis. Amusant non ?

Il y a peut-être une démarche plus directe, autre qu'une vérification, cela m'intéresse pour le principe.

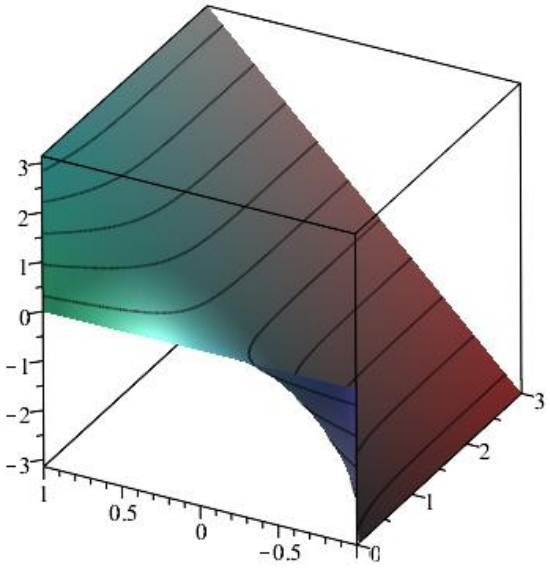

A la fin nous avons :

$$V(x,y) = \frac{2}{\pi} \cdot V_0 \cdot \arctan[th(x) \cdot \tan(y)]$$

Appendix C

Terms and dependencies of fringe fields spin dynamics

Motion Coslike and Sinlike functions

$$C(X) = 1 - \beta \cdot \left[A \cdot I_{11} + B \cdot \left(I_{12} - \frac{(X-a)^2}{2} \right) \right] + \beta^2 \cdot \left[A^2 \cdot J_{11} + A \cdot B \cdot (J_{12} - J_0 - J_{41}) + B^2 \cdot \left(J_{22} - L_2 - J_{42} + \frac{(X-a)^4}{24} \right) \right]$$

$$S(X) = X - a - \beta \cdot \left[A \cdot K_{11} + B \cdot \left(K_{12} - \frac{(X-a)^3}{6} \right) \right] + \beta^2 \cdot \left[A^2 \cdot L_{11} + A \cdot B \cdot (L_{12} - L_0 - Js_{42}) + B^2 \cdot \left(L_{22} - L_1 - Js_{41} + \frac{(X-a)^5}{120} \right) \right]$$

$$C'(X) = 0$$

$$S(X) = 1$$

Terms R11 fringe

$$R_{11\,CI=0} = 1 - \frac{\alpha^2(\gamma 0^2 - \gamma m^2)^2(\int_0^S k0[s]\,ds)^2}{8\gamma 0^2(-1+\gamma m^2)^2}$$

$$\frac{\partial R_{11}}{\partial x_0} = 0$$

$$\frac{\partial R_{11}}{\partial p_{x0}} = 0$$

$$\frac{\partial R_{11}}{\partial p_{y0}} = \frac{i\alpha(\gamma 0^2 - \gamma m^2)\int k0[s]\,ds}{2\gamma 0(-1+\gamma m^2)}$$

$$\frac{\partial R_{11}}{\partial \delta} = \frac{\alpha^2(\gamma 0^2 - \gamma m^2)(\int_0^S k0[s]\,ds)((\gamma 0^2 - \gamma m^2)\int k0[s]\,ds + (2+\gamma 0^2 - 3\gamma m^2)\int_0^S k0[s]\,ds)}{4\gamma 0^2(-1+\gamma m^2)^2}$$

$$\frac{\partial^2 R_{11}}{\partial {x_0}^2} = -\frac{\alpha^2(\gamma 0^2 - \gamma m^2)^2(\int_0^S k0[s]\,ds)\int C[s]\dot{C}[s]\dot{k}0[s]\,ds}{4\gamma 0^2(-1+\gamma m^2)^2}$$

$$\frac{\partial^2 R_{11}}{\partial {p_{x0}}^2} = -\frac{\alpha^2(\gamma 0^2 - \gamma m^2)^2(\int_0^S k0[s]\,ds)\int \dot{k}0[s]S[s]\dot{S}[s]\,ds}{4\gamma 0^2(-1+\gamma m^2)^2}$$

$$\frac{\partial^2 R_{11}}{\partial {p_{y0}}^2} = -\frac{\alpha^2(\gamma 0^2 - \gamma m^2)^2(\int_0^S k0[s]\,ds)^2}{8\gamma 0^2(-1+\gamma m^2)^2}$$

$$\frac{\partial^2 R_{11}}{\partial \delta^2} = -\frac{1}{8\gamma 0^4(-1+\gamma m^2)^2}\alpha^2(4\gamma 0^2(\gamma 0^4 + \gamma 0^2(2-4\gamma m^2) + \gamma m^2(-2+3\gamma m^2))(\int k0[s]\,ds)\int_0^S k0[s]\,ds + (3\gamma 0^6 + \gamma m^2(-2+3\gamma m^2) - 5\gamma 0^4(-3+4\gamma m^2) + \gamma 0^2(6-26\gamma m^2+21\gamma m^4))(\int_0^S k0[s]\,ds)^2 + \gamma 0^2(\gamma 0^2 - \gamma m^2)^2(\int_0^S k0[s]\,ds))$$

$$\frac{\partial^2 R_{11}}{\partial x_0 p_{x0}} = \frac{\alpha^2(\gamma 0^2 - \gamma m^2)^2(\int_0^S k0[s]\,ds)\int \dot{k}0[s](\dot{C}[s]S[s] + Cc[s]\dot{S}[s])\,ds}{4\gamma 0^2(-1+\gamma m^2)^2}$$

$$\frac{\partial^2 R_{11}}{\partial x_0 p_{y0}} = -[i\alpha^2((\gamma 0^2 - \gamma m^2)^2(\int_0^S \mathrm{k0}[s]\,ds)\int \mathrm{C}[s]\dot{\mathrm{k}}0[s]\,ds - 2\int \mathrm{C}[s](-\gamma 0(\gamma 0^2 - \gamma m^2)(-1 + \gamma m^2)\mathrm{k0}[s] - 2\gamma 0(-1 + \gamma m^2)^2 \mathrm{k0}[s]^2 + (\gamma 0^2 - \gamma m^2)^2(\int_0^S \mathrm{k0}[s]\,ds)\dot{\mathrm{k}}0[s])\,ds)]/[4\gamma 0^2(-1 + \gamma m^2)^2]$$

$$\frac{\partial^2 R_{11}}{\partial p_{x0} p_{y0}} = -[i\alpha^2((\gamma 0^2 - \gamma m^2)^2(\int_0^S \mathrm{k0}[s]\,ds)\int \dot{\mathrm{k}}0[s]\mathrm{S}[s]\,ds - 2\int (-\gamma 0(\gamma 0^2 - \gamma m^2)(-1 + \gamma m^2)\mathrm{k0}[s] - 2\gamma 0(-1 + \gamma m^2)^2 \mathrm{k0}[s]^2 + (\gamma 0^2 - \gamma m^2)^2(\int_0^S \mathrm{k0}[s]\,ds)\dot{\mathrm{k}}0[s])\mathrm{S}[s]\,ds)]/[4\gamma 0^2(-1 + \gamma m^2)^2]$$

$$\frac{\partial^2 R_{11}}{\partial x_0 \delta} = 0$$

$$\frac{\partial^2 R_{11}}{\partial p_{x0} \delta} = 0$$

$$\frac{\partial^2 R_{11}}{\partial p_{y0} \delta} = \frac{i\alpha \int \mathrm{k0}[s]\,ds}{\gamma 0}$$

Terms R12 fringe

$$R_{12_{CI=0}} = \frac{\alpha(\gamma 0^2 - \gamma m^2)\int_0^S \mathrm{k0}[s]\,ds}{2\gamma 0(-1+\gamma m^2)}$$

$$\frac{\partial R_{12}}{\partial x_0} = (\alpha^2(\int_0^S \mathrm{C}[s]\mathrm{k0}[s](\gamma 0^2 - \gamma m^2 + (2+\gamma 0^2 - 3\gamma m^2)\mathrm{k0}[s])\,ds + (\gamma 0^2 - \gamma m^2)\int(\dot{\mathrm{C}}[s]\dot{\mathrm{k}}0[s]\eta_1[s] + \mathrm{C}[s](\mathrm{k0}[s] + \mathrm{k0}[s]^2 + \dot{\mathrm{k}}0[s]\eta_{\mathrm{p1}}[s]))\,ds))/(2\gamma 0(-1+\gamma m^2))$$

$$\frac{\partial R_{12}}{\partial p_{x0}} = (\alpha^2(\int_0^S \mathrm{k0}[s](\gamma 0^2 - \gamma m^2 + (2+\gamma 0^2 - 3\gamma m^2)\mathrm{k0}[s])\mathrm{S}[s]\,ds + (\gamma 0^2 - \gamma m^2)\int(\mathrm{k0}[s]\mathrm{S}[s] + \mathrm{k0}[s]^2\mathrm{S}[s] + \dot{\mathrm{k}}0[s](\dot{\mathrm{S}}[s]\eta_1[s] + \mathrm{S}[s]\eta_{\mathrm{p1}}[s]))\,ds))/(2\gamma 0(-1+\gamma m^2))$$

$$\frac{\partial R_{12}}{\partial p_{y0}} = (i\alpha^2(\gamma 0^2 - \gamma m^2)((\gamma 0^2 - \gamma m^2)(\int \mathrm{k0}[s]\,ds)\int_0^S \mathrm{k0}[s]\,ds - 2\int((\gamma 0^2 - \gamma m^2)(\int_0^S \mathrm{k0}[s]\,ds)\mathrm{k0}[s] - \gamma 0(-1+\gamma m^2)\dot{\mathrm{k}}0[s]\eta_1[s])\,ds))/(4\gamma 0^2(-1+\gamma m^2)^2)$$

$$\frac{\partial R_{12}}{\partial \delta} = -\frac{\alpha((\gamma 0^2 - \gamma m^2)\int \mathrm{k0}[s]\,ds + (2+\gamma 0^2 - 3\gamma m^2)\int_0^S \mathrm{k0}[s]\,ds)}{2\gamma 0(-1+\gamma m^2)}$$

$$\frac{\partial^2 R_{12}}{\partial {x_0}^2} = \frac{\alpha(\gamma 0^2 - \gamma m^2)\int \mathrm{C}[s]\dot{\mathrm{C}}[s]\dot{\mathrm{k}}0[s]\,ds}{2\gamma 0(-1+\gamma m^2)}$$

$$\frac{\partial^2 R_{12}}{\partial {p_{x0}}^2} = \frac{\alpha(\gamma 0^2 - \gamma m^2)\int \dot{\mathrm{k}}0[s]\mathrm{S}[s]\dot{\mathrm{S}}[s]\,ds}{2\gamma 0(-1+\gamma m^2)}$$

$$\frac{\partial^2 R_{12}}{\partial {p_{y0}}^2} = 0$$

$$\frac{\partial^2 R_{12}}{\partial \delta^2} = \frac{\alpha(2\gamma 0^2(2+\gamma 0^2 - 3\gamma m^2)\int \mathrm{k0}[s]\,ds + (2+2\gamma 0^4 - 3\gamma m^2 + \gamma 0^2(11-12\gamma m^2))\int_0^S \mathrm{k0}[s]\,ds)}{4\gamma 0^3(-1+\gamma m^2)}$$

$$\frac{\partial^2 R_{12}}{\partial x_0 p_{x0}} = \frac{\alpha(\gamma 0^2 - \gamma m^2)\int \dot{\mathrm{k}}0[s](\mathrm{Ccp}[s]\mathrm{S}[s] + \mathrm{C}[s]\dot{\mathrm{S}}[s])\,ds}{2\gamma 0(-1+\gamma m^2)}$$

$$\frac{\partial^2 R_{12}}{\partial x_0 p_{y0}} = -\frac{i\alpha(\gamma 0^2 - \gamma m^2)\int \mathrm{C}[s]\dot{\mathrm{k}}0[s]\,ds}{2\gamma 0(-1+\gamma m^2)}$$

$$\frac{\partial^2 R_{12}}{\partial p_{x0} p_{y0}} = -\frac{i\alpha(\gamma 0^2 - \gamma m^2)\int \dot{\mathrm{k}}0[s]\mathrm{S}[s]\,ds}{2\gamma 0(-1+\gamma m^2)}$$

$$\frac{\partial^2 R_{12}}{\partial x_0 \delta} = \frac{1}{2\gamma 0^3(-1+\gamma m^2)}\alpha^2\Big(\int_0^S -\mathrm{C}[s]\mathrm{k0}[s](\gamma 0^2(2+\gamma 0^2-3\gamma m^2)+(2+2\gamma 0^4-3\gamma m^2+\gamma 0^2(11 \\ -12\gamma m^2))\mathrm{k0}[s])\,ds + \gamma 0^2\int(-\dot{\mathrm{C}}[s]\dot{\mathrm{k}}0[s]((2+\gamma 0^2-3\gamma m^2)\eta_1[s]+(-\gamma 0^2+\gamma m^2)\eta_2[s]) \\ +\mathrm{C}[s](2(-1+\gamma m^2)\mathrm{k0}[s]-2(2+\gamma 0^2-3\gamma m^2)\mathrm{k0}[s]^2-\dot{\mathrm{k}}0[s]((2+\gamma 0^2-3\gamma m^2)\eta_{\mathrm{p1}}[s]+(-\gamma 0^2 \\ +\gamma m^2)\eta_{\mathrm{p2}}[s]))\,ds\Big)$$

$$\frac{\partial^2 R_{12}}{\partial p_{x0} \delta} = \frac{1}{2\gamma 0^3(-1+\gamma m^2)}\alpha^2\Big(\int_0^S -\mathrm{k0}[s](\gamma 0^2(2+\gamma 0^2-3\gamma m^2)+(2+2\gamma 0^4-3\gamma m^2+\gamma 0^2(11 \\ -12\gamma m^2))\mathrm{k0}[s])\mathrm{Ss}[s]\,ds + \gamma 0^2\int(2(-1+\gamma m^2)\mathrm{k0}[s]\mathrm{Ss}[s]-2(2+\gamma 0^2-3\gamma m^2)\mathrm{k0}[s]^2\mathrm{S}[s] \\ -\dot{\mathrm{k}}0[s](\dot{\mathrm{S}}[s]((2+\gamma 0^2-3\gamma m^2)\eta_1[s]+(-\gamma 0^2+\gamma m^2)\eta_2[s])+\mathrm{S}[s]((2+\gamma 0^2-3\gamma m^2)\eta_{\mathrm{p1}}[s] \\ +(-\gamma 0^2+\gamma m^2)\eta_{\mathrm{p2}}[s]))\,ds\Big)$$

$$\frac{\partial^2 R_{12}}{\partial p_{y0} \delta} = \frac{1}{4(\gamma 0-\gamma 0\gamma m^2)^2}i\alpha^2\Big((\gamma 0^4+\gamma 0^2(4-6\gamma m^2)+\gamma m^2(-4+5\gamma m^2))(\int \mathrm{k0}[s]\,ds)\int_0^S \mathrm{k0}[s]\,ds - 2\int((\gamma 0^4 \\ +\gamma 0^2(4-6\gamma m^2)+\gamma m^2(-4+5\gamma m^2))(\int_0^S \mathrm{k0}[s]\,ds)\mathrm{k0}[s]+\gamma 0(-1+\gamma m^2)\dot{\mathrm{k}}0[s](-(2+\gamma 0^2 \\ -3\gamma m^2)\eta_1[s]+(\gamma 0^2-\gamma m^2)\eta_2[s]))\,ds-(\gamma 0^2-\gamma m^2)^2\int_0^S \mathrm{k0}[s]\,ds^{\,2}\Big)$$